Final Technical Report

Real Time Monitor and Control of MBE Growth of HgCdTe by Spectroscopic Ellipsometry

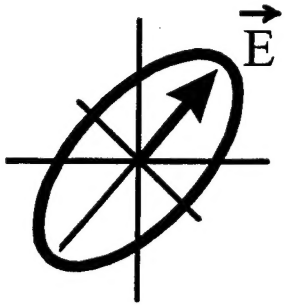

J.A. Woollam Co., Inc.

Author: Blaine Johs

Final Technical Report

Real Time Monitor and Control of MBE Growth of HgCdTe by Spectroscopic Ellipsometry

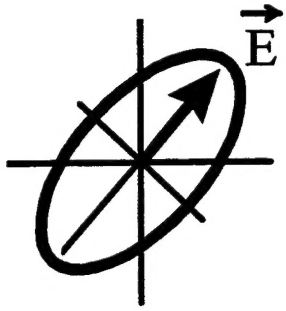

J.A. Woollam Co., Inc.

Author: Blaine Johs

REPORT DOCUMENTATION PAGE

Form Approved
OMB No. 0704-0188

1. AGENCY USE ONLY (Leave blank)	2. REPORT DATE	3. REPORT TYPE AND DATES COVERE
	October 8, 1996	**Final Scientific and Technical Report, covered from: May 19, 93 to Sept. 30, 96**

4. TITLE AND SUBTITLE

Real Time Monitor and Control of MBE Growth of HgCdTe by Spectroscopic Ellipsometry

5. FUNDING NUMBERS

C
Contract No. DAAB07-93-C-U008

6. AUTHOR(S)

Blaine Johs, Shakil Pittal, Ping He, and John A. Woollam

7. PERFORMAING ORGANIZATION NAME(S) AND ADDRESS(ES)

J. A. Woollam Co., Inc. 645 M Street, Suite 102, Lincoln, NE 68508

8. PERFORMAING ORGANIZATION REPORT NUMBER
Final - MBE II

9. SPONSORING/MINITORING AGENCY NAME(S) AND ADDRESS(ES)
U.S. Army CECOM
AMSEL-ACCC-A-CB
Fort, Monmouth, NJ 07703-5008

10. SPONSORING/MONITORING AGENCY REPORT NUMBER
D1-MISC-80711

11. SUPPLEMENTARY NOTES

12a. DISTRIBUTION/AVAILABILITY STATEMENT

Distribution statement A. Approved for public release: Distrubution is unlimited

12b. DISTRIBUTION CODE

U

13. ABSTRACT (Maximum 200 words)

The primary goal of this contract was develop a real-time monitoring capability for HgCdTe composition during MBE growth. This goal was realized by demonstrating a ± 0.001 accuracy in the composition values determined by the Spectroscopic Ellipsometry (SE) in situ sensor, which was confirmed by exsitu FTIR measurements. Attaining this level of success required significant improvements in the ellipsometer system hardware and data analysis software, the creation of accurate optical constant libraries for the CdZnTe Substrate and HgCdTe film materials, and the development of a systematic methodology for acquiring and analyzing insitu SE data in the MBE growth environment. These improvements and developments are part of an extensive 'knowledge base' which evolved throughout this contract, and is encapsulated in this report. This knowledge base is not specific only to HgCdTe growth; it is also directly relevant to the insitu SE monitoring of any epitaxial semiconductor growth process. In addition to the HgCdTe composition monitoring capabilities, insitu SE was also found to be very useful in monitoring the temperature and the surface condition of the CdZnTe substrate before growth, surface roughening during the initiation of HgCdTe growth, and the surface morphology during ECR etching of HgCdTe films.

14. SUBJECT TERMS
Ellipsometry, insitu monitoring, MBE growth, HgCdTe, etching, epitaxial growth, insitu sensors, feedback control

15. NUMBER OF PAGES
155

16. PRICE CODE
CPFF

17. SECURITY CLASSIFICATION OF REPORT	18. SECURITY CLASSIFICATION OF THIS PAGE	19. SECUIRTY CLASSIFICATION OF ABSTRACT	20. LIMITATION OF ABSTRACT
Unclassified	**Unclassified**	**Unclassified**	**UL**

Contents

6. Data Analysis Results 82

7. Growth Manager Software 108

Acknowledgments

I would like to thank the scientists at NVESD for their dedicated work which made this contract a success: Jack Dinan, Art Cornfeld, David Benson, James Johnson, and Krissy Singley. I greatly appreciate your patience in enduring the many software bugs and hardware glitches which cropped up throughout this contract. Thanks for being so persistent in 'making things work'. It was a pleasure working with you.

B.J.

1. Introduction

Goal of this Contract

$Hg_{1-x}Cd_xTe$ (abbreviated 'HgCdTe' or 'MCT' throughout this report) is a II-VI semiconductor material which is used extensively in infrared (IR) imaging and night vision electronics. To obtain acceptable yields in such devices, it is extremely important to control the bandedge of the HgCdTe detector material. This requirement directly translates into a need for precise composition control of the HgCdTe films which are grown for IR detector applications.

To satisfy the production requirements of current IR detector technology, a composition reproducibility of ±0.001 is required for state of the art devices. To achieve this level of composition reproducibility, some kind of real-time monitoring and control of the HgCdTe growth process is essential. In this contract, insitu Spectroscopic Ellipsometry (SE) was proposed as a means of providing real-time information about the HgCdTe composition during the molecular beam epitaxy (MBE) growth of the film.

While Spectroscopic Ellipsometry systems have been commercially available for many years, it has only been recently that SE systems have been adapted to provide insitu measurements in the epitaxial semiconductor growth environment. Some insitu SE work also had been performed on the MBE growth of III-V semiconductor systems (e.g., $Al_xGa_{1-x}As$) prior to the start of this contract. However, for the II-VI material systems (especially HgCdTe), it is much more difficult to achieve high quality epitaxial growth; this in turn complicates the process of using the insitu SE sensor to extract real-time composition information from the growing layer. Furthermore, the level of absolute composition accuracy which is required for HgCdTe detector applications (±0.001) had never been demonstrated by the SE measurement technique (prior to this contract).

Based on the Phase I work of this contract, it was clear that significant improvements were required not only in the insitu SE hardware and software technology, but also in the fundamental understanding of how to apply the insitu SE sensor to the HgCdTe MBE film growth process. It was therefore the goal of this contract to develop a methodology for using the insitu SE sensor to study the MBE growth of HgCdTe films, and then apply this knowledge to monitor and control the composition in real-time during growth.

Overview of this Report

The basic purpose of this report is to document how the insitu SE technology was evolved and applied to provide real-time composition monitoring during the MBE growth of HgCdTe. In the interest of time, space, and clarity, this report does not contain all of the work which was performed under this contract; more importantly, it attempts to summarize the *successful* methods and approaches which were developed. In this sense, the report reads more like a 'how to' manual on insitu ellipsometry. It is hoped that this 'manual' style approach to the final report provides a useful reference to the staff at NVESD, where the ellipsometer systems are being used for related ongoing work. It is also hoped that this 'manual' is useful to other J.A. Woollam Co. insitu SE customers; most of the material of this report is applicable to the insitu SE monitoring of epitaxial growth of semiconductors in general.

This manual is somewhat self-contained, in that most of the concepts necessary to understand how to acquire and analyze insitu SE data are described herein. However, it is beyond the scope of this report to provide all of the details, such as how to install the WVASE32 software program, or how to change a lamp in the ellipsometer light source, for example. For these details, the reader should consult the J.A. Woollam Co. WVASE32 and/or Ellipsometer Hardware User's Manuals.

A brief synopsis of each chapter is as follows:

1. In the **Introduction** chapter, the goals of the contract are clearly stated. The format and purpose of this report are also discussed, and a summary of the work performed in this contract is presented.
2. An **Ellipsometry Overview** is presented in this chapter. The theory behind the ellipsometric measurement and data analysis process are covered, such that a user can gain an appreciation of how sample parameters, such as composition and thickness, can be extracted from ellipsometric Ψ and Δ values. In other words, the 'magic black box' is removed from the ellipsometric analysis problem, exposing the concise and elegant equations and algorithms which are used to interpret the data. Future chapters rely heavily on the concepts presented in this chapter.
3. The **Ellipsometry Hardware** chapter describes how ellipsometric measurements are implemented in practice, and more specifically, it details the operation of the J.A. Woollam Co. M-XX line of insitu SE systems which were used in this contract.
4. Practical methods for performing ***Insitu* Real-Time Ellipsometry** in the MBE deposition environment are discussed in this chapter. Techniques for visualizing and displaying the vast of amount of SE data acquired during a growth run are also presented.
5. **Optical Constant Libraries** are required to quantitatively extract parameters (such as composition) from the insitu SE data. This chapter outlines a systematic methodology for building temperature and composition dependent optical constant libraries for the substrate (CdZnTe) and film (HgCdTe) materials used in this contract.
6. Using the optical constant libraries from the previous chapter, **Data Analysis Results** are presented in this chapter. This results constitute the 'meat' of this report: from the insitu SE data analysis, the CdZnTe substrate temperature and oxide thickness were determined before

growth, the compositions of HgCdTe layers were extracted and accurately correlated with exsitu FTIR compositions, and other interesting effects (such as surface roughening during the HgCdTe growth initiation) were observed.

7. The **Growth Manager Software** which is described in this chapter provides a user-friendly front end to the insitu SE system. It also was used to integrate the SE and MBE systems, such that feedback controlled growth of HgCdTe was demonstrated.
8. **ECR Etching Results** which were obtained via insitu SE are briefly described in this chapter.
9. The **Conclusions** chapter summarizes the accomplishments of this contract, and offers some thoughts on the continuation of this work.

Summary of Work Performed in this Contract

To enable insitu SE measurements, a modified Fisons V80H MBE chamber was delivered and retrofitted at NVESD. This modified chamber included ports to provide optical access at ≈75° with respect to the substrate normal, and an improved substrate manipulator design which provided improved rotational wobble and optical access to the back side of the substrate for optical temperature measurements.

Under this contract, two insitu spectroscopic ellipsometer systems where delivered to NVESD: an M-88 system which is installed on the MBE reactor, and an M-44 system which is mounted on the ECR etching chamber. The M-XX ellipsometer technology is the 2nd generation of insitu ellipsometer systems developed by J.A. Woollam Co. The design objectives of the M-XX ellipsometer technology were:

- to provide a compact multi-wavelength ellipsometer system,
- capable of acquiring fast and accurate insitu ellipsometric data in a typical deposition system environment (rotating substrate, etc.),
- that is robust and easy to use,
- with powerful analysis software to provide real-time data analysis,
- which can be integrated to provide feedback control of the deposition system,
- at an affordable system cost.

While the basic M-XX technology existed at Woollam Co. before the start of this contract, the technology was certainly tested, evolved, and extended throughout this contract. A giant leap in M-XX technology was made with the delivery of the 1st J.A. Woollam Co. M-88 ellipsometer system to NVESD. The M-88 effectively doubles the number of measured wavelengths (from 44 to 88) compared the original M-44 technology.

An number of enhancements were made to the data acquisition capabilities of the WVASE32 software. Most importantly, the ellipsometer calibration and data acquisition algorithms were improved to make them more robust in the MBE growth environment. More specifically, the rotating substrate in the MBE system degraded the signal-to-noise of the ellipsometer signal. To improve the signal integrity during substrate rotation, the ellipsometer electronics' gain switching algorithm was enhanced to compensate for the wide fluctuations in signal intensity during rotation. To improve the robustness of the calibration algorithm, user definable acceptance

limits were added. This prevents unacceptable calibrations from corrupting the current calibration parameters and thereby generating inaccurate ellipsometric data.

Significant advances were made in the real-time analysis capability of the WVASE32 software: the FastDyn layer and the multi-model analysis features (which are used in chapters 5 and 6), were added in part to support the data analysis requirements of this contract. The data selection and visualization capabilities were also revamped to provide more flexibility and improved performance, and to support real-time user interaction during the data acquisition process.

A user-friendly 'push-button' interface suitable for a manufacturing environment, along with ellipsometer-MBE system integration to support feedback control of growth, was provided by the development of the Growth Manager software which is described in Chapter 7. This software underwent many iterations throughout this contract. The final version is highly customizable, and has also been successfully used at other insitu SE installations to monitor III-V semiconductor growth by both MBE and MOVPE technologies.

While the above list of hardware and software developments which were performed on this contract is impressive, a large portion of the time spent on this contract was dedicated analyzing the insitu SE data that was acquired on the NVESD MBE chamber. The successful methods and approaches which were developed in this process (and summarized in this report) represent a major contribution to the work performed on this contract.

2. Ellipsometry Overview

Ellipsometry is a powerful characterization technique which is highly sensitive to layer thickness and composition, and can be performed both insitu and exsitu. In this chapter, a brief overview of ellipsometry is given. Only the basic concepts essential for applying ellipsometry to insitu measurements are provided; for a more in-depth discussion of this topic, please refer to the 'A Short Course in Ellipsometry' chapter in the J.A. Woollam Co. *WVASE32 User's Manual.*

What Spectroscopic Ellipsometry (SE) measures

Measurement Geometry

Ellipsometry measures the *change* in polarization state of light which is reflected off the surface of a sample. The geometry for the ellipsometric measurement is shown in the figure 2.1 below. To perform the ellipsometric measurement, light with a known polarization state (typically linear) is made incident at an oblique angle on the sample to be measured. The reflection of the light from the sample surface changes the polarization state of the beam (to an elliptical polarization state, in general), which is then detected and quantified by the ellipsometer system.

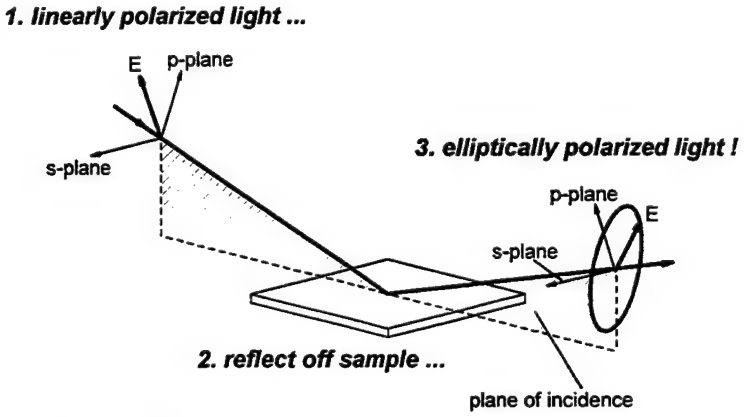

Figure 2.1. Measurement geometry for ellipsometric experiments

The coordinate system for the measurement is defined relative to the plane of incidence. The p- direction is parallel to the plane of incidence, and the s- direction is perpendicular to the plane of incidence. The p- and s- directions are mutually orthogonal to each other and to the direction of the light beam propagtion, thereby forming an orthogonal right-handed coordinate system. Any polarized beam of light which is reflected off the sample can be broken into p- and s- components (since these are the eigenmodes of propagation for the beam of light). At oblique angles of incidence, all materials reflect p- and s- polarized light differently, which is the fundamental reason why ellipsometry works!

The Ellipsometry Equation

Mathematically, the reflection of polarized light from a sample is traditionally described by the ellipsometric equation shown in equation 2.1. In this equation, R_p and R_s are the complex electric field reflection coefficients (also know as the Fresnel coefficients) for p- and s- polarized light respectively; ρ is the complex reflectivity ratio. The parameters Ψ (Psi) and Δ (Delta) are the 'ellipsometric parameters': Ψ is the intensity ratio of p- to s- reflected light, and Δ is the phase difference between p- and s- reflected light.

$$\rho = \frac{R_p}{R_s} = \tan(\Psi) \cdot e^{i \cdot \Delta} \qquad (2.1)$$

Advantages of Ellipsometry

Ellipsometry is related to the technique of reflectance, which measures the absolute intensity of light reflected from a sample (typically at normal angle of incidence). However, ellipsometry has two fundamental advantages over reflectance:

1. Ellipsometry measures a ratio, which makes it much easier to reproducibly perform accurate measurements.
2. Ellipsometry measures a complex number; the 'phase' information from the ellipsometric Δ parameter is extremely surface sensitive.

However, compared to reflectance, ellipsometry does require more complicated instrumentation to perform the measurement. The availability of commercial ellipsometer systems, such as the ones delivered on this contract, negates this potential disadvantage.

Spectroscopic + Ellipsometry = SE

A single Ψ, Δ pair corresponds to an ellipsometric measurement at a single wavelength of light and at a given angle of incidence. From a single Ψ, Δ ellipsometric measurement, at most 2 things can be determined about the sample. Additional information about the sample can be derived by performing ellipsometric measurements at multiple wavelengths. If sufficient wavelengths are used (>10), a 'spectrum' of ellipsometric Ψ, Δ parameters vs. wavelength can be acquired. The term 'Spectroscopic Ellipsometry' (or its acronym 'SE') is used to describe this type of measurement. SE greatly increases the information content of the measurement; however, an SE measurement with 50 wavelengths does not imply that 100 parameters can be uniquely determined about the sample. Subsequent sections in this

chapter will discuss the analysis techniques for extracting sample parameters from the information-rich SE data sets.

Another way of increasing the information content of ellipsometric measurements is to acquire data at multiple angles of incidence. When combined with spectroscopic measurements, this technique is know as Variable Angle Spectroscopic Ellipsometry (or VASE®, which is a registered trademark of the J.A. Woollam Co., Inc.). However, in the insitu environment it is not feasible to perform measurements at multiple angles of incidence. For this reason, the relative merits of variable angle measurements will not be discussed here. Fortunately (from the standpoint of performing insitu measurements), ellipsometric measurements at multiple wavelengths almost always provide more uncorrelated information content than ellipsometric measurements at multiple angles.

Since SE data spectra are plotted vs. wavelength, it is pertinent to list the different units which can be used to specify the wavelength of light: Photon Energy (eV), nanometers (nm), Angstroms (Å), and microns (μm). Assuming a given λ specified in Angstroms, Table 2.1 shows how to convert between the various units. From this table, it is clear that higher Photon Energies correspond to shorter wavelengths. The WVASE32 program allows the user to select the default units of light which will be used to manipulate and display the SE data. For most of this report, units of Photon Energy (eV) are used, as the dielectric function for most semiconductor materials is more appropriately displayed in terms of eV.

To convert from λ in Angstroms:
$nm = 0.1 \cdot \lambda$
$\mu m = 0.0001 \cdot \lambda$
$eV = 12400 / \lambda$

Table 2.1. Conversion formulae for different light units.

Basic Thin Film Optics Equations

Regime of Validity

To successfully interpret SE data, a fundamental understanding of how light interacts with the measurement sample is required. Fortunately, this interaction can be concisely encapsulated by the equations given in this section. The validity of these equations is predicated by the following assumptions (these assumptions also impose a limit to the applicability of the ellipsometric measurement technique):

1. The lateral dimensions of the measurement sample must be much greater than the measurement wavelength of light (for most SE measurements, the wavelength of light lies within the 0.2 - 1.7 μm range). This requirement is not a problem for insitu measurements on unpatterned samples, as the macroscopic dimensions of the sample are essentially infinite compared to the wavelength of light.
2. The surface and/or interfacial roughness of the sample must be much less (< 0.1) than the wavelength of the measurement beam. This requirement basically states that the sample must be specular. If the roughness levels exceed this limit, part of the light beam will be

scattered as opposed to reflected. Scattered light must be described by a completely different formalism, and does not lend itself to simple analytic equations except in some limiting cases. Fortunately, in the case of epitaxial crystal growth, a nearly atomically smooth surface is typically present, such that this requirement is also easily met. (If the crystal surface scatters a significant amount of light, the layer quality is probably very poor and not acceptable for device applications anyway.)

3. The light beam collimation and spectral purity, film thickness, and sample uniformity in the area of the measurement beam must be such that the reflected beam contains a single polarization state. In other words, the sample and/or measurement conditions do not depolarize the light beam. For most insitu measurement conditions, this requirement is also met. While the WVASE analysis software does provide some capability to model these non-idealities, it is certainly more straightforward to analyze the ellipsometric data when this requirement is satisfied.

Optical Constants

The optical properties of the materials strongly influence the interaction of light with the sample. The material optical constants quantify how light propagates through the material. The electronic polarizability of a material (which is related to its band structure, composition, microstructure, etc.) determines its optical constants. Optical constants are usually specified in terms of the complex index of refraction,

$$\tilde{n} = n + i \cdot k \qquad (2.2)$$

or the material dielectric function,

$$\tilde{\varepsilon} = \tilde{n}^2 = \varepsilon_1 + i \cdot \varepsilon_2 \qquad (2.3)$$

The '~' symbol above the variables simply denotes that the value may be complex. The imaginary parts of these quantities ('k' or 'ε_2') are proportional to the optical absorption within the material. The real parts of these quantities are related to the velocity of light when traveling in the material. Throughout this report, the terms 'optical constants' and 'dielectric function' are used interchangeably, as the both describe the same material property (equation 2.3 can be used to convert between the two quantities). Also for simplicity, the complex dielectric function values ε_1 and ε_2 are sometimes referred to as e1 and e2.

When performing *spectroscopic* ellipsometry (SE), it is very important to recognize that the optical constants (or equivalently, the dielectric function) of a given material *vary* as a function of wavelength. This is in contrast to single wavelength ellipsometry, in which one can refer to *the* index of refraction, 'n'. In SE, there are actually many discrete 'n' and 'k' values (or 'e1' and 'e2' values) associated with a given material (one for each wavelength of light in the experimental data set). Figure 2.1b shows the dielectric function spectra for $Hg_{0.8}Cd_{0.2}Te$ at growth temperature. Note the 'bumps' in the e2 spectra near 2.2 and 2.8 eV. These 'bumps' correspond to the E_1 and $E_1+\Delta_1$ interband electronic transitions in the material, and are referred to as 'critical points'. The shape and position of the critical point structures in semiconductor materials are sensitive to the composition and temperature of the materials; this is how SE derives its sensitivity to these sample properties.

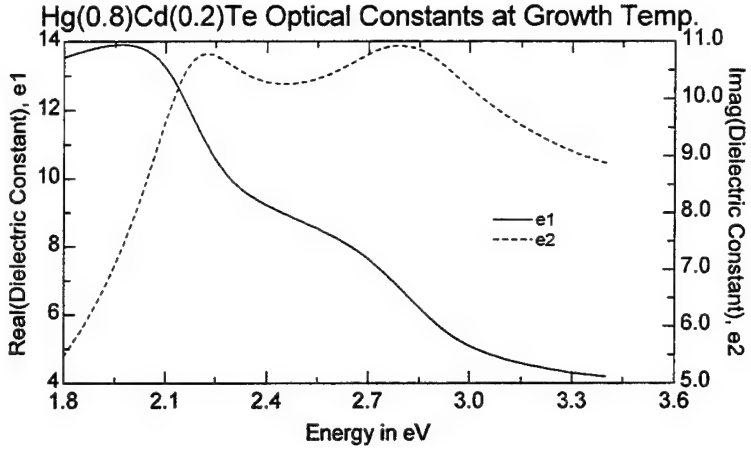

Figure 2.1b. Dielectric function for $Hg_{0.8}Cd_{0.2}Te$ at growth temperature.

'Mixed' Materials: the EMA Approximation

Sometimes it is helpful to model the optical constants of a material consisting of a 'mixture' of different constituents. A number of different electromagnetic theories (which use differing underlying assumptions) can be used to predict the 'effective' optical constants of such a mixture. In practice, most of the underlying assumptions are not rigorously satisfied, and the resulting 'effective' optical constants only approximate the optical behavior of the mixture. Nevertheless, it is still very common to utilize these approximations in the analysis of ellipsometric data. The most commonly used expression is the Bruggeman Effective Medium Approximation (EMA), which is given by (2.4). In this expression, f_a and f_b are the volume fractions of the 2 constituents, ε_a and ε_b are the dielectric constants of the 2 constituents, and ε is the effective dielectric constant of the mixture.

$$f_a \frac{\varepsilon_a - \varepsilon}{\varepsilon_a + 2\varepsilon} + f_b \frac{\varepsilon_b - \varepsilon}{\varepsilon_b + 2\varepsilon} = 0 \qquad (2.4)$$

To ellipsometrically model surface roughness on a given material, a layer consisting of a 50% EMA mixture of the material with 'void' (dielectric constant ≡ 1) is typically employed.

Reflection from a Bulk Substrate

The geometry for the reflection of light from a bulk substrate is shown in Figure 2.2 below. n_0 and n_1 denote the optical constants of the ambient and substrate respectively (the optical constants of the ambient are normally assumed to be 1.0). Φ_0 is the angle of incidence of the incident beam with respect to the sample normal (Φ_0' is the angle of reflection, which is equal to the angle of incidence for a specular reflecting sample). Φ_1 is the angle of refraction, and is given by Snell's law:

$$\tilde{n}_0 \sin\phi_0 = \tilde{n}_1 \sin\tilde{\phi}_1 \qquad (2.5)$$

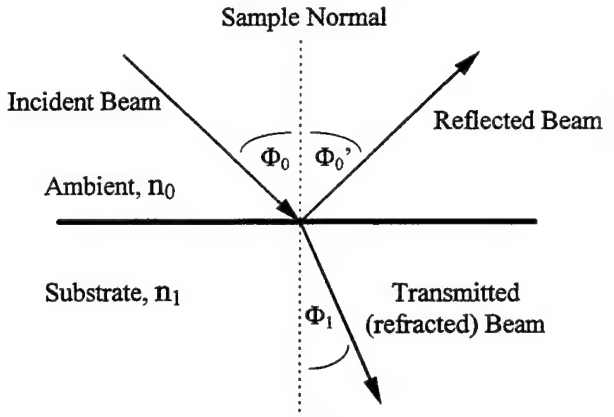

Figure 2.2. Geometry for light reflection from a bulk substrate

Equations (2.6) and (2.7) quantify the reflection of p- and s- polarized light from a bulk substrate. The r_p and r_s parameters are known as the Fresnel reflection coefficients. These equations can also be used to calculate the reflectivity at any material interface, e.g. between a film and substrate, by simply using the appropriate optical constants and renaming the subscripts as appropriate.

$$\tilde{r}_p = \frac{\tilde{n}_1 \cos\phi_0 - \tilde{n}_0 \cos\tilde{\phi}_1}{\tilde{n}_1 \cos\phi_0 + \tilde{n}_0 \cos\tilde{\phi}_1} \qquad (2.6)$$

$$\tilde{r}_s = \frac{\tilde{n}_0 \cos\phi_0 - \tilde{n}_1 \cos\tilde{\phi}_1}{\tilde{n}_0 \cos\phi_0 + \tilde{n}_1 \cos\tilde{\phi}_1} \qquad (2.7)$$

The 'pseudo' dielectric function, <ε>

Substituting equations (2.6) and (2.7) into the ellipsometric equation (2.1), it is easy to see how the ellipsometric parameters Ψ and Δ can be calculated for a bulk substrate (assuming that the substrate optical constants and angle of incidence are known). In this case, it is also possible to invert equation 2.1 to obtain the substrate optical constants as a function of the ellipsometric parameters and the angle of incidence:

$$\langle\varepsilon\rangle = \langle\varepsilon_1\rangle + i\cdot\langle\varepsilon_2\rangle = \sin^2\Phi_0 \cdot \left(1 + \tan^2\Phi_0 \cdot \frac{1-\tan\Psi\cdot e^{i\cdot\Delta}}{1+\tan\Psi\cdot e^{i\cdot\Delta}}\right) \qquad (2.8)$$

<ε> is denoted the 'pseudo' dielectric function of the material, as it is the dielectric function of the material *assuming* that the sample can be optically represented as a bulk substrate, and that the angle of incidence is accurately known. If these assumptions are true, then the 'pseudo' dielectric function may actually equal the true dielectric function of the material. This is one of the few cases where the ellipsometric Ψ and Δ parameters can be directly inverted to extract information about the sample.

Reflection from a Thin Film Layer

The reflection of light from a thin film layer on top of a substrate can also be analytically described. Figure 2.3 shows the geometry used for this calculation: n_0,

n_1, and n_2 are the optical constants of the ambient, film, and substrate respectively. The film thickness is given by the parameter 'd'. Inside the film, the light beam actually undergoes multiple reflections between the ambient-film and film-substrate interfaces. However, as long as the film thickness is thin enough to maintain beam coherence, the multiple beams constructively and/or destructively combine into a single coherent reflected beam.

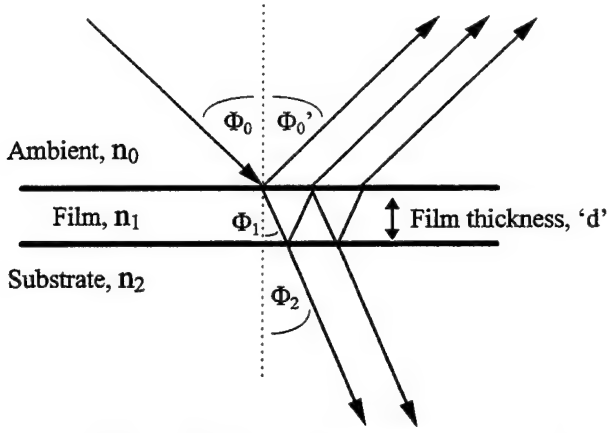

Figure 2.3. Geometry for light reflection from a thin film on a substrate

Using equations (2.9) and (2.10), it is possible to analytically calculate the reflectance of light from a thin film layer on a substrate. These equations are valid for both p- and s- polarized light. r_{01} denotes the reflectivity of the ambient-film interface, r_{12} and denotes the reflectivity of the film-substrate interface; these values are calculated using the Fresnel equations given by (2.6) and (2.7), evaluated with the appropriate optical constants. The 'β' parameter is known as the phase propagation constant, and defines the 'optical' thickness of the film.

$$r = \frac{\tilde{r}_{01} + \tilde{r}_{12} e^{-i2\beta}}{1 + \tilde{r}_{01}\tilde{r}_{12} e^{-i2\beta}} \qquad (2.9)$$

$$\text{where } \beta = 2\pi\tilde{n}_1 \frac{d}{\lambda}\cos\tilde{\phi}_1 = 2\pi\frac{d}{\lambda}\sqrt{\tilde{n}_1^2 - n_0^2 \sin^2\phi_0} \qquad (2.10)$$

Calculating Ψ and Δ for an Arbitrary Film Stack

To calculate the ellipsometric Ψ and Δ parameters from a more complicated multiple layer film stack, it is possible to iteratively evaluate equation (2.9) for each layer, starting at the substrate and appropriately renaming the subscripts for subsequent layers. On the surface, it may seem that this calculation is rather trivial. In practice, however, this calculation is rather intensive, as (2.9) relies on (2.10), (2.5), (2.6), and (2.7), all of which require complex arithmetic. Furthermore, this calculation must be repeated for both p- and s- polarized light, and the results inserted into (2.1) to provide the final Ψ and Δ values. For SE data, this must also be performed for each measured wavelength. While it is not tractable to write down the complete analytic expression for the ellipsometric calculation of an arbitrary film stack, it can be readily handled by the current generation of high speed digital computers. The WVASE32 analysis software supplied with the J.A. Woollam Co. ellipsometer systems uses highly optimized C++ and assembly language routines to evaluate these equations in the most efficient manner possible.

Analysis of SE data

The Data Analysis Flowchart

Analyzing spectroscopic ellipsometry (SE) data is not a trivial task. Like many other characterization techniques, SE provides only an indirect measure of the desired sample properties. In other words, SE measures Ψ and Δ parameters, but what is really desired are the sample parameters such as layer thickness, composition, temperature, etc. To extract these parameters from the 'raw' SE data, a data modeling procedure using the optics equations described in the previous section is employed. Schematically, this is represented in figure 2.4 below.

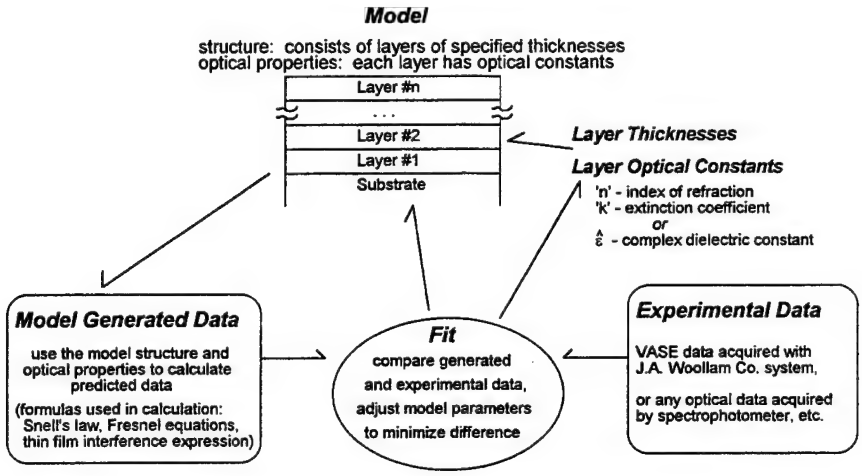

Figure 2.4. Flowchart of the data analysis procedure for an ellipsometric experiment.

The procedure starts with the specification of an optical Model, consisting of a substrate on which 'n' discrete layers with differing optical constants and thicknesses are placed. Ideally, the optical model should correspond with the actual physical structure of the sample. The next step is the generate 'predicted' ellipsometric data from the model, using the thin film optics equations from the previous section. This generated ellipsometric data is then compared with the measured experimental ellipsometric data. If generated and experimental data are not in *agreement*, the data Fit algorithm will iterative adjust the model parameters (such as layer thicknesses and composition) to improve the agreement between the model generated and experimental data.

Fitting the Data, or Minimizing the MSE

The key concept in the data analysis flowchart previously described is that the model is adjusted to improve the *agreement* between the model generated data and the experimentally measured data. To implement such an approach, it is necessary to quantify what constitutes a good *agreement* between the generated and experimental data. One objective measure of the goodness of fit is the Mean Squared Error parameter defined in (2.11). (Actually, this equation defines the Root Mean Squared Error, but for historical reasons the term MSE is still used.) This parameter is also related to the chi-square (χ^2), which is another maximum likelihood estimator that is commonly used in the statistical analysis of data.

$$MSE^2 = \frac{1}{2N-M}\sum_{i=1}^{N}\left[\left(\frac{\psi_i^{mod}-\psi_i^{exp}}{\sigma_{\psi,i}^{exp}}\right)^2+\left(\frac{\Delta_i^{mod}-\Delta_i^{exp}}{\sigma_{\Delta,i}^{exp}}\right)^2\right]=\frac{1}{2N-M}\chi^2 \qquad (2.11)$$

In (2.11), 'N' is the number of ellipsometric data points, 'M' is the number of adjustable model fitting parameters, the 'mod' and 'exp' superscripts denote the model generated and experimentally measured ellipsometric data respectively, and the 'σ' values represent the standard deviations of the experimentally measured ellipsometric data. A smaller MSE corresponds to a better 'fit' or agreement between the model generated and experimental ellipsometric data.

The Levenberg-Marquardt (L-M) Algorithm

To minimize the MSE, the Levenberg-Marquardt (L-M) algorithm is employed to iteratively adjust the model fitting parameters. The details of this algorithm are beyond the scope of this report. However, it is sufficient to say that this algorithm is extremely efficient at finding the best model which fits the experimental data, as long as the following conditions are met:

1. The starting model is reasonably close to the best fit solution. The L-M algorithm only performs a local optimization, and does not search the global fit parameter space. In general, this is not a fundamental limitation, as in most insitu applications, the crystal grower knows the nominal growth rates and compositions which can be input as model parameter starting values.
2. A unique best fit model exists. In some cases, there may be many different models which all provide an equivalent fit to the experimental data; this phenomena is know as parameter *correlation*, i.e., multiple parameter sets provide the same solution. In this circumstance, the L-M algorithm can not objectively select the best fit model. The only ways to break the parameter correlation problem are to add more information to the analysis (additional ellipsometric data), or to simplify the model by reducing the number of fitting parameters. The best way to determine if correlation is present in a given model is to restart the fit with different initial starting values for the parameters. If the model does not converge to the same final solution, parameter correlation is present.

Determining when a Fit is 'Acceptable'

When is a fit 'good enough', i.e., when is the MSE 'low enough'? This is a difficult question to answer in general. Unfortunately, it is not possible to numerically define what an acceptable MSE value is, as it depends on the type and signal-to-noise of the data which is being analyzed and the complexity of the model (for some analysis, an MSE of 5 might be considered acceptable, while for other analysis, MSE's less than 1 are expected). Certainly, the more complicated the model is (and the more fitting parameters which are defined) the better the data fit should be. However, overly complicated models tend to have parameter correlation which can dramatically skew the analysis results. The best strategy is to start with the simplest model which adequately fits the ellipsometric data, and then to incrementally add complexity to the model until no significant improvements are seen in the MSE. For example, if adding another fit parameter to the current model lowers the MSE by 1%, the additional model complexity is not justified. On the other hand, if adding a surface roughness layer to the model reduces the MSE by a factor of 2, then it is reasonable to conclude that the roughness layer should be included in the model.

There is still a fair amount of art and subjectivity that goes into the model dependent analysis of SE data. One of the goals of report is to document the data analysis experience gained during this contract and thereby provide some guidelines and strategies for the analysis of SE data acquired during the MBE growth of HgCdTe. Most of this experience is also directly applicable to the ellipsometric monitoring of epitaxial semiconductor growth in general.

Accuracy of Ellipsometrically Determined Parameters

Once an appropriate model has been constructed and fit to the experimental ellipsometric data, it is reasonable to ask how accurate are the parameters which are extracted from the analysis. Once again, this is a difficult question to answer, due to the indirect nature of the ellipsometric data analysis procedure. To ultimately answer this question, it is necessary to perform some independent characterization technique to confirm the ellipsometric results. For example, ellipsometrically determined layer composition values could be verified by X-Ray diffraction or FTIR analysis.

A *relative* indicator of ellipsometric parameter accuracy is found by looking at the 90% parameter confidence limits which are returned for each fit parameter from the L-M algorithm. The statistical formulas which are used to calculate these limits assume that the only source of discrepancies between the model generated data and the experimental data is *random* noise with a Gaussian profile. This assumption is rarely the case in ellipsometric data analysis (normally *systematic* errors dominate the fit discrepancies). For this reason, it is not appropriate to consider the 90% parameter confidence limits as absolute parameter error bars. However, it is still useful to consider these limits as 'error bars' in a loose and relative sense. For example, if the ellipsometric analysis reports a thickness to be 12.32±20.43 Å, it is clear that the ellipsometric data does not have much sensitivity to this thickness. On the other hand, if a thickness resulting from an SE data analysis is reported to be 12.32±0.13 Å, it does not imply that the ellipsometer can accurately measure thicknesses down to a tenth of an Angstrom accuracy, only that the ellipsometric data is quite sensitive to this parameter.

Another way of looking at the 90% confidence limits is that they give a reasonable indication of the reproducibility of the ellipsometric measurement and analysis process. That is, if you were to measure a sample multiple times and perform the same model analysis, the resulting distribution of a given fit parameter vs. measurement number would approximately lie within the parameter's 90% confidence limits.

Performing SE Data Analysis with WVASE32

Most of the information presented in this chapter has been rather theoretical in nature. In practice, the WVASE32 software (shown in figure 2.5) which is supplied with the J.A. Woollam Co. ellipsometer systems takes care of all of the low level issues associated with SE data analysis. For an introduction to the installation, basic navigation, and use of WVASE32, please refer to the *WVASE32 User's Manual.*

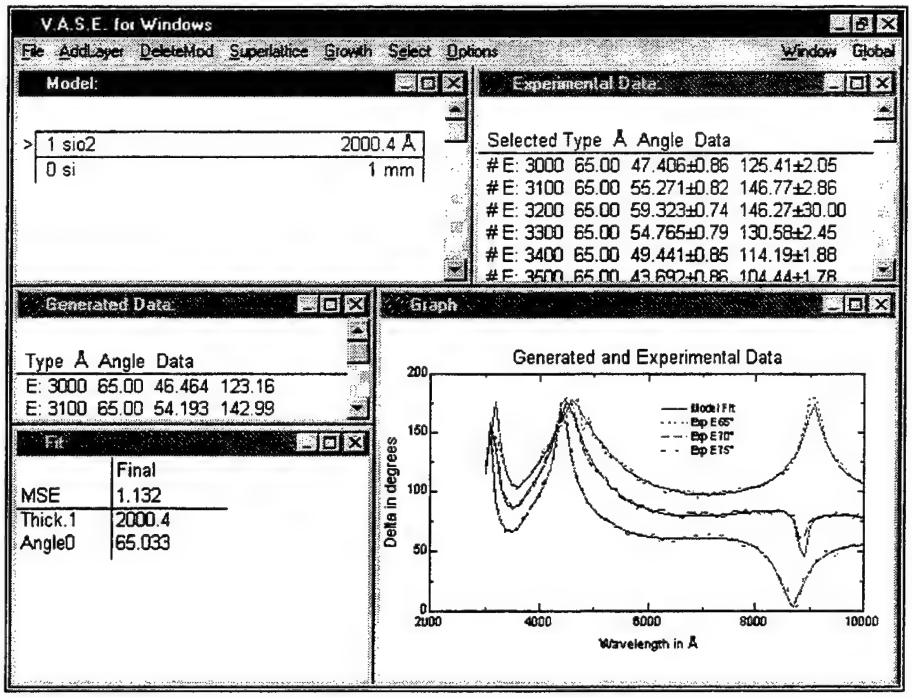

Figure 2.5. Screen dump of the J.A. Woollam Co. WVASE32 Analysis Software

Hopefully, the theoretical background in this chapter will provide the reader with an understanding and appreciation of what goes on inside the WVASE32 software. To utilize the WVASE32 software to its full potential, it is still necessary to have an intuitive understanding of the concepts presented in this chapter. The steps below summarize the general WVASE32 SE data analysis procedure. The actual implementation details of each step will be illustrated in the SE data analysis examples which are presented throughout this report.

1. In the WVASE32 'Experimental' Window, select the experimental ellipsometric data to be analyzed. It may be desirable to include only a specific spectral or time range of ellipsometric data in the analysis.
2. In the WVASE32 'Model' Window, build an appropriate optical model to represent the sample. Initialize the model parameters such as layer thicknesses and compositions to reasonable starting values. Define which model parameters will be adjustable during the fitting process.
3. In the WVASE32 'Generated Data' Window, generate ellipsometric data from the Model defined in step 2. Verify that the generated and experimental data are in reasonable agreement by visualizing the data in the WVASE32 'Graph' Window. If the data are not in agreement, return to step 2.
4. In the WVASE32 'Fit' Window, initiate a data fit. WVASE32 will use the L-M algorithm to iteratively adjust the model fitting parameters.
5. Evaluate the results of the data fit. This can be done by visualizing the data fit in the 'Graph' Window, observing the final MSE in the 'Fit' Window, and viewing the Fit Statistics (90% confidence limits and parameter correlation matrix) in the 'Fit' Window. It is this part of the analysis procedure that is the most subjective. To further optimize the fit, repeat the analysis procedure, possibly modifying the selected experimental data range, model, and/or defined fit parameters.

3. Ellipsometer Hardware

There are a variety of different optical configurations which can be used to acquire ellipsometric data. A brief review of these different configurations can be found in the 'Ellipsometer principles and configurations' section of the *WVASE32 User's Manual*. In this chapter, the focus is on the RAE configuration, and more specifically, the implementation of this configuration embodied in the J.A. Woollam Co. M-XX line of ellipsometer systems.

The Rotating Analyzer Ellipsometer (RAE) configuration

Description and Advantages

In the RAE configuration, the light beam path is as follows:

Light Source ⇒ Input Polarizer ⇒ Sample ⇒ Rotating Analyzer ⇒ Detector.

The Input Polarizer sets the polarization state of the light incident on the sample. The Rotating Analyzer is used to measure the polarization state of the light reflected from the sample. This unit consists of a polarizer element which is mechanically rotated in a continuos manner. Since the speed of the mechanical rotation is in the 10-60 Hz range, this imposes a limit on the measurement speed of the instrument. However, with M-XX technology this seeming limitation on measurement speed actually becomes an advantage, as it allows the detector unit (which converts light intensity into an electrical signal) to simultaneously acquire ellipsometric data at multiple wavelengths during a single analyzer rotation period.

The Rotating Analyzer Ellipsometer (RAE) configuration is one of the simplest ellipsometer configurations: it is constructed with only two polarizers elements (a polarizer and an analyzer). The are several advantages to using only polarizers as optical elements in an ellipsometer system:

- Polarizers can be made with nearly ideal optical behavior.
- Polarizers are achromatic over wide spectral ranges.
- Polarizers are relatively inexpensive optical elements.
- Polarizers are relatively easy to align within a system.

There is, however, one main disadvantage to the RAE configuration:

- Sensitivity is lost when the ellipsometric Δ parameter is near 0° or 180°.

This disadvantage is not a serious problem when acquiring ellipsometric data on HgCdTe or most semiconductor materials, as the optical absorption of these materials in the measured visible spectrum is high enough to keep Δ away from the less sensitive regions near 0° or 180°

How an RAE Measures Ellipsometric Data

The following examples show the detector signal for different polarization states of light after passing through a rotating analyzer. Three different input polarization states of light are considered: linear, circular, and elliptical.

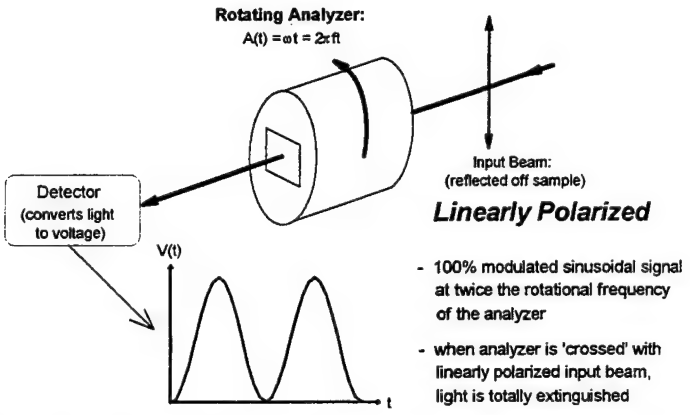

Figure 3.1. Detector signal for a linearly polarized beam entering the rotating analyzer polarization detector.

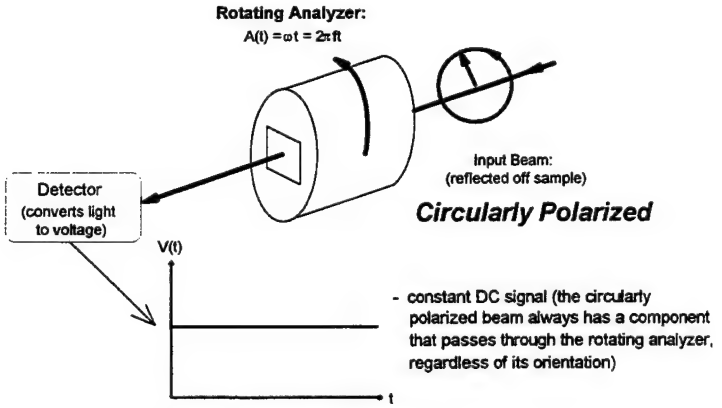

Figure 3.2. The detector signal associated with a (right or left) circularly polarized beam entering the rotating analyzer polarization detector.

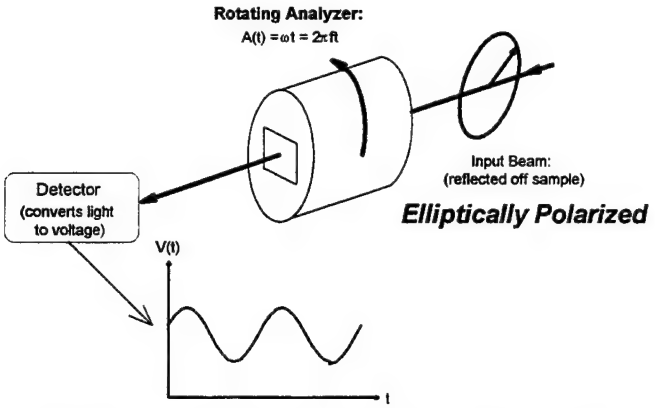

Figure 3.3. The detector signal associated with an arbitrarily elliptically polarized beam entering the rotating analyzer polarization detector.

For a general elliptical polarization state, the detected signal is a sinusoid with a DC offset of the form:

$$V(t) = DC + a\cos(2\omega t) + b\sin(2\omega t). \qquad (3.1)$$

The two important quantities measured by an RAE are α and β, which are the normalized Fourier coefficients of the detector signal. They can be represented in terms of the Ψ and Δ values for the sample and the input polarizer azimuthal angle as follows:

$$\alpha = \frac{a}{DC} = \frac{\tan^2\Psi - \tan^2 P}{\tan^2\Psi + \tan^2 P} \qquad (3.2)$$

$$\beta = \frac{b}{DC} = \frac{2\tan\Psi\cos\Delta\tan P}{\tan^2\Psi + \tan^2 P} \qquad (3.3)$$

This result is obtained from a Jones matrix analysis of the RAE optical system, which can be found in the *WVASE32 User's Manual*. Ψ and Δ are the ellipsometric parameters that characterize the sample, and P is the input polarizer azimuth with respect to the plane of incidence. (P = 0° is in the plane of incidence.) The above equations may be inverted to obtain Ψ and Δ from the measured α and β and the known P.

$$\tan\Psi = \sqrt{\frac{1+\alpha}{1-\alpha}}\cdot|\tan P| \qquad (3.4)$$

$$\cos\Delta = \frac{\beta}{\sqrt{1-\alpha^2}}\cdot\frac{\tan P}{|\tan P|} \qquad (3.5)$$

These equations form the basis of the ellipsometric measurement with the rotating analyzer ellipsometer (RAE). To summarize, the detector signal is measured as a function of time, the measured signal is Fourier analyzed to obtain the Fourier coefficients α and β, and finally Ψ and Δ are calculated from α and β and the known azimuthal angle of the input polarizer, using (3.4) and (3.5).

M-XX: Multi-Wavelength RAE Technology

Optics Configuration

The patented M-XX technology is a multi-wavelength extension to the standard Rotating Analyzer Ellipsometer configuration. There are two members of the J.A. Woollam Co. M-XX family of ellipsometer systems: the M-44 and the M-88, which simultaneously measure ellipsometric data at 44 and 88 wavelengths respectively. The key elements of this technology are shown in Figure 3.4.

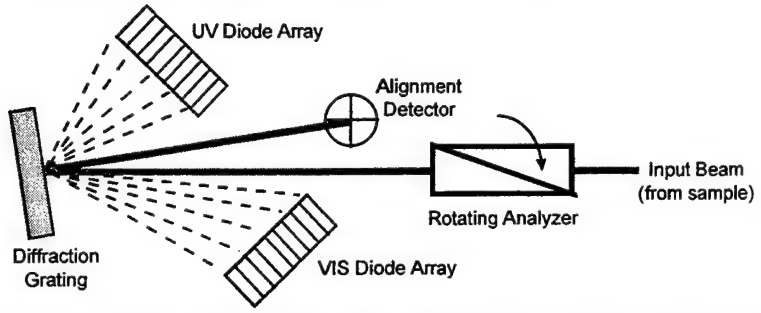

Figure 3.4. Schematic of an M-88 RAE system (the M-44 uses only the VIS diode array)

The collimated beam of light which is reflected from the sample passes through the Rotating Analyzer, and directly to the diffraction grating, without any of the focusing optics which are used in a traditional monochromator system. The light is then diffracted by the grating onto the 46-element (only 44 of the elements are used) photo-diode array(s), again without any additional focusing optics. The simplicity of this design makes for a low cost, easy to manufacture system. The Alignment Detector, which monitors the position of the specular (zero order) reflection from the diffraction grating, is used to align the optics of the M-XX detector unit with respect to the input beam, thereby verifying the wavelength calibration of the instrument.

To calibrate the wavelengths of each diode element, a monochromator is scanned across the spectral range of the instrument, and the detected intensity at each channel is recorded vs. input wavelength. Figure 3.5 shows the results of a typical wavelength calibration scan for an M-44 system. This procedure is performed at the factory for each M-XX system, and does not have to be repeated under normal operating conditions. Inside the detector assembly, the diode array is tilted to achieve a uniform angular dispersion of about 7 nm/mm. The average bandwidth of each detector is about 10 nm, which can be modeled (if necessary) by the WVASE32 data analysis software.

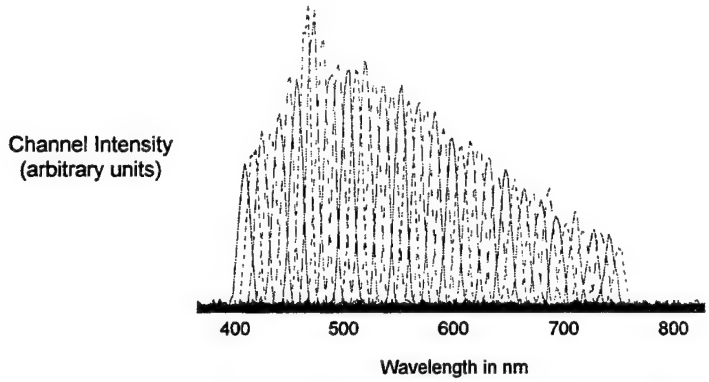

Figure 3.5. Typical wavelength calibration spectra for an M-44 system.

Diode Array Electronics

Many spectroscopic diode array based instruments use CCD technology to read out the light from the individual diodes. While this technology is readily available and very scaleable (CCD diode arrays with more than 2048 elements are commercially available), there are some major disadvantages to using CCD read out technology in an ellipsometer. These limitations are discussed in the literature by R.W. Collins, and include: image persistence, non-linearity, stray light, and limited scanning speed. To overcome these limitations, a *linear* photo diode array, along with custom read out electronics, are used in the M-XX technology (Figure 3.6). These electronics allow high speed scanning of the photo diode array: it is scanned 28 times during each revolution of the rotating analyzer (which continuously rotates at 25 Hz in an M-44 instrument). The individual op amps on each diode ensure excellent channel isolation and linearity, such that the detected signal at each wavelength does not require any correction factors to compensate for signal read out anomalies (as is the case with the CCD-based ellipsometer systems built by Collins et. al.).

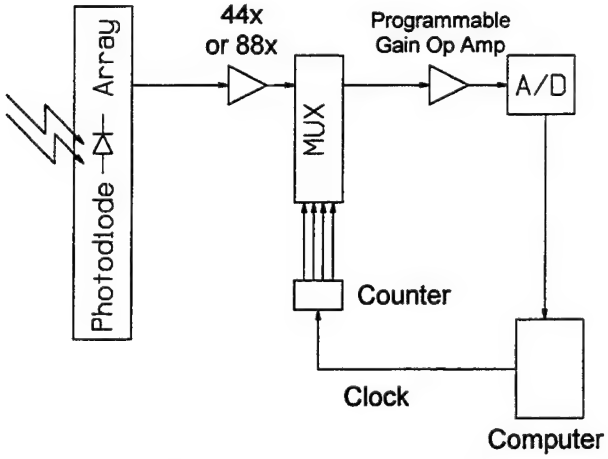

Figure 3.6. M-XX detector read-out electronics.

System Components

The basic components of an M-XX system are shown in Figure 3.7. In this figure, the system is shown mounted on an exsitu multi-angle base. This configuration is

useful for testing the system and performing the system calibrations which will be described in the next section. Each component of the ellipsometer system will now be individually described.

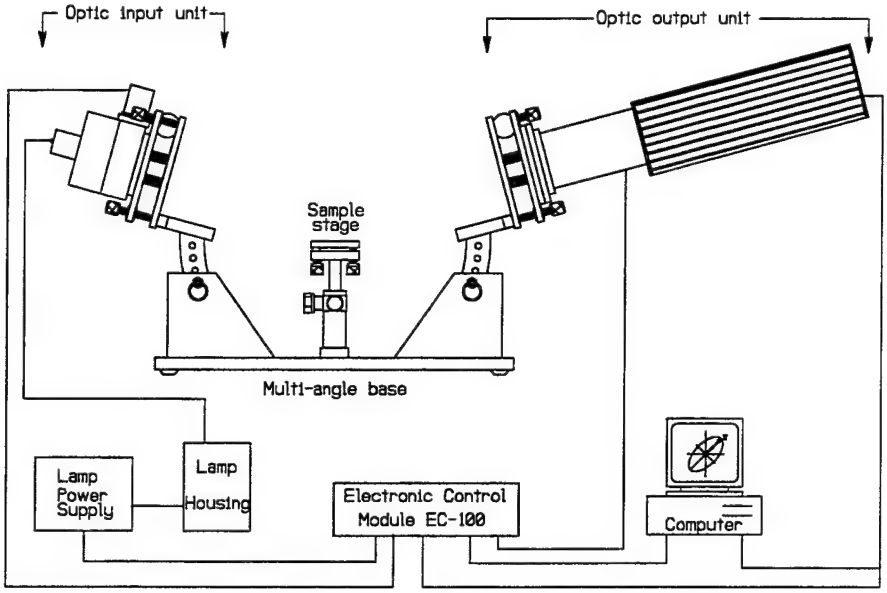

Figure 3.7: Block diagram of M-XX system on a "bench top" base.

Light Source

The purpose of the light source is to provide a high intensity, stable source of white light for the ellipsometric measurement. The light source consists of: a 75W xenon short arc lamp, a focusing mirror, and a light shutter unit (in more recent production versions of the instrument, the shutter has been moved into the 'optic input unit'). The lamp is mounted vertically in the lamp housing. The focusing mirror is used to focus the broad band white light from the lamp into a fiber optic connector. An electronic shutter is used to block and unblock the light during the system calibration procedure. A power supply with an initial 20 kV arc is used to trigger the Xenon lamp, and to apply regulated DC power to the lamp after its ignition.

Optic input unit

This unit consists of a collimating lens, a polarizer and a tilt stage. An optic fiber couples light from the light source into the collimating lens assembly of the optic input unit. The lens couples the light from the fiber into a uniform and collimated beam. The prism polarizer transforms the incident unpolarized light into linearly polarized light. The polarizer is mounted on a high-accuracy rotational stage (with a typical accuracy of ±0.01° and precision of 0.005°), to enable accurate setting of the input polarization state with respect to the sample. It is driven by a microstepping drive unit located in the electronics control module EC-100. A tilt stage is provided to tilt the optic input unit during system alignment. A pin actuated iris diaphragm is provided to adjust the size of the beam.

Optic output unit

The optic output unit consists of: a second prism polarizer called the analyzer, a continuously rotating stepper motor, a diffraction grating, a silicon photodiode array(s), and a four-quadrant alignment detector. The prism polarizer is mounted in

a hollow shaft within the stepper motor. The stepper motor is driven by a stepper drive unit located in the electronics control module. The alignment detector is a four quadrant detector used for aligning the light beam falling on the grating. A schematic layout of the optic output unit is shown in Figure 3.4.

System Specifications

	M-44	M-88
Spectral Range in nm	415 - 750	280 - 760
Number of channels	44	88
Average channel bandwidth	10	8
Maximum data acquisition rate, in Hz (for complete spectra)	24.8	21.7
Typical data acquisition rate, in Hz	.25 - 2	.25 - 2
Typical Psi repeatability	to 0.015°	to 0.015°
Typical Delta repeatability	to 0.08°	to 0.08°

Calibration of the M-XX Ellipsometer System

Accurate ellipsometer system calibration is paramount to acquiring high quality ellipsometric data. This section provides the conceptual background necessary to understand the various M-XX ellipsometer calibration procedures. In practice, the WVASE32 software automates the calibration procedures which are required for the M-XX ellipsometer systems. Please refer to the *WVASE32 User's Manual* for a hands on discussion of how to perform these calibration procedures.

System (Straight-Through) Calibration

The M-XX optics configuration does introduce one non-ideality into the ellipsometer system: the reflectivity of the diffraction grating which is positioned behind the rotating analyzer element depends on the polarization state of the light incident on the grating. This effect is known as polarization dependent sensitivity (PDS). Since the analyzer element is continuously rotating, the PDS of the grating imposes an additional modulation on the detector signal. To minimize the effect of PDS on the ellipsometer signal, M-XX systems have a retarder inserted into the beam path after the rotating analyzer (this is also part of the patented M-XX technology). While this retarder minimizes the effect of the PDS (by converting the linearly polarized light from the rotating analyzer into elliptically polarized light), it does not completely eliminate it.

Fortunately, the literature (S.H. Russev, *Appl. Opt.*, 28 (1989) 1504) provides an analytical model for this effect, such that an exact correction can be made to the ellipsometric data. Equation (3.6) quantifies the effect of the PDS on the α and β parameters measured by a RAE. In this equation, α' and β' are the experimentally measured values of the normalized Fourier coefficients which include the PDS effect. The PDS is described by the x_p and f_d parameters, which quantify the magnitude and azimuthal orientation (with respect to the sample plane of incidence) of the PDS. For example, if x_p=0 no PDS is present, and if x_p=1 the grating is actually acting like a

polarizer element. If the PDS parameters x_p and f_d are known, (3.6) can be used to calculate the 'ideal' α and β values which can be directly substituted into (3.4) and (3.5) to obtain accurate ellipsometric Ψ and Δ parameters.

$$\alpha = \frac{\alpha' - x_p \cdot \cos 2f_d}{1 - 0.5 \cdot x_p \cdot (\alpha' \cos 2f_d + \beta' \sin 2f_d)}$$
$$\beta = \frac{\beta' - x_p \cdot \sin 2f_d}{1 - 0.5 \cdot x_p \cdot (\alpha' \cos 2f_d + \beta' \sin 2f_d)} \qquad (3.6)$$

To determine the PDS parameters for an M-XX system, a straight-through 'system' calibration procedure is performed. In the straight-through configuration, the optics input unit is pointed directly into the optics output unit, such that no sample is present in the beam path. (The ellipsometric parameters for 'air' are definitely known and constant, Ψ=45° and Δ=0°, which greatly simplify the system calibration process.) To perform this type of calibration, it is necessary to remove the ellipsometer system from the vacuum chamber, and install it on the exsitu base.

In addition to extracting the PDS parameters, the straight-through calibration procedure also determines the electronic attenuation and phase offset for each detector channel, which characterize the AC-DC transfer functions of the op amps on each individual channel.

When the 'Straight-Through' Calibration option is selected in WVASE32, the program will move the input polarizer to a range of different azimuthal settings, and acquire normalized Fourier coefficient data α and β at each polarizer setting. To extract the calibration parameters from the measured $\alpha(P)$ and $\beta(P)$ data, a model-based regression analysis of the data is performed for each channel. The model basically consists of equations (3.2) and (3.3), and the 'inverse' of equations (3.6). (This technique is analogous to the SE data analysis procedure given in Chapter 2, and is described in further detail in "Regression calibration method for rotating element ellipsometers," B. Johs, Thin Solid Films, **234**, 395-398 (1993).) A typical data fit for straight-through calibration data is shown in Figure 3.8 (the 'Residual' function plotted on the graph is defined as $1-\alpha^2-\beta^2$). Note that the model fit data, which is represented by the dashed curves, lie directly on top of the experimentally measured $\alpha(P)$ and $\beta(P)$ curves, demonstrating that the signal-to-noise of the detector signal is excellent, and that the optical behavior of the ellipsometer system is accurately described by the equations given in this chapter.

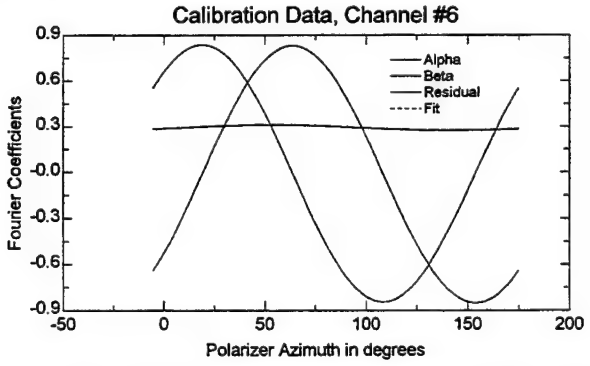

Figure 3.8. Typical Straight-Through calibration data fit for a M-44 system

Figures 3.9 - 3.12 show the calibration parameters which are determined by the straight-through calibration procedure (these graphs are from an M-44 system; the

calibration graphs from an M-88 contain the same information, but may have slightly different shapes). The PDS parameters are reported in 'rectangular' coordinates, that is: $X_c = x_p \cdot \cos(2 \cdot f_d)$ and $X_s = x_p \cdot \sin(2 \cdot f_d)$. Each calibration parameter is independently determined at each channel. This information is stored into a disk file (C:\WVASE32\MXX-CAL.CNF), and is used for all subsequent ellipsometer calibrations and data acquisition.

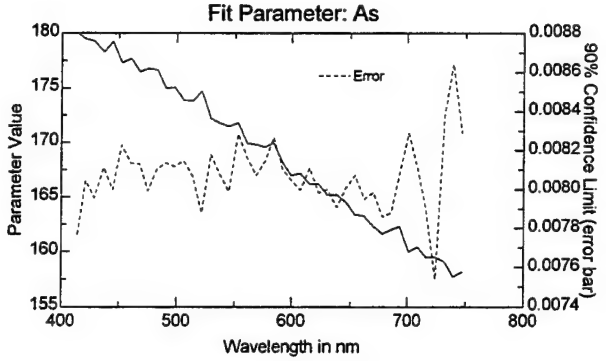

Figure 3.9. Channel 'Phase' parameters from straight-through calibration

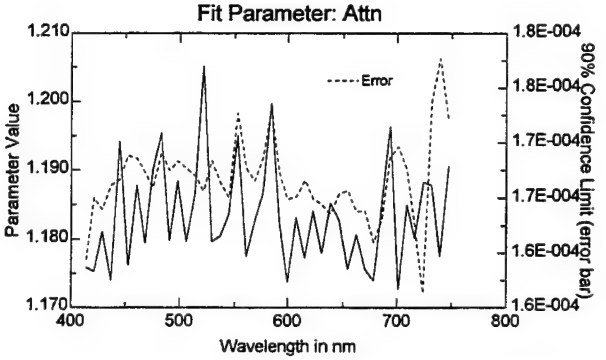

Figure 3.10. Channel 'Attenuation' parameters from straight-through calibration

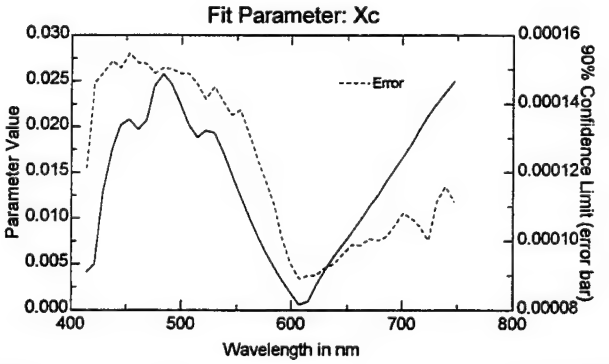

Figure 3.11. 'X_c' PDS parameters from straight-through calibration

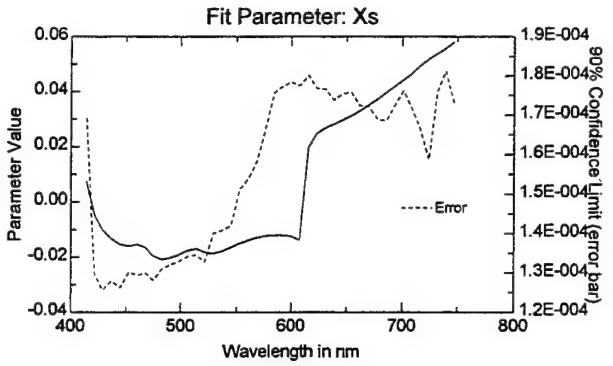

Figure 3.12. 'X_s' PDS parameters from straight-through calibration

Important Notes about System Calibration

In theory, the system calibration procedure should only have to be performed once for a given M-XX system. However, in practice, some changes in the system calibration constants have been observed over time. Due to the intermittent nature of these changes, and the fact that they typically occur over long periods of time (more than a few months), it is difficult to reproduce and study the cause of these drifts. It may be appropriate to perform the system calibration procedure at regular intervals (for example, once a month) or whenever the quality of the normal calibration fits begin to degrade.

Coarse Calibration

After a successful system calibration, the ellipsometer system can be remounted and aligned (see Chapter 4) on the vacuum chamber. The next type of ellipsometer calibration that needs to be performed is 'Coarse Calibration'. In this calibration, the calibration parameters to be determined are the azimuthal orientation of the ellipsometer's optical elements with respect to the sample's plane of incidence. These calibration parameters are given the following designations:

- $\mathbf{P_s}$ (angular offset of the input polarizer)
- $\mathbf{A_s}$ (angular offset of the rotating analyzer)
- $\mathbf{F_d}$ (angular offset of the detector box PDS)

Calibration data are acquired in a manner similar to the system calibration, that is, $\alpha(P)$ and $\beta(P)$ are collected over a range of input polarizer settings. Since the software has no prior knowledge about the angular orientation of the optical elements with respect to the sample plane of incidence (the user can mount the input and output optics in any orientation), it is necessary for the software to perform a 'global' search of the parameter space. As multiple branches exist in the global parameter space for the Ψ and P_s parameters ($\Psi'=90°-\Psi$ and $P_s'=90°+P_s$ correspond to equivalent solutions), it is necessary for the coarse calibration algorithm to *assume* that $\Psi<45°$ in order to get the correct P_s value. This assumption easily satisfied as long as the sample used for the coarse calibration procedure is 'bulk-like', i.e., a substrate with no (or a very thin) film overlayer. Again, a regression analysis is used to fit the calibration data; typical results of such a fit are shown in Figure 3.13. If the 90% confidence limits of the three calibration parameters (P_s, A_s, and F_d) extracted from the coarse calibration fit are within the acceptable limits defined in the WVASE32 program, the program will save the values into the calibration file (C:\WVASE32\MXX-CAL.CNF) for subsequent use.

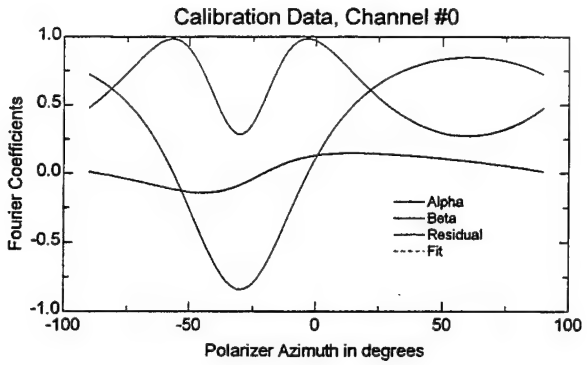

Figure 3.13. Typical Coarse Calibration data fit

When to Perform a Coarse Calibration

The Coarse Calibration procedure must be performed each time the ellipsometer system is re-mounted on a chamber or the exsitu base. This is because the calibration angles of the optics with respect to the sample change when the instrument is mounted in a different setting. It should not be necessary to run the Coarse Calibration procedure in the day to day operation of the instrument (running a Coarse Calibration followed by a Normal Calibration does not improve the overall calibration accuracy of the instrument). However, if for some reason the Normal Calibration fails (sometimes an unexpected computer 'lockup' can cause the reference angles for the optics to become corrupted, thereby invalidating the current calibration angles), it may be necessary to perform another Coarse Calibration before attempting the Normal Calibration procedure again.

Normal Calibration

The Normal Calibration procedure must be used in the day to day operation of the ellipsometer. Each time the WVASE32 program is started and/or the ellipsometer hardware is reinitialized, it is necessary to perform the Normal Calibration procedure. This is because the angular offset of the rotating analyzer element (that is, the A_s calibration parameter) randomly depends on the initial motor position when the hardware is initialized (there is no reference position sensor on the rotating analyzer motor shaft). In the insitu environment, it is also important to perform a Normal Calibration each time a sample is loaded into the chamber, as the reproducibility of most sample manipulators does not come close to the ±0.01° accuracy desired for the calibration angles of the optical elements with respect to the sample plane of incidence.

The Normal Calibration procedure is very similar to the Coarse Calibration procedure in that the same three calibration parameters are determined: P_s, A_s, and F_d. However, with Normal Calibration, it is assumed that the previous P_s and F_d calibration values are very close to the current values, such that a global search of parameter space is not required (it is still necessary to globally search for the A_s parameter, but this is much easier as there are no ambiguities for A_s in the solution space). Since good starting values for the P_s and F_d calibration parameters are known, the Normal Calibration procedure typically uses fewer calibration data points (fewer input polarizer settings) and a smaller range of input polarizer settings. Figure 3.14 shows a typical data fit from a Normal Calibration.

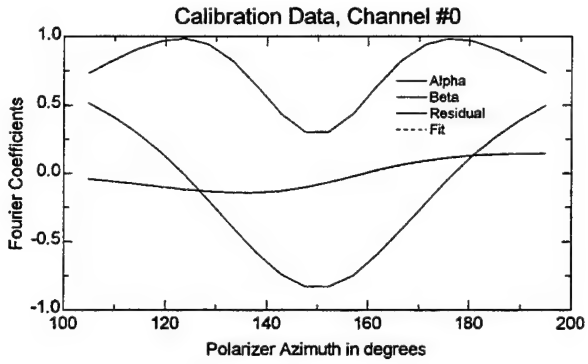

Figure 3.14. Typical Normal Calibration data fit

Notes about Normal Calibration

The results of each successful Normal Calibration are stored in the Hardware Log file in WVASE32. By viewing this file, one can track the reproducibility of the ellipsometer calibration over time. Comparing the MSE and 90% parameter confidence limits (± values) of the calibrations gives an indication of the quality of the calibration data fits over time. The P_s and F_d calibration parameters should also be fairly constant over time, although this may depend somewhat on the reproducibility of the sample position inside a vacuum chamber. (As stated in the previous section, the A_s calibration parameter will be different each time the hardware is reinitialized.)

As part of the regression fitting of the Normal Calibration data, ellipsometric Ψ and Δ values for the sample are also extracted from the fit. This data is shown in the WVASE32 'Graph' window, and can be saved to disk from the WVASE32 'Experimental Data' window. The ellipsometric data resulting for the Normal Calibration data fit is extremely accurate, as it represents the best possible solution averaged over multiple input polarizer angles (this helps to minimize and cancel any 2^{nd} order systematic errors in the ellipsometer system). One good check on the systematic accuracy of the ellipsometer system is to compare the ellipsometric data extracted from a Normal Calibration with ellipsometric data 'acquired' after the calibration. If these two data sets are in good agreement (the Ψ and Δ values are within 0.1° of each other for most wavelengths), then the ellipsometer is system is acquiring very accurate data.

Calibration Acceptance Limits

WVASE32 uses acceptance limits to determine if a given System, Coarse, and/or Normal calibration is successful. These limits can be found in the C:\WVASE32\MXX-CAL.CNF file. After each calibration, the 90% confidence limits of each calibration parameter are checked against the corresponding acceptance limit. If a limit is exceeded, the calibration will not be accepted and WVASE32 will display a 'Calibration not Successful' message. To improve the calibration accuracy (i.e., reduce the 90% confidence limits on the calibration parameters), try increasing the following calibration parameters and repeating the calibration: # of Revs (for acquiring each calibration data point), # of Calibration Data Points, and/or the Polarizer Span.

Under some circumstances (for example, the rotating substrate in an MBE system) the signal-to-noise of the ellipsometer signal is degraded such that it is not possible for the calibration to succeed using the default acceptance limits. In these cases, it

may be necessary to increase the acceptance limits in the MXX-CAL.CNF file such that ellipsometric data can still be acquired. Even though the calibration may be less than ideal in these circumstances, it still should be adequate to acquire ellipsometric data with reasonable accuracy.

4. *Insitu* Real-Time Ellipsometry

Acquiring accurate insitu ellipsometric data in the HgCdTe MBE growth environment, in which the substrate is rotating and small substrates are used, is no small task. In this contract, a methodology for overcoming this challenge was developed. This chapter summarizes the overall strategy which was used to obtain accurate SE data under actual HgCdTe MBE growth conditions.

Ellipsometer Beam Alignment

The first challenge in acquiring insitu data is to reflect the ellipsometric measurement beam off the sample and into the detector unit. This is not necessarily a trivial issue, when you consider that the size of the CdZnTe substrates used for the epitaxial growth of HgCdTe are quite small: 1.5 x 1.5 cm is a typical size, although sometimes wafers ½ or ¼ of this size are used for growth, as the CdZnTe substrate material is very expensive. Due to the MBE chamber dimensions and the location of the optical access ports, the distance between the ellipsometer input unit and the substrate (and the ellipsometer output unit as well) is ≈ 50 cm. Furthermore, to promote compositional and thickness uniformity, it is absolutely necessary to rotate the substrate during the MBE growth.

Substrate Wobble

Figure 4.1 shows the geometry of the beam movement during substrate rotation, where Φ is the angle of incidence, θ is the angle between the substrate normal and axis of rotation (the substrate angular wobble), and 'd' is the substrate to detector distance. Simple trigonometry, shown in equations (4.1) and (4.2), predict the length 'l' and width 'w' of the ellipsoidal beam trajectory at the detector plane due to the substrate rotation.

$$l = 2 \cdot d \cdot \tan(\theta) \qquad (4.1)$$

$$w = 2 \cdot d \cdot \tan(\theta) \cdot \cos(\Phi) \qquad (4.2)$$

If the angular wobble θ of the substrate is $\pm 0.1°$ (which is the nominal specification of the upgraded Fisons manipulator), d = 500 mm and $\Phi = 75°$ (which are appropriate values for the V80H system), the reflected beam will move in a 1.7 x 0.5 mm ellipsoidal trajectory at the detector plane. While this would probably be acceptable for most ellipsometric measurements, in practice we typically observed beam trajectories which ranged from 2-5 times larger than this, implying that the

substrate wobble was much greater than the nominal Fisons specification. However, substrate mounting procedures, i.e., how the CdZnTe wafer is attached to the substrate block which mates into the MBE substrate manipulator system, could account for much of the increase and variation in observed substrate wobble from run to run.

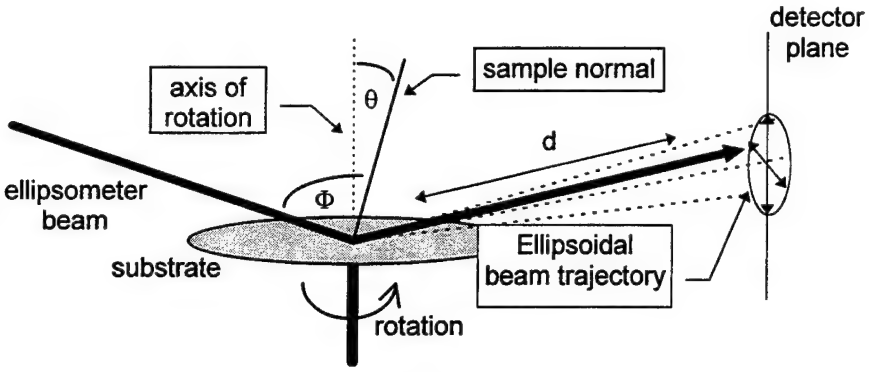

Figure 4.1. Geometry of beam movement at the detector during substrate rotation

Since the aperture of the detector unit is only about 1 mm in diameter, it is important to collect as much of the beam reflected off the substrate as possible during rotation. If the beam trajectory due to substrate wobble is very large, then the size of the reflected ellipsometer beam at the detector aperture must be very big if the ellipsometer system is to collect light throughout the complete period of substrate rotation. This is an important issue to keep in mind as the two approaches described in the following sections are considered.

Focused Beam Approach

Initially, we considered the approach of trying to focus the ellipsometer beam completely on the small CdZnTe substrate. Figure 4.2 illustrates the geometry of the ellipsometer optical system, where 'i1' is the diameter of the input fiber, 'i2' is the beam diameter at the sample, 'f1' is the focal length of the lens, and 'f2' is the distance from the lens to the sample.

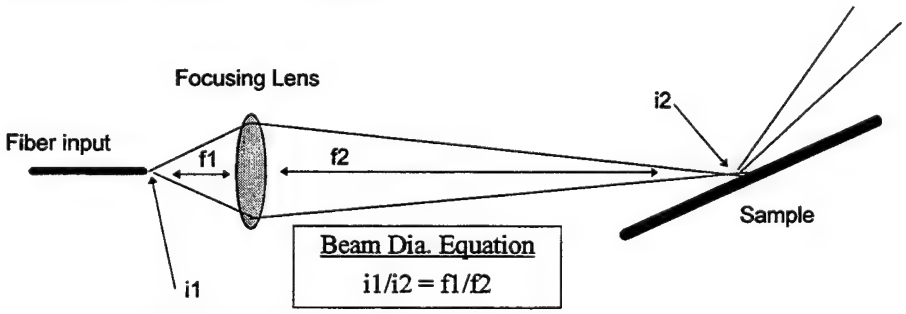

Figure 4.2. Geometry to focus ellipsometer input beam on sample

For the modified Fisons V80H MBE chamber f2 ≈ 500mm and for the standard M-XX input optics unit f1 ≈ 60 mm. If a 200 μm diameter input fiber is used, this implies that a beam diameter of less than 2 mm on the substrate should be achievable by the simply adjusting the input fiber-to-lens distance to focus the beam on the substrate.

Due to the very oblique angle of incidence (≈ 75°), the ellipsometer beam significantly elongates on the surface of the substrate. The length of the ellipsometer

beam on the sample is calculated from the geometry and equation shown in Figure 4.3: 'w' is the diameter of the beam on the sample, and 'l' is the length of the elongated beam on the sample at the oblique angle of incidence Φ. For Φ = 75° l/w=3.86, which implies that the beam is almost 4 times longer than the beam diameter on the substrate surface.

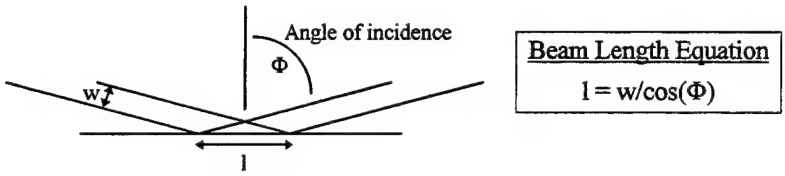

Figure 4.3. Geometry of ellipsometer beam on sample at oblique angle of incidence.

From the preceding discussion, it should be theoretically possible to place a 2 x 8 mm beam on the 15 x 15 mm CdZnTe substrate mounted inside the MBE chamber and acquire ellipsometric data. However, in practice this proved to be quite difficult. The limited degree of optical access to the MBE chamber made it difficult to visualize and position the beam on the sample *and* keep the reflected beam centered on the detector aperture. If the CdZnTe substrate was not precisely centered, the beam would not stay only on the substrate during rotation. Furthermore, as the substrate rotated, the trajectory of the beam on the detector aperture was such that for much of the rotation period, no light was entering the detector unit.

The 'Floodlight' Approach

To improve the signal-to-noise of the ellipsometric signal, we needed to increase the amount of light collected by the detector optics during substrate rotation. Instead of trying to keep the ellipsometer beam completely on the small CdZnTe substrate, we tried a completely different approach: a very large beam which overfilled the substrate was used. Since the substrate mounting block and manipulator have a rough non-specular finish, only the part of the beam that hits the CdZnTe substrate is reflected into the ellipsometer detector. This is the basis of the 'floodlight' approach, as illustrated in Figure 4.4: flood the sample with as many light rays as possible; the rays which fall on the substrate are reflected into the detector, and the rays which fall off the substrate are scattered away. The large input beam greatly simplifies the alignment overall alignment procedure: it is not necessary to re-adjust the input unit each time a sample is loaded, as the large beam always illuminates the sample.

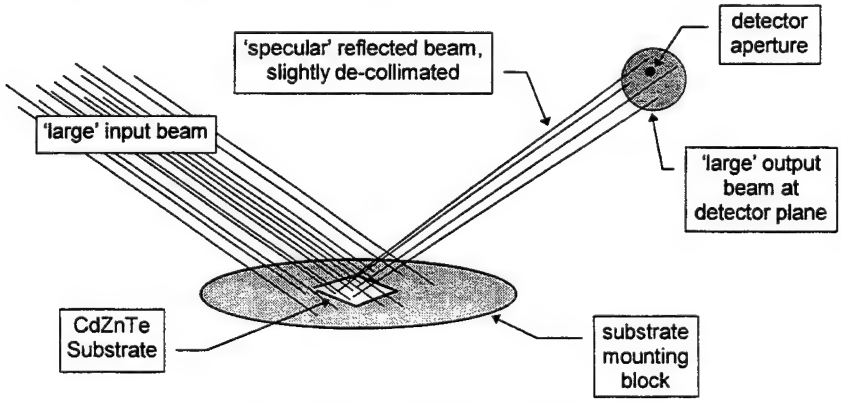

Figure 4.4. The 'floodlight' approach to sample illumination.

To increase the size of the light beam on the detector aperture, the ellipsometer beam was intentionally de-collimated by the following means:

1. Larger core diameter input fibers (400μm and 600μm) were used. This effectively launches more light rays into the system. At the same time, the beam is less collimated, as the larger core diameter looks less like a 'point source' of light.
2. A shorter focal length input lens was also tried. This also gathers more light rays from the input fiber, at the expense of beam collimation.
3. The input fiber to lens distance was adjusted to mildly focus the beam on the sample.

In practice, we found that combining #1 and #3 yielded the best results on the NVESD chamber with small CdZnTe substrates. Other systems with different samples sizes, chamber geometries, and/or substrate wobble may benefit from using #2 as well. The 'floodlight' approach certainly has some limits:

- Flooding the sample with an extremely large beam not only 'wastes' light, it also increases the chance that some of the 'scattered' light will enter the ellipsometer detector
- If the beam is too de-collimated, the intensity of the beam at the detector will decrease.

For optimal ellipsometer signal-to-noise, the trick is to make the beam at the detector plane large enough such that a part of the beam is always collected while the substrate is rotating (see Figure 4.5). However, if the beam is too large, much of the light reflected from the sample is wasted, as it is never collected by the detector. The next section summarizes the practical aspects of the beam alignment procedure which were implemented on the NVESD chamber to optimize the amount of light collected by the ellipsometer detector.

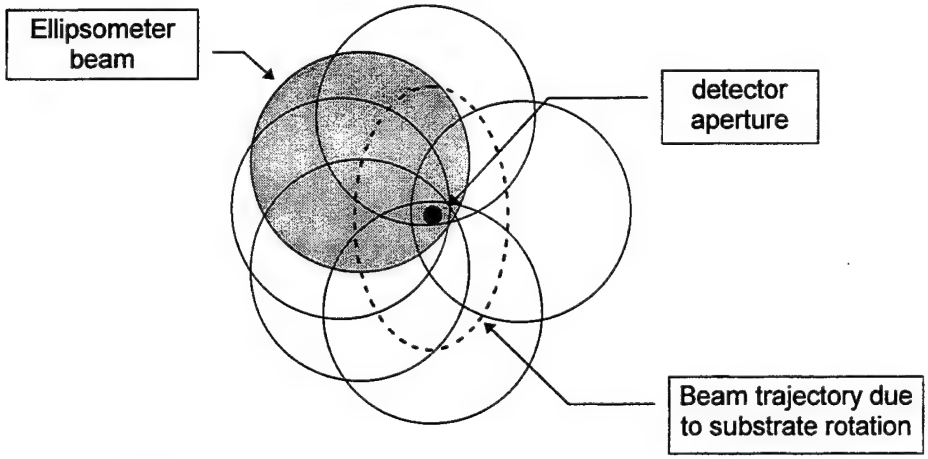

Figure 4.5. 'Large' ellipsometer beam at the detector aperture with substrate rotation.

NVESD Alignment Procedure

The following steps were used to align the ellipsometer beam on the NVESD MBE chamber with the small CdZnTe substrates used for HgCdTe growth:

1. Mount the ellipsometer input optics, on the MBE chamber, using the standard insitu mounting hardware included with the M-XX system.
2. Install a larger core diameter input fiber (400μm or 600μm).

3. Start the light source by turning on the power and igniting the arc lamp.
4. Load the CdZnTe substrate into the MBE chamber, and turn on the substrate rotation.
5. Adjust the tilt stage of the optics input unit to center the 'overfilled' ellipsometer beam on the CdZnTe substrate (use the MBE system's pyrometer port to see the beam on the substrate).
6. Verify that the ellipsometer beam which is reflected off the sample exits the other optical viewport. If this is not the case, go back to step #5 and adjust the input tilt stage such that the beam does exit the port and still is fairly centered on the substrate.
7. Mount the ellipsometer 'alignment jig' on the output optical viewport, using the standard insitu mounting hardware included with the M-XX system. Loosen the locking screws and translate the output stage to center the reflected beam (which is moving due to the substrate rotation) on the aperture of the alignment jig. If the substrate wobble is too large to keep some portion of the beam in the aperture during the complete rotation period, install a larger core fiber and/or adjust the distance of the input fiber relative to the input lens to increase the beam size. When the moving beam is 'centered' on the detector aperture, tighten the locking screws on the translation stage.
8. Adjust the tilt of the output stage to center the beam on the reticule of alignment jig.
9. Remove the alignment jig, and mount the ellipsometer output optic (detector) unit. Connect all the ellipsometer cables, power up the ellipsometer computer and control electronics box.
10. Start the WVASE32 software and initialize the ellipsometer hardware. Go to the alignment screen. Adjust the output tilt stage to center the alignment crosshair trajectory.
11. Evaluate the alignment: A 'good' alignment on the NVESD MBE system will have an 'Intensity' value (which is shown on the alignment screen) greater than 2.0, although any value greater than 0.5 is also probably acceptable. A fairly elliptical trajectory should be observed on the alignment screen (if the crosshair randomly jumps around during part of the substrate rotation period, the beam is probably not staying on the detector aperature for the complete rotation period, and the alignment needs to be improved). Figure 4.6 shows a typical WVASE32 alignment screen with the substrate rotation enabled. The size of the ellipse does vary from sample to sample; for some samples the trajectory will be larger than that shown in the figure. This is still acceptable, as long as some part of the beam is always collected by the detector, and the intensity value is acceptable.
12. If necessary, repeat the alignment procedure (starting with step #5) in an iterative manner. To increase the signal intensity on the alignment screen, it may also be helpful to tweak the alignment screws on the lamp housing to maximize the light source output. Slightly adjusting the input fiber to lens distance may also improve the light collection at the detector unit. Sometimes the only way to achieve an acceptable sample alignment under substrate rotation conditions is to remount the sample.

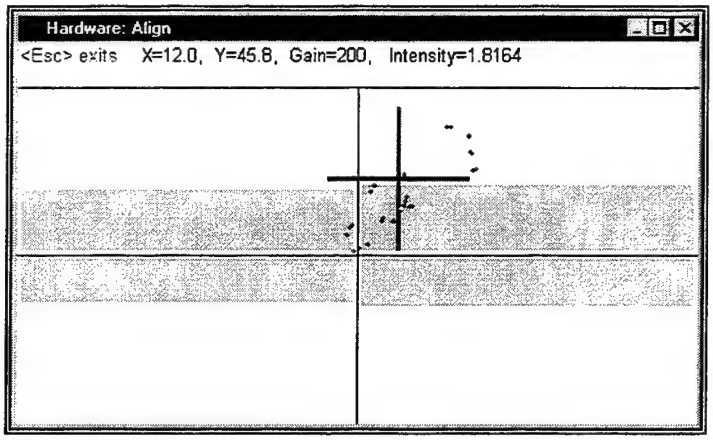

Figure 4.6. Typical alignment screen with substrate rotation.

Data Acquisition Parameters

Signal Averaging Time

Once the ellipsometer system has been properly aligned, the system needs to be calibrated, and then accurate real-time insitu ellipsometric data can be acquired. For an overview of the various calibration procedures used with the M-XX ellipsometer systems, see Chapter 3. It is important to perform the ellipsometer alignment and calibration procedures under the same conditions that growth will be performed, i.e., with substrate rotation enabled and on the actual substrate that will be used for the growth. The ellipsometer signal averaging time is an important parameter that needs to be specified for both the calibration procedure and the data acquisition routine.

During the 1st trip to NVESD in which insitu ellipsometric data was acquired, the ellipsometer signal averaging (data acquisition) time was arbitrarily set to 8 seconds (this corresponds to ≈ 200 analyzer revolutions, or revs/measurement, on the M-44 system). Figure 4.7 shows oscillations in the measured ellipsometric data, due to substrate rotation, which were observed under these data acquisition conditions. For this growth run, the beam precessed on the detector iris ≈0.5cm. Given the substrate to detector distance of ≈50cm, this yields an angular beam wobble on the order of ±0.3°.

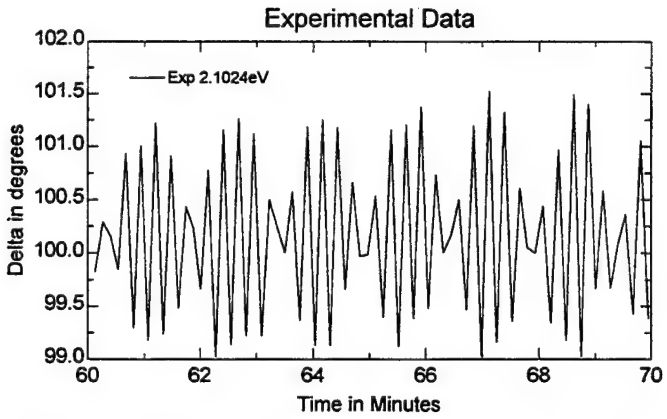

Figure 4.7. Oscillations in ellipsometric data due to substrate rotation.

The higher frequency oscillations observed in the data have the same period as the substrate rotation, which was about 17 seconds/revolution. The slower 'beat frequency' observed in the data is caused by the interaction of the ellipsometer sampling period (8 seconds/measurement) with the sample rotation. The simple MATHCAD simulation shown below demonstrates the exact behavior seen in the experimental ellipsometric data shown above.

$$\text{Substrate}(t) := \sin\left(\frac{t}{.29}\cdot 2\cdot\pi\right)$$

Periodic rotation of substrate:
1 revolution every 0.29 minutes
(17.4 seconds)

$t := 0, .133 .. 10$ Data acquisition every 0.133 minutes (8 seconds)

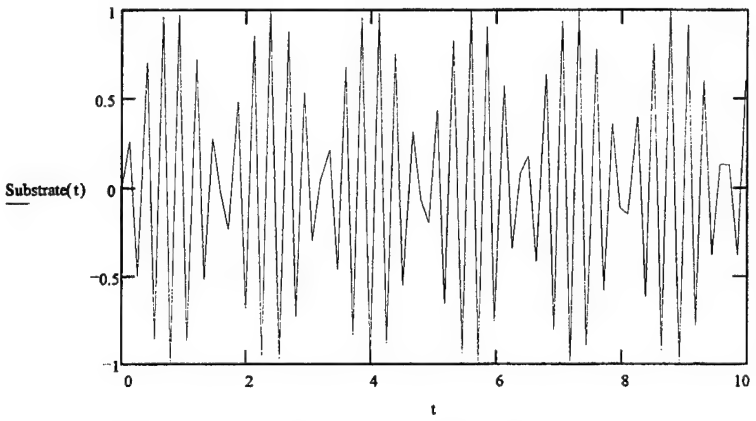

Figure 4.8. MATHCAD simulation of 'beat frequency' from the interaction of the substrate rotation period with the ellipsometer sampling frequency.

To reduce the magnitude of the oscillations in the ellipsometric data, the ellipsometer data acquisition time was simply adjusted to match the substrate rotation period. A stop watch was used to time the substrate rotation period. It is not necessary to have the ellipsometer data acquisition time exactly equal the substrate rotation period: as long as they are fairly close (within a few %), the magnitude of the oscillations is greatly reduced, as each measurement averages over a complete substrate rotation period. The period of the beat frequency also increases as the ellipsometer data acquisition time approaches the substrate rotation period (if they were exactly equal, the period of the beat frequency would be infinite). To increase the allowable rate of the ellipsometer data acquisition, the substrate rotation period was decreased to 8.5 seconds.

'High Accuracy' Mode

For all insitu ellipsometric data acquired on the NVESD MBE chamber, the WVASE32 'High Accuracy' mode of data acquisition was used. In this mode of acquisition, ellipsometric data was acquired with the input polarizer at +P and -P angles, and the two scans were averaged to produce each measurement point (this is also know as 'zone averaging'). The input polarizer angle P was chosen to be 15°, which is approximately the average of the ellipsometric Psi values which were measured throughout a HgCdTe growth run (the condition of input polarizer angle $\approx \Psi$ optimizes the sensitivity and accuracy of an ellipsometric measurement by a RAE).

The 'High Accuracy' mode is useful for canceling out small systematic errors in ellipsometer alignment and calibration, and window effects. Even if the system is perfectly aligned and calibrated at the beginning of the run, it is possible that thermal effects in the MBE substrate manipulator throughout the course of a very long growth run could cause the position of the substrate to change. Any changes in the substrate position would effect the ellipsometer alignment and calibration. To the first order, the 'High Accuracy' data acquisition mode cancels these effects.

Since two scans were required for each point, the time for each ellipsometric measurement was twice the substrate rotation period, or 17 seconds. This seemingly slow data acquisition rate was considered acceptable for the HgCdTe growth environment, as the most important parameter to monitor was how the composition of the material varies throughout the duration of the growth run. Since the HgCdTe growth runs could be very long (>5 hours), acquiring data a higher rate does not provide any useful information for most of the growth (once the film is optically thick, the data should be a flat line for the rest of the growth if the composition is constant). Even with a data acquisition time of 17 seconds, huge volumes of ellipsometric data were acquired during each run. For example, acquiring data with an M-88 system during a 6 hour growth run yields 88 wvls/acquisition x 6 hours/growth x 60 minutes/hour x 60 seconds/minute / 17 seconds/acquisition = 111,760 data points!

Signal-to-Noise in the Ellipsometric data

Using the data acquisition parameters described in the previous sections, ellipsometric data with excellent signal-to-noise (S/N) could be acquired on small CdZnTe substrates, even with the substrate rotation enabled. Figure 4.9 and 4.10 show typical real-time insitu ellipsometric data (at a few selected wavelengths) acquired during a HgCdTe growth run. At this scale, the noise in the ellipsometric data is barely discernible. Figure 4.11 shows a complete spectrum of ellipsometric data, at a selected time midway through a growth run. Again, the signal-to-noise is quite good, especially for the lower photon energy (longer wavelength) data. Data in the UV (higher energies or shorter wavelengths) will always exhibit more noise, due to the lower light intensity levels from the light source and reduced sensitivity in the silicon photodiode array detector in this region of the spectrum.

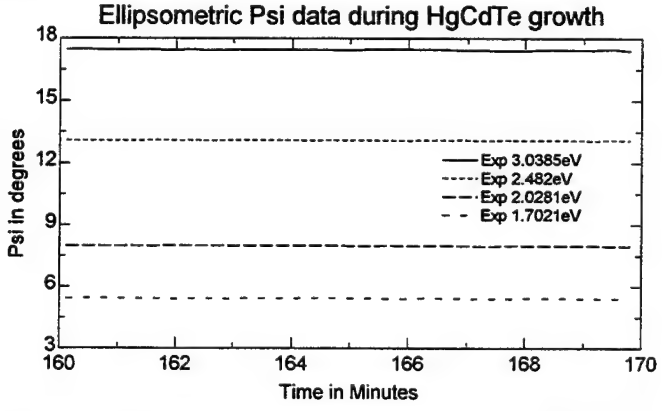

Figure 4.9. Real-time insitu ellipsometric Psi data during a typical HgCdTe growth run.

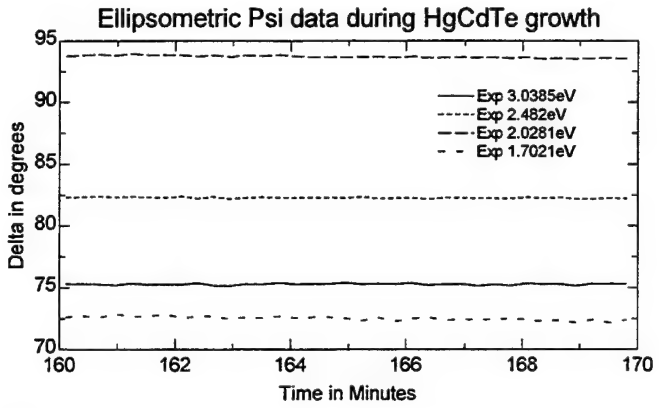

Figure 4.10. Real-time insitu ellipsometric Delta data during a typical HgCdTe growth run.

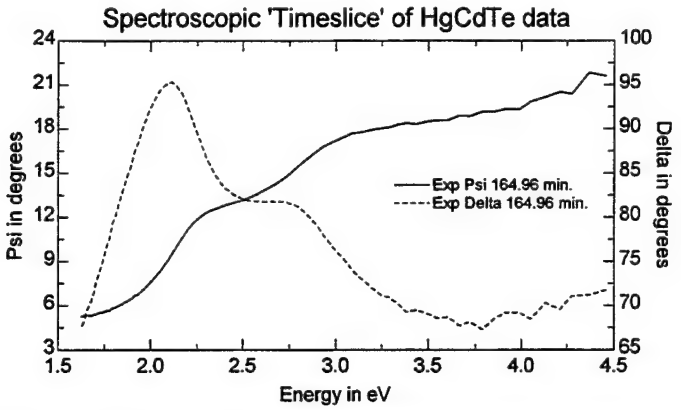

Figure 4.11. SE data at a selected time during a typical HgCdTe growth run.

While the data displayed in the graphs above is somewhat typical of the insitu ellipsometric data acquired throughout this contract, this quality of data was not achieved for every growth run. Smaller CdZnTe wafers usually resulted in slightly degraded S/N in the ellipsometric data. However, the factor which most influenced the acceptability of the ellipsometric data was the mounting of the small CdZnTe wafer to the substrate block. The wafer surface must be mounted extremely parallel to the substrate block to minimize the beam wobble due to substrate rotation. As long as the wobble was such that some part of the ellipsometric beam always entered the detector aperture, ellipsometric data with acceptable S/N could be acquired. If the beam wobble was excessive, the substrate had to be removed from the MBE chamber and remounted.

Systematic Drift in Data

In some of the earlier NVESD HgCdTe growths, the insitu ellipsometric data exhibited a large systematic drift throughout the run (see Figure 4.12). No corresponding drift was observed in the ellipsometric Delta data. If the composition and morphology of the HgCdTe surface were constant throughout the growth run, the measured insitu ellipsometric data should also be constant (after the film becomes optically thick). Upon observing the large systematic drift, we were suspicious that drift was not a real effect caused by the changes in the HgCdTe film, but that it was possibly due to some ellipsometric data acquisition and/or analysis artifact.

At first, we tried explaining the drift in Psi with a surface light scattering model in which some portion of s-polarized light scattered off the sample and was not collected by the detector system. This assumption results in the following relation for the measured ellipsometric Psi value: $\Psi_{measured} = \Psi_{ideal} \times \sigma$, where 'σ' is proportional to the amount of 'surface scattering' (σ=1 implies no scattering). This simple 'surface scattering' correction provided a quantitative fit to the 'drifting' data, and enabled the extraction of a constant HgCdTe composition from the ellipsometric data. However, this approach was not based on a physically sound argument, as the resulting HgCdTe sample is highly specular and mirror like, and the ex-situ VASE measurements show no evidence of such a scattering layer.

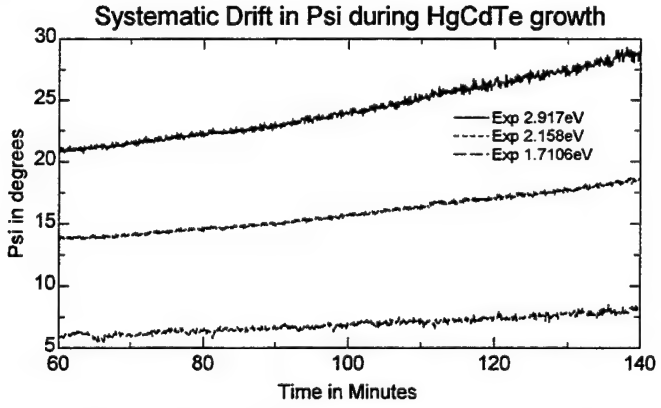

Figure 4.12. Systematic drift observed in Psi during some HgCdTe growth runs.

By a process of elimination, the scientists at NVESD were able to determine the true cause of the systematic drift in Psi: under certain conditions, the input polarizer position slowly changed over long periods of time (it was necessary to note the exact polarizer dial reading and wait for 15 - 60 minutes to observe the change). Electrical interference from a particular heater tape / power supply combination was found to be the culprit. When the heater was unplugged, the input polarizer position was stable and the drift was eliminated from the ellipsometric data. Equations (3.4) and (3.5) explain why the drift was only observed in the Psi data, as the ellipsometric Delta parameter does not depend on the value of the input polarizer position (only the 'sign' of the input polarizer is used in the determination the measured Delta value).

Window Effects

Data Accuracy Issues

Since ellipsometry accurately measures the change in polarization state induced by the sample, it is very important that the windows which are used to provide optical access to the sample inside the chamber do not affect the polarization state of the ellipsometric measurement beam. This implies that the windows must be free of strain induced birefringence. To satisfy this requirement, special windows from the BOMCO corporation were used on the ellipsometer ports of the NVESD MBE chamber. These windows are specifically designed to minimize the strain induced birefringence of the window. For the most part, the BOMCO windows on the NVESD chamber, as well as most of the other insitu ellipsometer installations in which we have used these windows, do work as advertised. However, at one installation we did observe some birefringence effects, even with the BOMCO windows. Therefore, it is very important to ensure that window effects are not

present at each installation. The best way to do this is to study the data fits resulting from the ellipsometer calibration procedure (such as that shown in Figure 3.14). As long as the experimental and model fit calibration curves lie directly on top of each other (as shown in the figure), it is very unlikely that window effects are corrupting the ellipsometric signal. If systematic discrepancies are observed in the curves, it may be necessary to remove and remount the window, taking care to gradually tighten the window flange bolts in an alternating sequence to prevent the flange from warping. If window effects are still present after remounting the window, it is necessary to send the window back to BOMCO to eliminate the window strain by a re-annealing process.

Coating Problems

As mentioned in the preceding section, window strain effects were not a problem on the NVESD MBE installation. However, due to the high flux of Hg in the MBE chamber during the growth of HgCdTe, the ellipsometer windows did become coated over time. Since ellipsometry measures a ratio (see equation 2.1), the accuracy of the measurement is not sensitive to decreases in the overall beam intensity caused by window coating. The S/N (precision) of the measurement does begin to degrade as the window becomes coated, though.

The BOMCO windows are designed in a manner such that they can be externally cleaned with a heat gun. While this procedure does work, it can be inconvenient and time consuming to hold a heavy heat gun in front of each window for 15 - 45 minutes to clean the windows each week. To overcome this problem, the scientists at NVESD designed a custom window heater assembly, consisting of resistive heating tape wrapped around the BOMCO window with an insulated enclosure. By applying an appropriate voltage to the heater winding, the window could be sufficiently heated to desorb the Hg (and any other coating, possibly Te) from the window surface. Unfortunately, the ellipsometric data measured on a static sample was observed to change as the window was heated from room temperature to the window cleaning temperature (this is most likely due to strain induced in the window from non-uniform heating). Therefore, it was not possible to keep the window hot while acquiring ellipsometric data during HgCdTe growth runs. The window surface does remain sufficiently clear during a complete growth run, such that a periodic cleaning of the windows in-between runs was acceptable.

Viewing the 'Raw' Data

Using the ellipsometer alignment, calibration, and data acquisition procedures described in this chapter, insitu ellipsometric data with excellent accuracy and S/N was acquired during the MBE growth of HgCdTe. A quantitative analysis of the insitu SE data is discussed in Chapter 6, and requires the optical constants libraries which are developed in Chapter 5. However, there is much information to be gleaned by simply viewing the 'raw' insitu ellipsometric data that is acquired in real-time during the growth process.

To illustrate the immense amount of insitu SE data which can be acquired during a HgCdTe growth run, consider the 3D plot of the ellipsometric Psi data vs. time and wavelength shown in Figure 4.13. This plot shows only a 15 minute subset (out of a 4 hour growth run) of insitu SE data. To visualize how the spectroscopic ellipsometric data evolves throughout the growth run, it is useful to plot 2D 'slices' of the data set, as a function of time (at a few selected wavelengths) or wavelength (at a few selected times). The WVASE32 software provides powerful capabilities for

selecting and viewing the insitu SE data. Before proceeding with the analysis of real-time insitu SE data, it is necessary to discuss the techniques to select, manage, and display specific portions of the large ellipsometric data set.

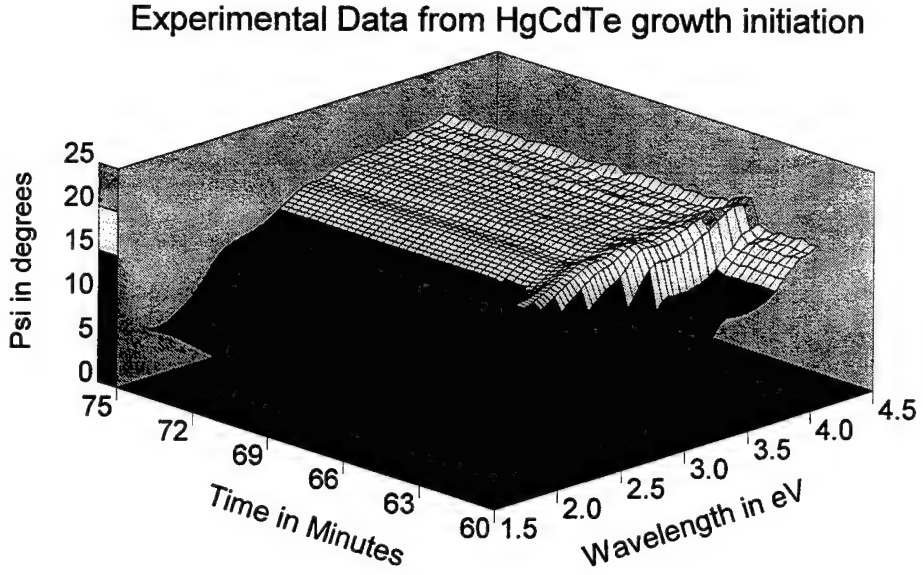

Figure 4.13. 3D plot of insitu SE data during HgCdTe growth inititation.

The 'Range Select' command

After the ellipsometric data from a growth run has been saved (the filename 'extension' for insitu ellipsometric data files is '.BDT', which stands for binary data format), it can be read into the 'Experimental Data' window of the WVASE32 program using the *File* | *Open Exp. File* menu option. The *Range Select* command, which is found in the 'Experimental Data' window of the WVASE32 program, is the basis for the manipulation and display of insitu SE data. Clicking on the WVASE32 *Range Select* option brings up the dialog box shown in Figure 4.14.

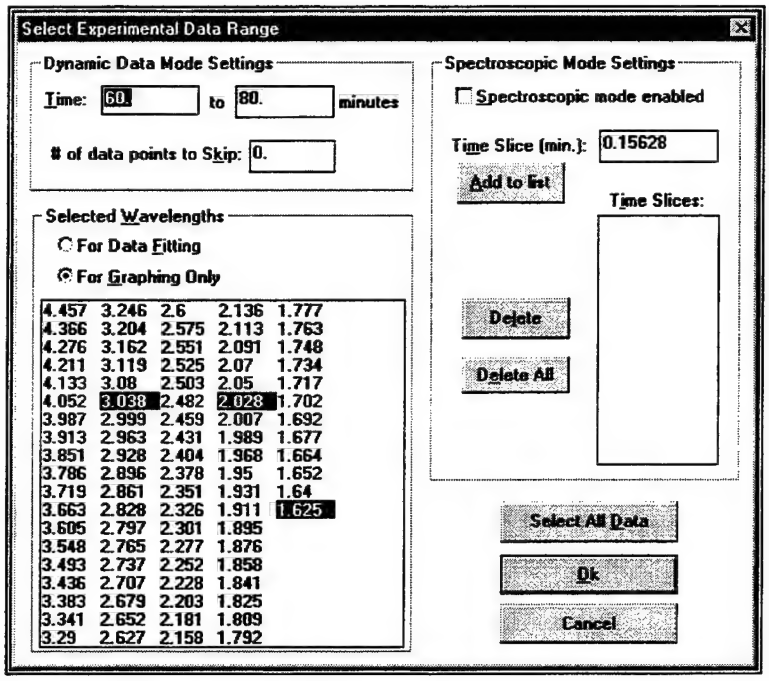

Figure 4.14. 'Range Select' dialog box with the Dynamic Data mode selected.

The Dynamic Data mode

The most important element of the dialog box in Figure 4.14 is the 'Spectroscopic mode enabled' checkbox which is found in the upper right-hand corner of the screen. When this box is **not** checked, the Dynamic Data mode will be used to display the SE data. In the Dynamic mode, the data is plotted as a function of time. The time range (in minutes) of the data that will be plotted is specified in the 'Time:' section of the dialog box.

To reduce the number of data points on the graph, the user can specify the '# of data points to Skip:', that is, instead of plotting each data point within the specified time range (which corresponds to the default 'Skip' value of zero), every n'th data point can be displayed by setting the 'Skip' value equal to 'n' (for example, to select every other data point, set the 'Skip'=1).

The 'Selected Wavelengths' list box shows which wavelengths will be used to Fit and Graph the data. To specify the wavelengths for graphing the Dynamic SE data vs. time, select the 'For Graphing Only' radio button, and click the mouse on the desired wavelengths in the list box. All of the measurement wavelengths which are contained in the experimental data file are shown in this box, using the WVASE32 default wavelengths units. In Figure 4.14, Photon Energy (eV) is used to specify the wavelength values; by selecting the *Global* | *Defaults* menu option, the wavelengths can also be listed (and graphed) in terms of nanometers (nm), Angstroms (Å), or microns (μm).

The 'Selected Wavelengths' list box is a standard multiple selection control: to use, click on the first desired wavelength, and then hold down the 'Ctrl' key while clicking the mouse on additional wavelengths. A range of wavelengths can be selected by holding down the mouse button and dragging the cursor over the desired wavelength range, or by holding down the 'Shift' key and clicking on the last wavelength in the desired range.

When graphing dynamic data, it is usually desirable to select only a handful of wavelengths (3-5) evenly distributed across the spectral range of interest. While more wavelengths can certainly be selected (it is possible to select all 44 or 88 wavelengths), this makes for a very cluttered graph which is difficult to read and interpret.

Clicking the 'OK' button on the 'Range Select' dialog box causes WVASE32 to select the specified subset of ellipsometric data, and update the WVASE32 'Graph' window accordingly. Figure 4.15 shows a graph of the ellipsometric Psi data which resulted from the 'Range Select' specifications shown in Figure 4.14.

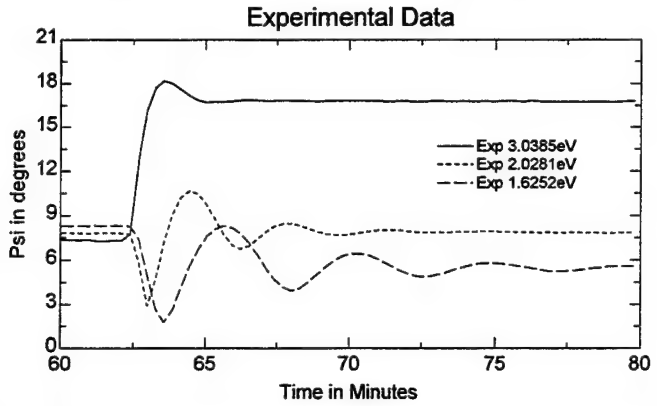

Figure 4.15. SE Psi data at 3 wavelengths displayed in the 'Dynamic' mode.

The Spectroscopic Data mode

The other display mode for SE data is the 'Spectroscopic' mode. In this mode, a spectrum of ellipsometric data vs. wavelength is displayed at a selected time (or times) during the growth run. Figure 4.16 shows a 'Range Select' dialog box which is set to the 'Spectroscopic' mode, by clicking the corresponding checkbox in the upper right corner of the screen.

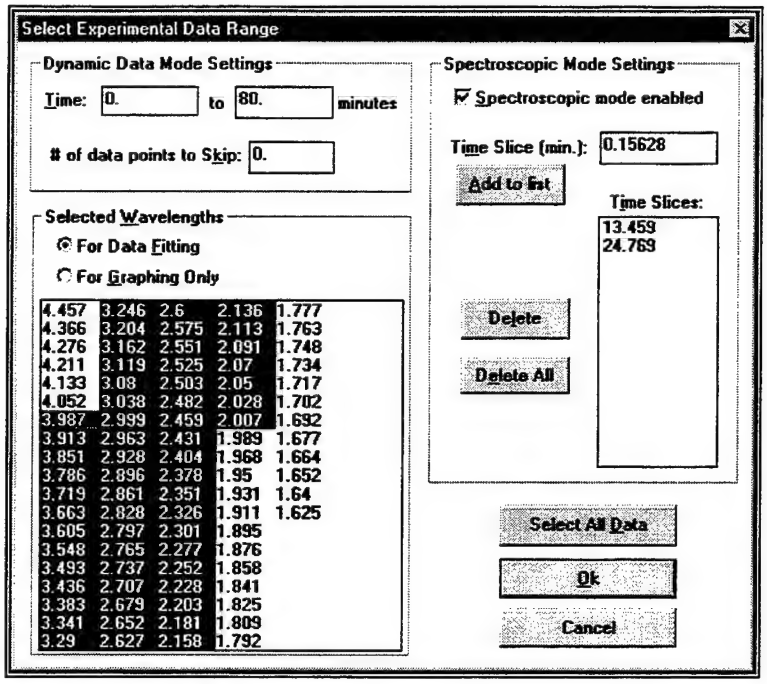

Figure 4.16. 'Range Select' dialog box with the 'Spectroscopic' mode selected.

In this dialog box, the spectroscopic 'timeslices' to graph can be specified by entering a value in the 'Time Slice (min.):' box, and clicking on the 'Add to list' button. To remove timeslices from the list, simply highlight the desired timeslice and click on the 'Delete' button. All the defined timeslices can be removed by selecting the 'Delete All' button.

To specify which wavelengths will be plotted in the spectroscopic mode graph, click on the 'For Data Fitting' radio button, and highlight the desired wavelengths in the 'Selected Wavelengths' list box. In Figure 4.16, the 2 - 4 eV spectral range is specified. Clicking on the 'OK' button accepts the range select specifications and displays a 'Spectroscopic' mode plot in the WVASE32 'Graph' window (Figure 4.17). In this graph, spectroscopic data at two times (t=13.72 and t=24.94) are displayed.

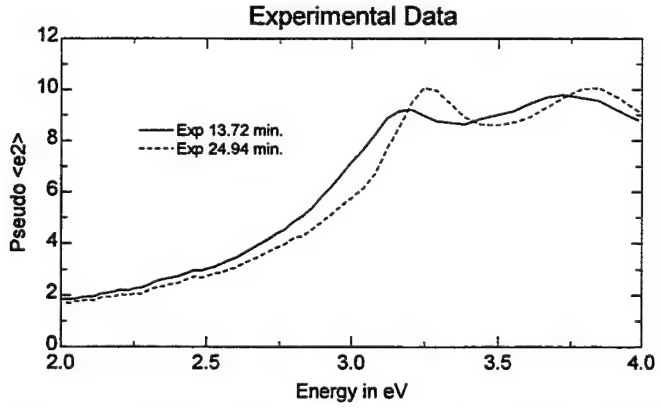

Figure 4.17. 'Spectroscopic' mode graph with two timeslices of SE data.

Data Selection Shortcuts

There is another very useful way to define spectroscopic timeslices. Start by Range Selecting a time range of data, using the 'Dynamic' mode. To define a timeslice, go to the WVASE32 'Graph' window, and right-click the mouse button at the desired 'x' position in time. A vertical line will appear on the graph to represent the location of the timeslice, as shown in Figure 4.18. To specify additional timeslices, hold down the 'Shift' key while right-clicking the mouse at the desired times. To quickly toggle between Dynamic and Spectroscopic modes without bringing up the Range Select dialog box, simply double click the mouse anywhere inside the 'Experimental Data' window.

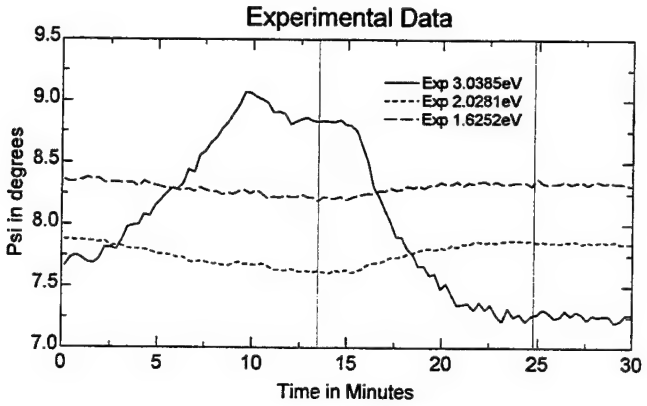

Figure 4.18. Defining Spectroscopic timeslices in the Dynamic Data mode.

Which parameters to plot?

Using the techniques described in the previous sections, different time and wavelength ranges can be selected and plotted in both Dynamic and Spectroscopic modes. The next question is: for a given time/wavelength range which parameter type is most useful to plot? The 'Type' menu option in the WVASE32 'Graph' window is used to select which ellipsometric parameter (or derived quantity) is plotted. The choices are: Psi, Delta, Tan(Psi), Cos(Delta), <e1>, <e2>, <n>, <k>, Re(rho), and Im(rho); the '<>' Pseudo dielectric and optical constant derived parameters are defined by (2.8), and the complex 'rho' parameters are defined by (2.1).

Which data type to plot is largely a matter of personal preference, but the general guideline is to plot the parameter which appears to have the most sensitivity to the current sample property of interest. For example, it may useful to monitor the ellipsometric Delta parameter during oxide desorption (as this parameter is more sensitive to the existence of thin overlayers), and the ellipsometer Psi parameter during sample heating. During the growth of the thick HgCdTe layer, it may be useful to view the Pseudo dielectric function parameters (for example, <e2>), as the composition of the HgCdTe layer is directly related to shifts in the critical point structure of its dielectric function. During most of the growth, the layer is optically thick and can be considered as a bulk material, such that the Pseudo dielectric function parameters derived from the ellipsometer Psi and Delta data are equal to the dielectric function of the growing layer.

When viewing the SE data, it may be helpful to switch between the different data types, especially when a data analysis is being performed. It is important that an analysis model fit both the ellipsometric Psi *and* Delta data (or correspondingly,

<e1> *and* <e2>). The *Style | 2D* menu option in the WVASE32 'Graph' window brings up a dialog box which allows the user to specify a 'Double Y axis' graph. This graph style, which is shown in Figure 4.19, provides a concise way to visualize and present spectroscopic timeslices of SE data along with the model analysis results.

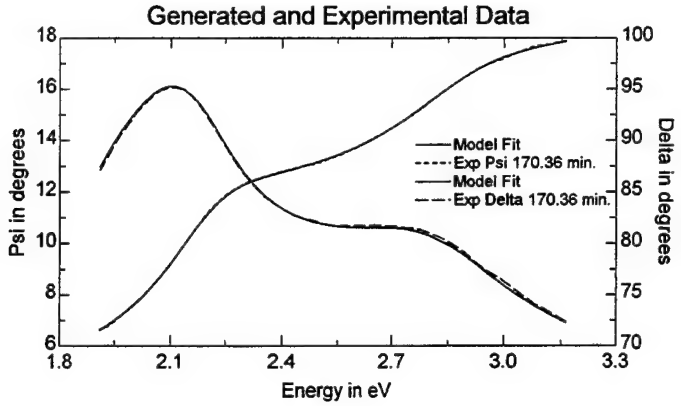

Figure 4.19. Double Y axis plot of SE data with Model Fit.

Ellipsometric Anatomy of a HgCdTe Growth Run

A typical Dynamic plot of the SE Delta data during a HgCdTe growth run is shown in Figure 4.20. For clarity, only two wavelengths are shown on this graph. Each wavelength, one shorter (2.83 eV) and one longer (1.63 eV), is more sensitive to different aspects of the growth process. The main phases of the growth are labeled on the graph:

1. The CdZnTe substrate is heated to 340° C (and held at this temperature for 10 minutes) to remove the oxide overlayer from the surface. The ellipsometric data is sensitive to both the temperature of the sample and the overlayer thickness (quantitative values for these parameters which were extracted from the analysis of the data are presented in chapter 6). By observing when the raw data near the end of this phase become constant, it is possible to determine when the substrate temperature and surface morphology are stable.

2. The CdZnTe substrate is cooled to 180° C in preparation for the HgCdTe growth. Once again, the raw ellipsometric signal can be used as an excellent indicator of the relative substrate temperature stability.

3. The growth of the HgCdTe layer is initiated at the beginning of this phase. The oscillations which are observed in the data (especially at the longer wavelength) are due to constructive and destructive interference in the light beam reflected from the sample, which is predicted by equation (2.9). At the shorter wavelength, which is more optically absorbing, the oscillation is damped out fairly quickly. Once the film reaches a critical thickness, light can no longer penetrate the depth of the film, and the oscillations are no longer observed (within a given spectral range). For that spectral range, the film can be considered 'optically thick', and from a data modeling standpoint it can be considered like a bulk substrate. From the constant nature of the raw ellipsometric signals in the optically thick regime, one can imply that the HgCdTe composition must also be relatively constant throughout the layer growth.

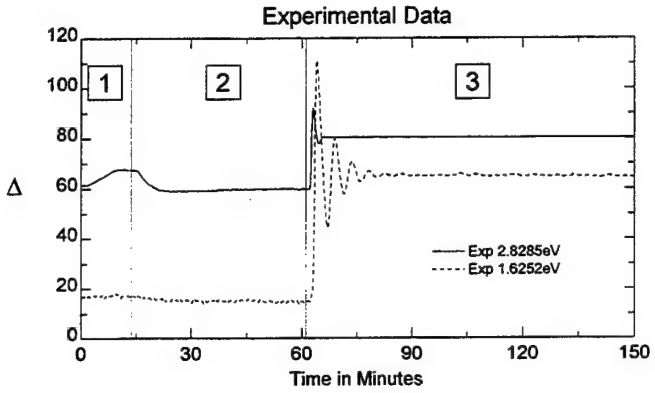

Figure 4.20. Raw real-time insitu ellipsometric data during HgCdTe growth run.

It is also informative to view a few spectroscopic timeslices of data at different phases of the growth. For example, Figure 4.21 shows the Pseudo <e2> function of the CdZnTe substrate measured during the cooldown transition between phases 1 and 2. The critical point structure near 3.2 and 3.8 eV sharpens and shifts to higher energies as the substrate cools. This behavior in the optical constants vs. temperature is typical for most semiconductor materials.

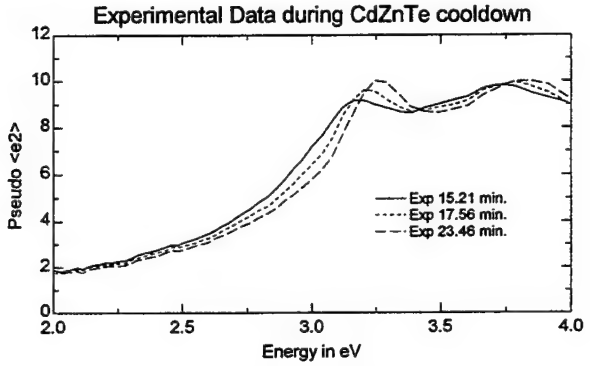

Figure 4.21. Timeslices of Pseudo <e2> data for CdZnTe substrate during cooldown.

Figure 4.22 shows a number of spectroscopic timeslices chosen during phase 3 of the growth in which the HgCdTe layer was optically thick. On this scale, all of the data lie almost directly on top of each other, indicating that the composition and surface morphology of the HgCdTe layer must be reasonably constant during this 4 hour portion of the growth.

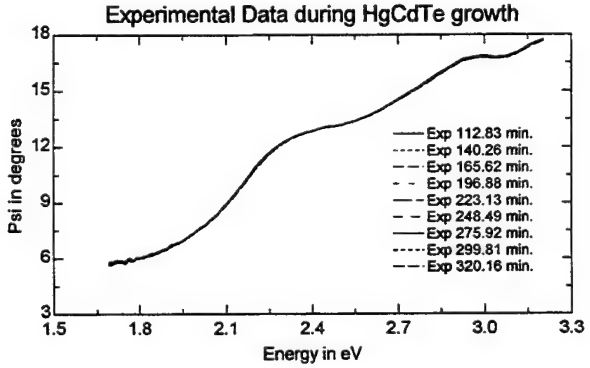

Figure 2.22. Spectroscopic timeslices during optically thick region of HgCdTe growth .

5. Optical Constant Libraries

As discussed in the Chapter 2, optical constants are required to perform quantitative analysis of SE data. Sometimes it is possible to find optical constants for the material of interest in the literature. However, for the case of insitu monitoring of semiconductor growth, very few published optical constants are available. Most of the semiconductor optical constants which do exist in the literature have been measured at room temperature.

Since the epitaxial growth of semiconductors is normally performed at elevated temperatures, the optical constants required for the SE data analysis must also be measured at these same growth temperatures. Furthermore, as the true substrate temperature during growth is not easy to precisely measure, it is often desirable to obtain a library of material optical constants as a function of temperature, such that the ellipsometer system can also be used to measure the substrate temperature.

For ternary semiconductor growth, a primary goal of the SE measurement is to determine the composition of the growing layer. The sensitivity of SE to composition is due to systematic changes in the material optical constants as a function of composition. Extracting the material composition from SE data requires a very accurate optical constant library consisting of the material optical constants measured at a range of known compositions at the growth temperature(s).

In this chapter, a systematic approach is outlined for acquiring the optical constant libraries needed to perform real-time analysis of the SE data. More specifically, a temperature dependent library for the CdZnTe substrate is described, and a composition dependent library for HgCdTe under growth conditions discussed. However, the methodology which was used to obtain these optical constant libraries is quite general and can be directly applied to the insitu SE monitoring of most epitaxial semiconductor growth applications.

Theoretical Considerations

The term 'optical constant' implies that this quantity is an invariant and intrinsic property of a given material. For some material systems, such as TiO_2, this statement is far from true: the index of refraction for a TiO_2 film can vary from 1.9 to 2.7 depending on the deposition conditions of the film. However, in the case of compound semiconductors, the optical constants of a material system (at a specified composition and temperature) are indeed quite constant, at least to the 1st order. (Doping and defect densities may cause some higher order variations in the semiconductor optical constants, but for most epitaxial growth applications, they are not significant.)

Assuming that compound semiconductor material systems do have invariant and intrinsic optical constants, can SE be used to accurately measure these values? While the next sections describe practical approaches for measuring semiconductor optical constants in an insitu growth environment, it is important to emphasize the difficulty of the optical constant measurement process. To accurately determine the intrinsic optical constants of a material using SE, a number of conditions must be met:

1. The ellipsometer system must acquire perfectly accurate Ψ and Δ data.
2. The ellipsometer beam angle of incidence must be exactly known.
3. The chamber windows used for optical access to the sample must be completely free of birefringence.
4. The surface quality of the material must be known; an atomically abrupt surface with no overlayer is desired.

Realistically, it is not possible to meet all of this conditions (or even verify that they have been met) in the insitu MBE environment. Of course, one can strive to minimize the possible sources of error in the measurement process, but in the end, the optical constants measured by SE are only an approximation to the intrinsic optical properties of the material.

Just how 'good' do the optical constants have to be? This depends on the application. For example, measuring the thickness of an SiO_2 layer on a Si substrate does not require perfectly accurate optical constants to achieve an excellent accuracy in the film thickness. Amazingly enough, the intrinsic optical constants of Si, which is the most important and well characterized material in the current semiconductor technology, are still a matter of debate in the literature. Even so, the SiO_2 layer thicknesses extracted from the SE data analysis using 3 different published sets of Si optical constants differed by less than 2Å for films ranging from 100 - 3500Å (work to be published by Craig Herzinger, et. al., J.A. Woollam Co.). In our experience with insitu SE, we also conclude that the accurate determination of layer *thickness* does not require perfect fits to the ellipsometric data or extremely 'perfect' optical constant libraries.

However, determining layer compositions from insitu SE data to the level of accuracy required for most device applications is a much more difficult problem. As you will see in the next chapter, the change in optical constants induced by a 0.001 change in HgCdTe composition is very small. In terms of the measured ellipsometric parameters, this small change in optical constants translates into a $\approx 0.01°$ change in Psi and a $\approx 0.05°$ change in Delta. While the current SE technology can easily provide this level of precision, it is not possible to achieve this level of absolute accuracy in the insitu environment (for starters, it is difficult to verify that the birefringence of the windows is $<0.1°$, which directly translates into systematic Delta errors on the order of $\approx 0.1°$). Extracting accurate HgCdTe compositions from SE data is a challenging problem which pushes the technique to its limit: to achieve the target level of HgCdTe composition accuracy (± 0.001 in x), you really have to 'split hairs'.

The good news is that it is not necessary to have perfect optical constants to achieve very good systematic reproducibility in the extracted from the SE data. Many potential sources of systematic errors (such as windows effects, assumed angle of incidence, systematic instrument errors) do remain fairly constant over time. As long as the measured SE data and the optical constant libraries were acquired under the same conditions, the sample parameters extracted from the data analysis should correlate nicely with the values from the optical constant libraries. Of course, if the optical constant libraries are used under different conditions (another growth

chamber and ellipsometer system), there may be some discrepancies in the SE data analysis results. If these discrepancies are fairly small and systematic, it may be possible to 'tune' them out by applying a simple correction factor to the results.

Hopefully, the optical constant libraries for the CdZnTe and HgCdTe material systems which were measured in this contract very closely approximate the true intrinsic optical constants of these materials. However, the only way to verify this is to use these libraries to fit ellipsometric data which is acquired by different ellipsometer systems on different growth chambers, etc. If the optical constant libraries both fit the data acceptably and return the correct results (in terms of compositions, temperatures, etc.), then the 'universality' of the library has been demonstrated and one might conclude that optical constant libraries do in fact represent the intrinsic properties of the material.

The conclusion of this lengthy theoretical discussion is that while it is may be very difficult to measure the true intrinsic optical constants of a given material system, this does not necessarily preclude using ellipsometry to extract systematically accurate parameters, such as composition, from the analysis of the data. Instead of considering the optical constants libraries presented in this chapter as 'the end result', one should realize that it is the systematic methodology for measuring (and validating) the optical constant library which is more important. Over time, the availability and absolute accuracy of optical constant libraries for use with insitu SE monitoring of semiconductor growth will certainly improve. For the time being, however, it will probably be necessary for most users to measure and validate their own optical constant libraries for each material system that they wish to monitor with SE. This is especially true in the case of demanding insitu monitoring applications which require very accurate optical constant libraries, such as with HgCdTe composition. One of the truly significant achievements of this contract is the development of a time efficient approach for measuring optical constant libraries (which is described in this chapter), and a systematic approach for validating the measured optical constant library (as is discussed in the following chapter).

Building a Substrate (CdZnTe) Optical Constant Library

Substrate Heat-Clean Procedure

A standard procedure for most epitaxial semiconductor growth is to heat the substrate to an elevated temperature to remove the oxide and/or any other contaminating overlayer from the surface before initiating the layer growth. This is an extremely critical part of the growth process, as any imperfections in the crystalline quality of the substrate surface will adversely affect subsequent epitaxial film growth. In the case of HgCdTe growth on CdZnTe substrates, the substrate temperature is typical raised to ≈340°C to fully desorb the oxide (a more volatile overlayer component, most likely amorphous Te, comes off at much lower temperatures). After holding at this elevated temperature for ≈10 minutes, the temperature is lowered and stabilized at ≈180°C before beginning the growth of the HgCdTe layer.

Since this process is so important, it would be very useful to monitor in real-time the substrate temperature and overlayer thickness. Ellipsometry is sensitive to both the oxide overlayer thickness (very sensitive) and the substrate temperature (fairly sensitive). This is dramatically shown in the raw ellipsometric data of Figure 5.1. In this graph, the 1st component of the CdZnTe overlayer (amorphous Te) desorbs from the surface at t=5 minutes. At about t=12 minutes, the remainder of the substrate overlayer desorbs. At t=18 minutes, the substrate cool down is initiated, and the

temperature is stabilized for growth (t>30 minutes). Note that the Psi and Delta curves exhibit differing amounts of sensitivity to the various events in this process. Other wavelengths of the SE data also show different structure throughout the heating process.

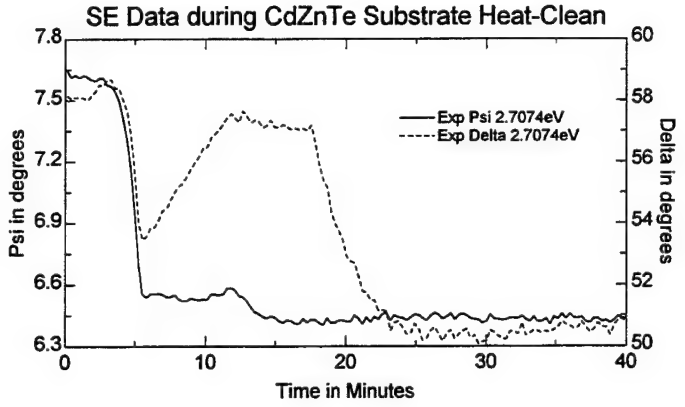

Figure 5.1. SE data at a single wavelength during CdZnTe substrate heating procedure.

Problems in Determining Substrate Optical Constants

While it is useful to qualitatively observe and associate the various events which occur in the substrate heat-clean procedure with changes in the raw SE data, it would be even more useful to quantitatively extract the substrate temperature and overlayer thickness from an analysis of the SE data. To do this, an optical constant library for the CdZnTe substrate as a function of temperature is required.

At first glance, it may seem like building an optical constant library for a substrate is a simple proposition: Equation (2.8) shows how to directly transform the ellipsometric data measured at each wavelength into the substrate dielectric function. However, there are two complications:

1. The insitu angle of incidence of the ellipsometric measurement beam with respect to the sample is not known *a priori.*
2. The assumption that the substrate is truly 'bulk-like' with no overlayer is questionable. It is not possible know when the substrate surface is perfectly clean and smooth (even RHEED can not *quantitatively* verify this).

The strategy used to overcome these complications is as follows: 1) an exsitu VASE measurement, in which the angle of incidence was accurately known to 0.01°, was performed on a CdZnTe substrate, and 2) it was *assumed* that the CdZnTe surface before growth (but after the heat-clean process) was perfectly 'clean' and could therefore be optically modeled as a bulk material.

Exsitu VASE Measurement of CdZnTe

Variable Angle Spectroscopic Ellipsometry (VASE) data for a CdZnTe sample was acquired at three angles of incidence over a 1.5-4.5 eV spectral range, using a J.A. Woollam Co. exsitu VASE ellipsometer system. The nominal composition of the sample (and all of the CdZnTe substrates used in this contract) was $Cd_{0.96}Zn_{0.04}Te$, which provides a better lattice match to the $Hg_{0.80}Cd_{0.20}Te$ films grown in this

contract. To extract the resulting CdZnTe optical constants from this data, an optical model consisting of a bulk substrate, with an overlayer was assumed (Figure 5.2). The true character of this overlayer is not known; it could be surface roughness, a native oxide, or possibly a non-stoichiometric overlayer (Te rich, for example). Fortunately, ellipsometry is not highly sensitive to the exact nature of the overlayer, i.e., it can not easily distinguish between a native oxide and surface roughness. Therefore, a surface roughness layer (consisting of a 50% percent EMA mixture of the bulk optical constants with void) was used to model the overlayer.

1	ema (cdznte)/50% void	25 Å
0	cdznte	1 mm

Figure 5.2. WVASE32 model for analysis of exsitu VASE data on CdZnTe substrate.

Without prior knowledge of the substrate optical constants, ellipsometry is also not sensitive to the *absolute* thickness of the overlayer. However, ellipsometry can still accurately determine the *relative* thickness of the overlayer. For this sample, I assumed that the overlayer thickness was 25Å. With this assumption, the overlayer thickness of the CdZnTe substrate measured insitu before growth was less than a few Å, which is quite reasonable. If I assumed that the overlayer thickness for the exsitu sample was 0Å, then the resulting overlayer thickness determined from the insitu sample would be about -25Å, which is not physical (although it is still accurate in a *relative* sense).

The ellipsometric data fits for the CdZn(.04)Te substrate are shown in Figure 5.3, and a graph of the resulting optical constants are shown in Figure 5.4. The CdZnTe optical constants are compared with CdTe optical constants which were measured by Aspnes and reported in the literature. The agreement in terms of position and shape of the critical point structures is quite good. The small systematic shift between the curves is easily explained by the 4% Zn which is present in the substrate material.

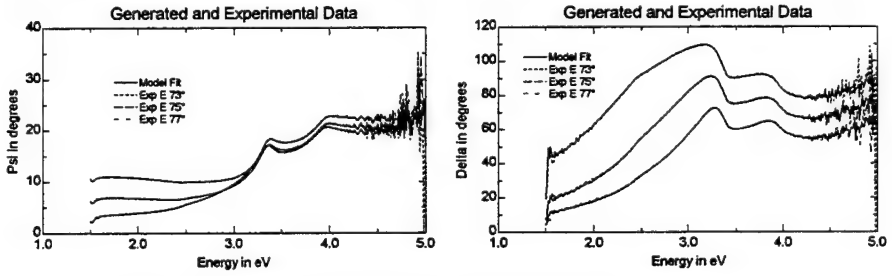

Figure 5.3. VASE data fits for the CdZnTe substrate measured exsitu.

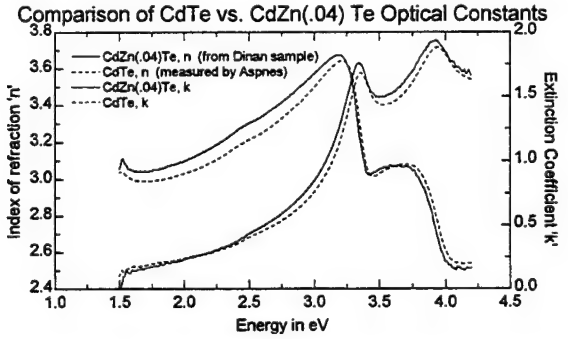

Figure 5.4. Comparison of $CdZn_{0.04}Te$ optical constants with published CdTe constants.

Determining the insitu Angle of Incidence

Using the exsitu determined CdZnTe optical constants from the preceding section, it was possible to fit for the insitu angle of incidence. The model used for this fit is shown in Figure 5.5; the 'srough' layer is simply a shortcut for a 50% EMA mixture of the substrate optical constants with void. The results of the fit are shown in Table 5.1, and a graph comparing the experimentally measured insitu SE data with the model generated data is shown in Figure 5.6.

1	srough	1.2252 Å
0	cdznte	1 mm

Figure 5.5. Model used to determine insitu angle of incidence and overlayer thickness.

Fit Parameter Name	Value, '±' numbers are the 90% confidence limits
MSE (Mean Squared Error)	0.9197
Thick.1 (surface roughness in Å)	1.2252±0.571
Angle0 (angle of incidence)	75.611±0.0123

Table 5.1. Fit parameters from insitu SE data analysis of CdZnTe substrate.

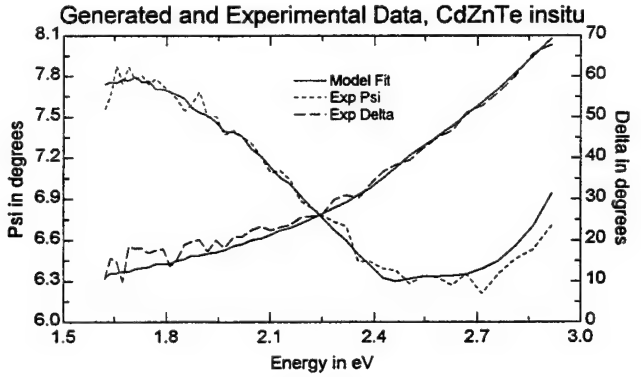

Figure 5.6. Insitu SE data fit for CdZnTe substrate before growth

The angle of incidence determined from the preceding data fit was used for all subsequent analysis of the SE data. In WVASE32, this is done by specifying the actual angle of incidence in the WVASE32 Experimental Window *Angles* menu option, as shown in Figure 5.7. This is also where the angle of incidence can be defined as a WVASE32 fitting parameter.

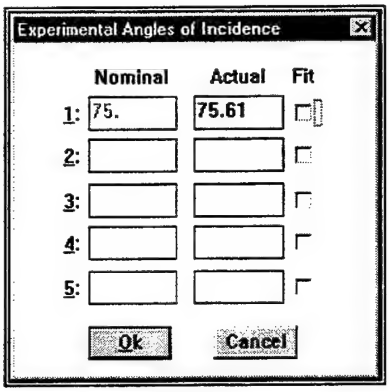

Figure 5.7. WVASE32 Experimental Angles dialog box.

While the data fits shown in Figure 5.6 are very good, there are still some potential sources of error in the angle of incidence: 1) the composition of the CdZnTe substrate material, which is assumed to be nominally constant for all substrates, may actually vary slightly from sample to sample, and 2) the temperature of the substrate during the SE measurement may not be exactly at room temperature, as the cryo-shields in the MBE system make it difficult to stabilize the substrate at room temperature (the optical constants used for the model analysis were measured at room temperature). These concerns aside, the maximum error in the fit angle of incidence is still estimated to be less than 0.1°.

Ramifications of Errors in the Angle of Incidence

Any error in the assumed angle of incident will translate into an error in SE determined layer thicknesses. The magnitude of this error depends on the material structure and optical constants, but for a 1000Å $Hg_{0.8}Cd_{0.2}Te$ film on a CdZnTe substrate, a 0.01° error in angle of incidence induces a 0.17% error in film thickness. This small systematic thickness error can be 'tuned' out of an existing optical constant library, if necessary.

However, angle of incident errors do not affect the SE determined layer compositions, as long as the optical constant spectra within the composition-dependent library were all acquired at the same nominal angle. In this case, the error in the optical constant library due to an inaccurate angle of incidence is systematically incorporated across all of the compositions in the library. When the optical constant library is used to analyze subsequently measured SE data, the fit will return the same 'inaccurate' angle of incidence value, but the fit composition will be systematically correct (assuming that the compositions in the library are accurate).

Extracting insitu Substrate Optical Constants

Two substrate temperatures were included in the CdZnTe optical constant library: 1) immediately before the layer growth, when the temperature should be stabilized at 180°C (according to the pyrometer), and 2) at the highest temperature of the heat-clean process, which is nominally 340°C (on the substrate thermocouple). In both cases, the oxide overlayer has already be desorbed, such that an ideal substrate optical model (no overlayer) can be used to extract the optical constants (using the previously determined angle of incidence).

The nominal temperature values of 180 and 340 may not be perfectly accurate, as the absolute substrate temperature is a very difficult property to measure insitu. However, these nominal values can easily be changed in the optical constant library

at a later time to correspond with another more accurate temperature measurement technique. Furthermore, the *reproducibility* of the SE-based temperature measurement is not affected by the relative accuracy of the nominal temperature values specified in the optical constant library.

To extract the insitu substrate optical constants at the two temperatures, spectroscopic timeslices were chosen at appropriate points in time throughout the substrate heat-clean procedure. Figure 5.8 shows how this was actually done in WVASE32, wherein multiple timeslices were selected during the region of constant substrate temperature before growth. WVASE32 was then switched to the 'Spectroscopic' mode, as shown in Figure 5.9. The data for the multiple timeslices lie essentially on top of each other. However, the purpose of selecting the multiple timeslices is to improve the signal-to-noise in the extracted optical constants by averaging the multiple sets of SE data.

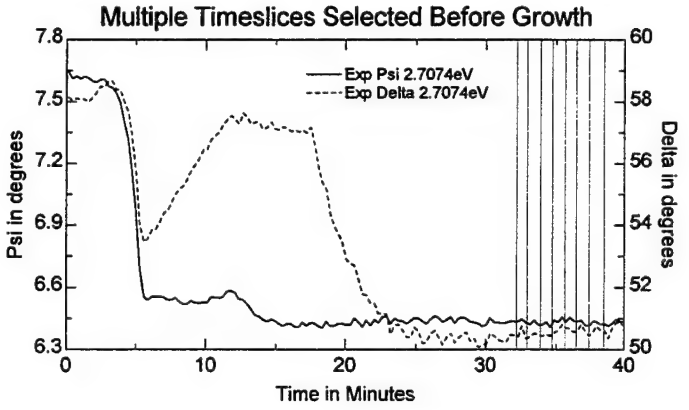

Figure 5.8. Selection of multiple timeslices at substrate T=180°C before growth.

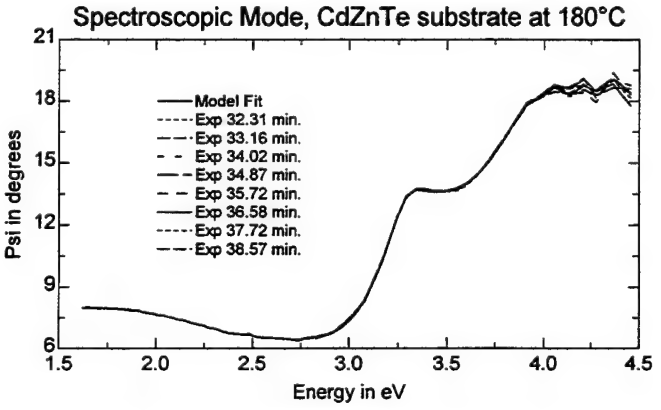

Figure 5.9. Spectroscopic SE data on the CdZnTe substrate before growth.

The next step is to build a simple substrate-only model in WVASE32, using the exsitu CdZnTe optical constants. The substrate optical constants are defined as fit parameters by clicking on the 'n' and 'k' boxes shown on the layer dialog (see Figure 5.10). The 'Normal Fit' menu option is then selected in the WVASE32 'Fit' window to extract the best fit optical constants for the selected SE data (the resulting fit in Psi is shown in Figure 5.9).

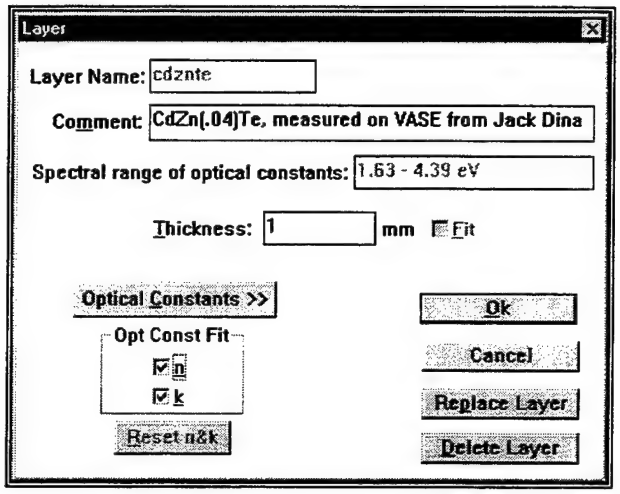

Figure 5.10. Defining the substrate optical constants as fit parameters in WVASE32

The resulting optical constants are saved to a file (named CZT-180) by clicking on the 'Optical Constants >>' button in the substrate layer dialog box (see Figure 5.10). This same process was repeated for the time range when the substrate was nominally at 340°C (time = 14 - 18 minutes, see Figure 5.8) to extract and save another set of CdZnTe optical constants.

Building an Optical Constant Library

Three sets of CdZnTe optical constants are now available: the room temperature constants measured exsitu, and the two sets of insitu constants extracted from SE data at 180° and 340° nominal temperatures in the preceding section. To compare these sets of optical constants, the WVASE32 model shown in Figure 5.11 was built. By selecting the *Data | All Layers (Opt. Const.)* menu option in the WVASE32 'Graph' window, the plot shown in Figure 5.12 was displayed. From this graph, it is clear that the CdZnTe critical point transitions at 3.3 and 3.8 eV broaden and systematically shift to lower energies as the temperature increases, as expected.

2	czt-340	0 Å
1	czt-180	0 Å
0	cdznte	1 mm

Figure 5.11. Model for comparing the CdZnTe optical constants at different temperatures.

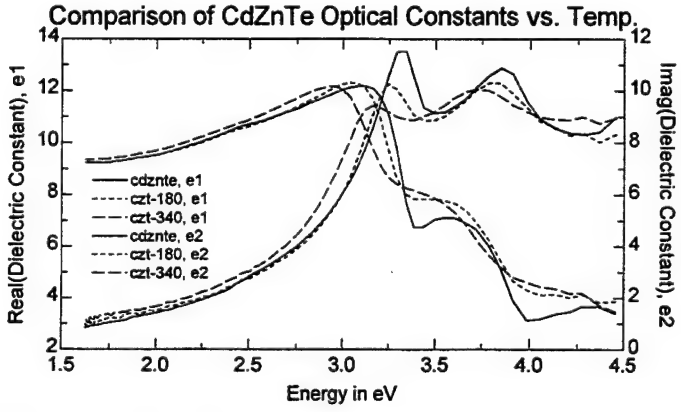

Figure 5.12. Comparison of the CdZnTe optical constants at different temperatures.

To use these temperature dependent optical constants in a practical manner, it is necessary to combine them into a 'library' file which enables the calculation of optical constant spectra at any arbitrary temperature. This is done by interpolating (or extrapolating) between the three discrete sets of CdZnTe optical constants. WVASE32 supports a simple file format to implement such a temperature-dependent optical constant library, which is shown in Table 5.2. This is an ASCII file which can be created by any text editor program (such as the Windows 'Notepad'). The optical constant values from the 3 discrete files are sequentially 'pasted' into this file, separated by blank lines. The syntax of header lines in the file must be exactly as shown in the table. The file must be saved with a '.MAT' extension (for example, CZT-T.MAT), such that WVASE32 can recognize it as a material file.

Temp. File Listing	Comments
CdZnTe, from Run1003	comment line
TEMP	'TEMP' keyword denotes temp library
eV	wavelength units used in this file
NK	optical constants specified in 'n' and 'k'
3	number of optical constant sets
22 180 340	temperatures of optical constant sets
	<blank line>
5 2.548 2.1361	optical constant data at 22°C,
4.99 2.9298 1.7164	column format: eV n k
4.98 2.4409 2.1853	
... ...	etc. for rest of 22°C opt. const. list
	<blank line>
4.4572 2.5553 1.6301	optical constant data at 180°C
4.3662 2.5227 1.5927	
4.2759 2.5981 1.6162	
... ...	etc. for rest of 180°C opt. const. list
	<blank line>
4.4572 2.5555 1.7518	optical constant data at 340°C
4.3662 2.5717 1.702	
4.2759 2.6566 1.6945	
... ...	etc. for rest of 340°C opt. const. list

Table 5.2. File format for WVASE32 temperature dependent optical constant library.

As an example of how the temperature-dependent file works in WVASE32, a model similar to that shown in Figure 5.11 was built, except that the temperature-dependent 'czt-t' file was used in place of the room temperature 'cdznte' file. The temperature of the layer can be specified (or defined as a fit parameter) by clicking on the layer to bring up its dialog box, as shown in Figure 5.13. In this figure, a layer temperature of 260°C is specified. The 'All Layers' optical constants graph shown in Figure 5.14 shows the interpolated CdZnTe optical constants at 260°C compared with the measured spectra at 180° and 340°.

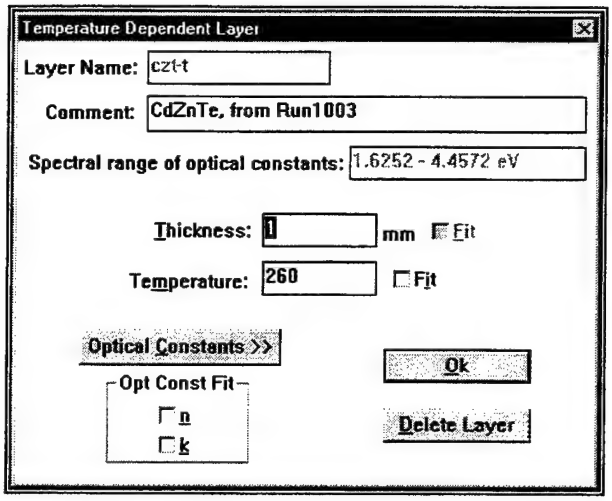

Figure 5.13. WVASE32 temperature-dependent layer dialog box.

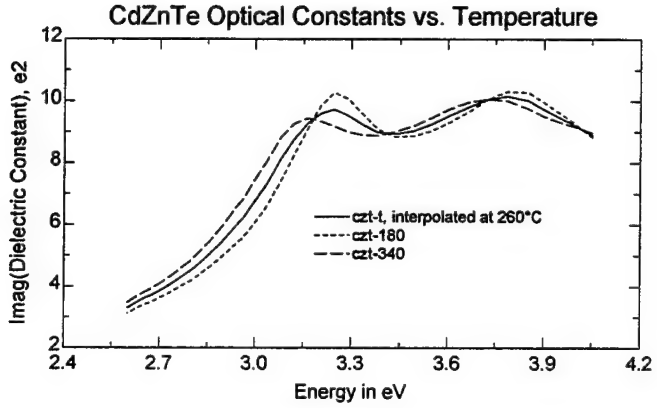

Figure 5.14. CdZnTe optical constants, with interpolated spectra at T=260°C.

Parameterizing an Optical Constant Library

The interpolated CdZnTe optical constants shown in Figure 5.14 do systematically vary between the endpoint spectra. This simple 3 temperature library does an adequate job of generating reasonable CdZnTe optical constant spectra vs. temperature. However, since a simple linear interpolation scheme is employed, the shapes of the critical points structure may be distorted or washed out for temperatures which are farther away from the measured spectra. Extrapolating optical constant spectra outside of the measured temperature range can also be inaccurate. These problems can be improved by measuring and extracting optical constants at more temperatures, but this is not always practical (in the case of CdZnTe, it is not easy to accurately measure the substrate temperature during the cool down phase of the heat-clean procedure).

Another way to improve and extend an optical constant library is to parameterize it. This reduces the number of values which are needed to describe the behavior of the optical constants ('n' and 'k' pairs at each wavelength are needed for each spectra in the simple interpolation scheme), and enforces a systematic consistency across the library. Parameterizing an optical constant library is not a trivial task, as the parameterization model must have enough flexibility to accurately describe the critical point structure which are typically found in semiconductor optical constant

spectra, and at the same time have a limited number of parameters such that it is tractable to build and fit. To satisfy these needs, a 'parametric semiconductor' layer was added to the WVASE32 analysis software.

The WVASE32 parametric semiconductor layer provides a very powerful tool for modeling the optical constants of semiconductors (and metals as well). The details of the parametric semiconductor model as implemented in this layer will be the subject of a future paper to be published by the J.A. Woollam Co. For now, it is sufficient to say that the parametric model used here is based on the summation of Gaussian-broadened low-order polynomial segments. These segments are 'hooked up' in a manner to represent the band structure scheme of a semiconductor. The Gaussian broadening guarantees that the real and imaginary parts of the optical constants are consistent with the Kramers-Kronig causality relationships.

Figure 5.15 shows the dialog box for a parametric semiconductor layer. An explanation on how to use this layer is beyond the scope of this report. Using the parametric model shown in this figure, the optical constant spectra for CdZnTe at 180°C was accurately described over the entire measured spectral range with only 15 adjustable parameters (this is far less than the 88 'n' and 'k' pairs in the tabulated optical constant spectra). The accuracy of the parametric fit to the optical constant spectra is excellent, as shown by Figure 5.16. Graphing the derivatives of the optical constant spectra (see Figure 5.17) enhances the critical point structure, and is thereby a good indicator of the true quality of any parametric fit to an optical constant spectra.

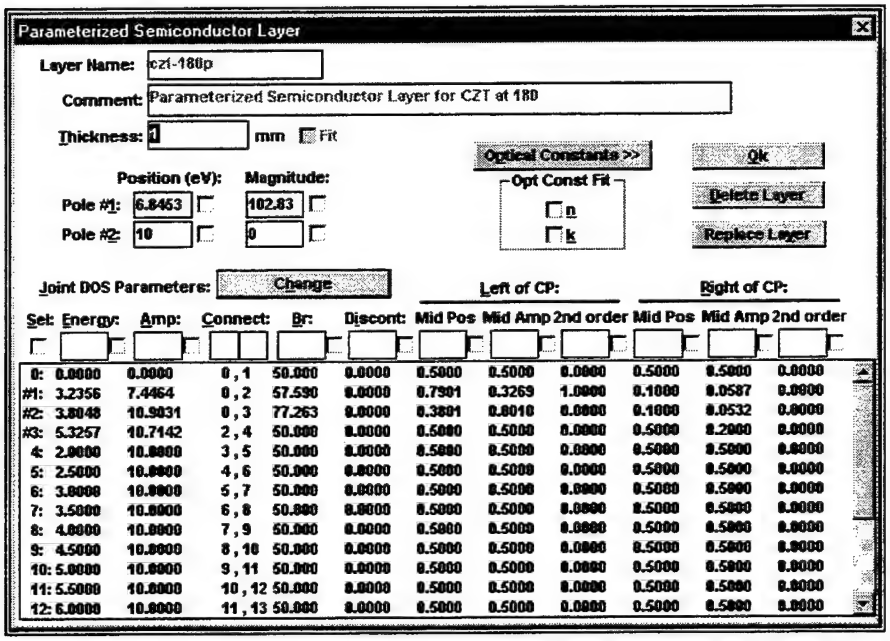

Figure 5.15. WVASE32 Parametric Semiconductor layer (for CdZnTe at 180°).

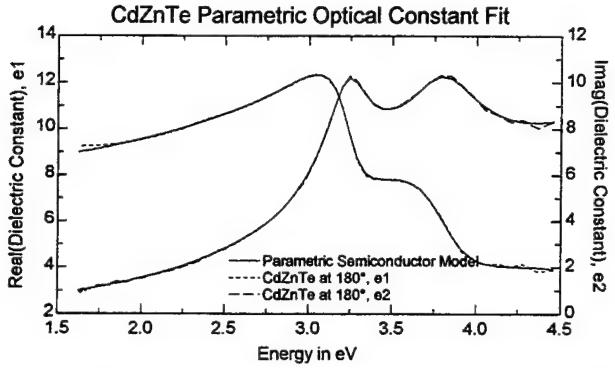

Figure 5.16. Parametric semiconductor model fit to CdZnTe optical constants at 180°C.

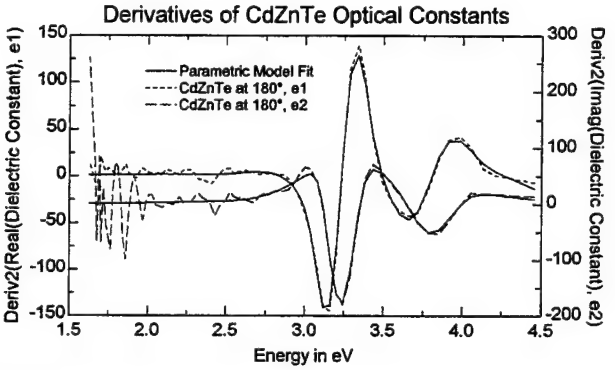

Figure 5.17. 2nd Derivative of the CdZnTe optical constant spectra, and its Parametric Semiconductor model fit.

Global Parametric Optical Constant Fit

While the parametric model fit for the CdZnTe optical constant spectra at 180°C is aesthetically pleasing, it does not in and of itself improve the interpolation ability of a temperature-dependent optical constant library. To meet this requirement, it is necessary to extend the parametric model *across* the temperature-dependent optical constant spectra. This capability is provided by the J.A. Woollam Co. 'Global Parametric Fit' program, which is shown in Figure 5.18 (at the current time, this program is only supported for in-house use). This generalized program supports the creation of parametric temperature and/or composition dependent optical constant libraries.

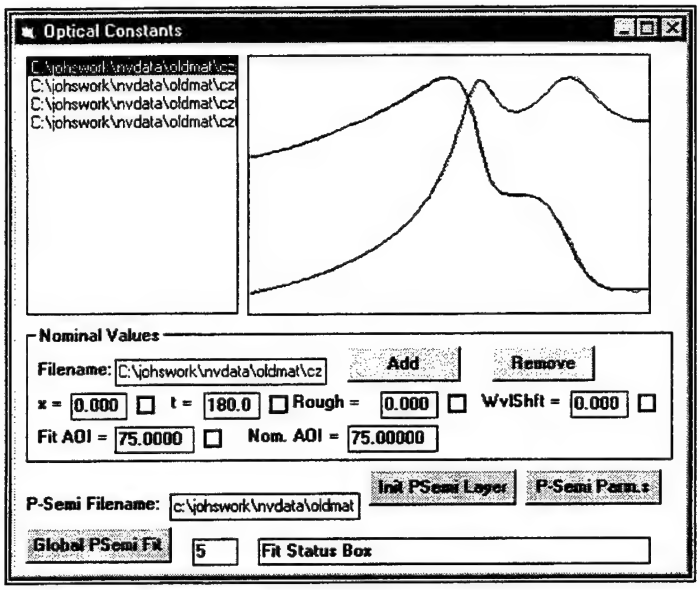

Figure 5.18. J.A. Woollam Co. Global Parametric Fit program.

In the screen shown in Figure 5.18, measured optical constant spectra at various temperatures and/or compositions are added to the list box in the upper left corner of the screen. Parameters which describe the corresponding selected spectra in the list box can be entered and defined as fit parameters in the 'Nominal Values' section. The graph in the upper right corner of the screen shows the global parametric fit model compared to each individual optical constant spectra.

Global parameters for the fit are defined in the dialog box shown in Figure 5.19. Each of the parameters found in the WVASE32 parametric model can itself be defined as a function of temperature and or composition. Mathematically, this can be stated as follows:

$$OC(\text{ Temperature, Composition }) \approx PS(\, p_i\,(x, T)\,) \qquad (5.1)$$

$$\begin{aligned} p_i\,(x, T) = {} & a_i + b_i{\cdot}x + c_i{\cdot}x^2 + d_i{\cdot}x^3 \\ & + e_i{\cdot}T + f_i{\cdot}x{\cdot}T + g_i{\cdot}x^2{\cdot}T + h_i{\cdot}x^3{\cdot}T \\ & + i_i{\cdot}T^2 + j_i{\cdot}x{\cdot}T^2 + k_i{\cdot}x^2{\cdot}T^2 + l_i{\cdot}x^3{\cdot}T^2 \\ & + m_i{\cdot}T^3 + n_i{\cdot}x{\cdot}T^3 + o_i{\cdot}x^2{\cdot}T^3 + p_i{\cdot}x^3{\cdot}T^3 \end{aligned}$$

Equation (5.1) states that the optical constant spectra at a given temperature and composition will be approximated by a Parametric Semiconductor model; each parameter of the Parametric Semiconductor model is in turn a function of composition 'x' and temperature 'T'. In practice, it is rarely necessary to fit for the p_i crossterm parameters in (5.1); very acceptable global fits to the optical constant spectra can usually be obtained by varying only the constant, linear, and quadratic terms in 'x' and 'T'.

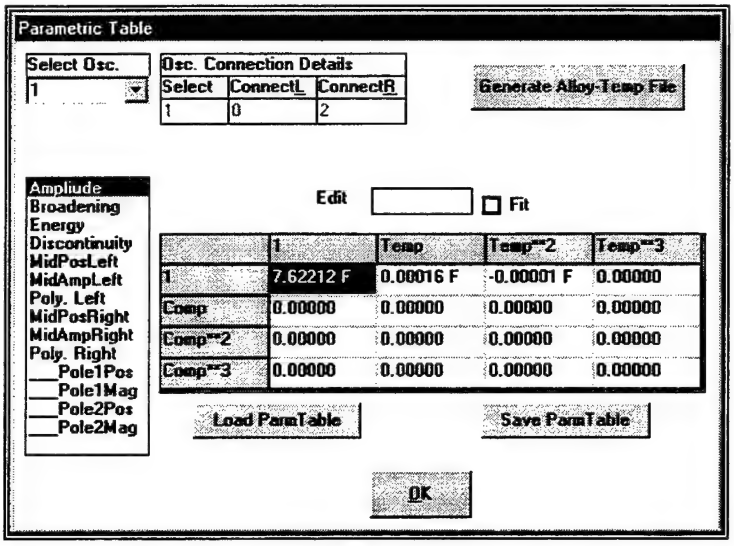

Figure 5.19. Global parameter definition dialog box.

After a global parametric fit has been performed, the results can be saved in a generated temperature-composition grid of optical constant spectra, which is specified in the dialog box shown in Figure 5.20 (the WVASE32 ALLOY-TEMP format is used for this file). WVASE32 can interpolate within this file to generate an optical constant spectra at an arbitrary composition and temperature. While this seems similar to the original interpolation file that was created, there are a few significant differences:

1. The global parametric model enforces a systematic consistency across the optical constant library. Any noise or artifacts in the discretely measured optical constant spectra can be averaged out by the parametric model.
2. The optical constant spectra grid which is saved into the ALLOY-TEMP file can be much denser (more temperatures and compositions) than the original optical constant library. For the reasons given in 1), the global parametric model can even extrapolate optical constant spectra outside the measured range.
3. The interpolation scheme used in the ALLOY-TEMP file is more sophisticated than the simple linear interpolation scheme used in the TEMP file. The ALLOY-TEMP file interpolation scheme uses the critical point energies, which are extracted as a function of temperature and composition by the global parametric fit, to 'shift' the constituent optical constant spectra before performing a weighted average interpolation. These scheme better maintains the shape of the critical point structure, and enables a single ALLOY-TEMP file to cover a wide range of compositions and temperatures without inducing any artifacts in the interpolated optical constant spectra.

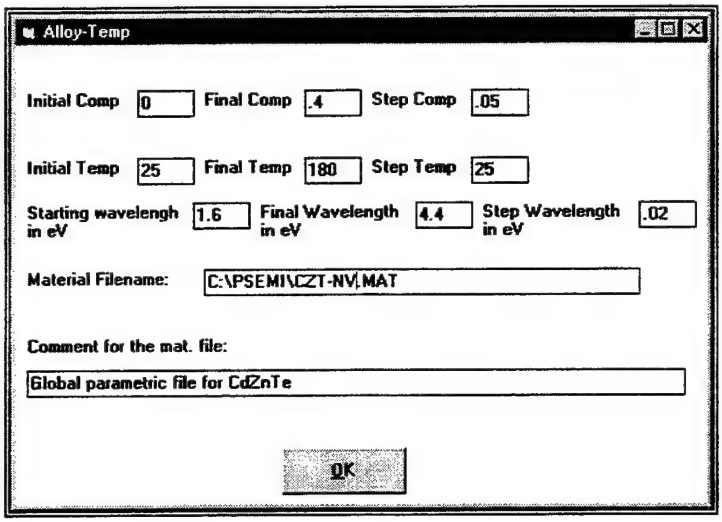

Figure 5.20. Dialog box for saving global parametric fit into an Alloy-Temp file.

Final CdZnTe Optical Constant Library (CZT-NV)

The global parametric temperature-dependent optical constant file for CdZnTe was saved as CZT-NV.MAT. Reading this material file into WVASE32 brings up the dialog box shown in Figure 5.21. Since this is an ALLOY-TEMP file, the dialog box has entries for both temperature and composition. However, since no optical constant spectra with different compositions were included in the global parametric fit (the only composition of interest is the $Cd_{0.96}Zn_{0.04}Te$ substrate material), the composition setting has no effect on the optical constants calculated by the layer.

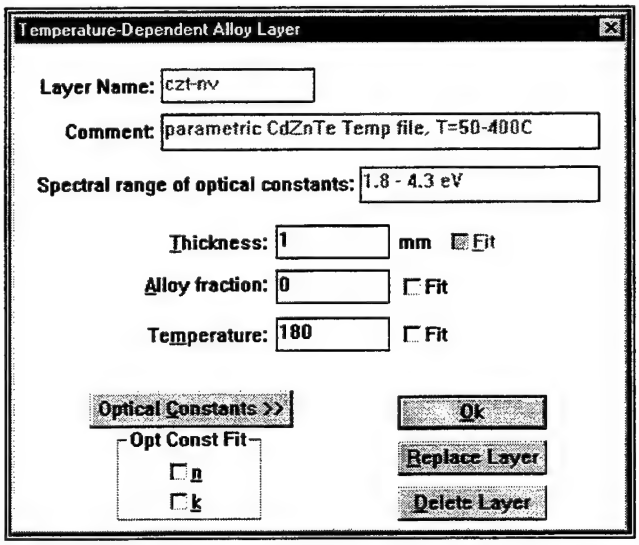

Figure 5.21. Dialog box for WVASE32 Temperature-Dependent Alloy layer.

Figure 5.22 shows a systematic series of CdZnTe optical constant spectra which were calculated from the CZT-NV.MAT ALLOY-TEMP layer in WVASE32. Note the noise-free and systematic behavior of the curves, especially at the critical point structures at higher energies, even when extrapolating to temperatures of 0° and 400° C, which are well outside the range in which optical constants were actually measured. This the optical file was used to extract in real-time the substrate

temperature and overlayer thickness; these results for many different growth runs will be presented in the next chapter.

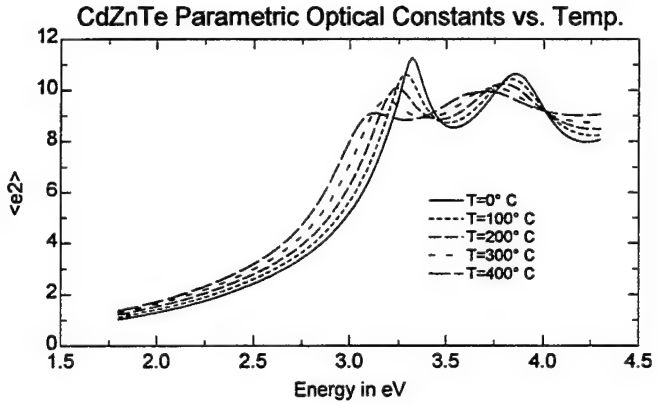

Figure 5.22. Calculated CdZnTe optical constant spectra vs. temperature, using the global parametric ALLOY-TEMP file CZT-NV.MAT.

One extremely important point to make about the temperature-dependent CdZnTe optical constants shown in Figure 5.22: the 'interesting' critical point structure for this material is at energies > 3.0 eV. To acquire data in this spectral range, the extended wavelength range of the M-88 ellipsometer system is required (an M-88 was installed during the later portion of this contract on the NVESD MBE chamber). The M-44 system, which was initially installed on the NVESD MBE chamber, only covers the 1.6 - 2.9 eV spectral range, and is therefore not as sensitive to the CdZnTe substrate temperature.

Building a Film (HgCdTe) Optical Constant Library

The methodology for obtaining the optical constant library for HgCdTe, which is an epitaxially grown layer, is a quite different from that which was used for the CdZnTe substrate. Below are some of the issues which complicate the creation of the HgCdTe optical constant library, which are also relevant for the creation of a growth temperature optical constant library for any ternary semiconductor material.

- The HgCdTe optical constants must be determined as a function of composition. Furthermore, at the beginning of this work, it was also though that temperature-dependent optical constants might be required for HgCdTe as well (it was later shown that this was not the case, as will be discussed in the next chapter). Building a 2-dimensional optical constant library vs. both temperature and composition is certainly more difficult than building a 1-dimensional library in temperature or composition only.
- The ellipsometric spectra for a growing film are more complicated than for a 'static' substrate, at least until the film becomes optically thick (this is shown in phase (3) of Figure 4.20). This is due to the interference oscillations, which dominate the spectra during the initial portion of the growth. Extracting optical constants from SE data with interference oscillations requires a more sophisticated analysis approach, when compared to the simple bulk substrate case.
- Material quality issues, particularly surface morphology, can also be a problem. For epitaxial semiconductor growth, one would like to

assume that the growth proceeds in an atomically smooth fashion. However, some amount of micro-roughness may still be present on the surface. For HgCdTe, which is a particularly difficult material to grow epitaxially, it was not known *a priori* how much a problem this would be. It also can not be assumed that the surface morphology and/or composition, from an optical standpoint, is the same for growing vs. static surfaces. This is especially the case with HgCdTe, in which the Hg is considerably more volatile than the other constituent atoms.

To address these issues, a general methodology for acquiring an insitu composition and/or temperature dependent optical constant library for epitaxially grown semiconductor films was devised, as outlined in the next section.

General Methodology

Ideally, one would like to determine exact, intrinsic, optical constant spectra for the ternary semiconductor system of interest for the complete range of growth temperatures and compositions, by performing insitu SE measurements during a systematic series of growth runs. The layer compositions and/or temperatures for each run should be accurately known and independently verified by other techniques, such as thermocouple, pyrometry, PL, X-ray diffraction, FTIR, etc., such that accurate values can be associated with each measured optical constant spectra. Unfortunately, this objective is **not** achievable in a reasonable time frame, as it would typically require a separate growth run and exsitu sample analysis for each composition. Building an optical constant library across multiple growth runs can introduce some inconsistency into the constituent optical constant spectra due to potential variations in the ellipsometer angle of incidence, material growth temperature, and surface quality.

It is more realistic to determine optical constant spectra for the ternary semiconductor system of interest at a few temperatures in the typical growth regime of the system, and at a limited number of representative compositions. Initially, only nominal values for temperature and composition would be assigned to the determined optical constant spectra. These nominal values may not be accurate in an absolute sense, but they will still enable the reproducible insitu determination of temperature and composition in a relative manner. The nominal values for temperature and composition assigned to each optical constant spectra can be replaced with more accurate values when that information becomes available (through extensive exsitu analysis of subsequently grown samples). For example, using a measured optical constant library with nominal values, one might reproducibly grow layers at 600°C (nominal) of composition 0.25 (also nominal). Two months later, after growing 20 of these layers at the exact same nominal temperature and composition, a very accurate pyrometer measures the actual wafer temperature to be 613°C, and PL measurements indicate that the actual composition is 0.268. These accurate absolute measurements do not invalidate the previously measured optical constant library; only the nominal temperature and composition values need to be replaced to improve the absolute accuracy of the optical constant library. The bottom line is that reproducibility (or relative accuracy) is more important and more readily achievable than absolute accuracy (which can still be developed over time).

The following procedure can be used to measure optical constants at nominal temperatures $t_x = t_1 \ldots t_n$ and compositions $c_y = c_1 \ldots c_m$; the proposed growth structure for this procedure is given in Figure 5.23.

1. Ramp wafer to blow-off oxide, and grow a thick buffer layer (which should be a binary semiconductor, if possible) to provide a smooth,

high-quality surface. During the buffer layer growth, the wafer temperature should be stabilized and maintained at t_1.

2. Grow a layer of composition c_y, with the temperature stabilized at t_x. For optimal results, the layer thickness should be greater than the ¼ wave optical thickness of the material. For semiconductors, a thickness of 500 - 1000Å is adequate. As the optical constants for c_y are different from the optical constants of the buffer layer, interference effects will be observed in the ellipsometric data. By performing a sophisticated growth-rate analysis on this data, highly accurate optical constants of the growing layer can be determined, even when the layer is grown on top of a complex multi-layer structure. In addition, the growth rate that is also extracted from the analysis may be used to estimate the composition of the layer. Because this analysis approach uses multiple instances of ellipsometric data acquired during the layer growth (as opposed to performing a single ellipsometric measurement of the material surface after the growth), the optical constants are 'over determined'. This minimizes inaccuracies in the determined optical constants due to ellipsometer measurement errors (no ellipsometer is perfectly accurate, especially when performing insitu measurements through 'strain-free' windows) and potential material interface and surface non-idealities.
3. Grow a 500 - 1000Å buffer layer with the temperature remaining stabilized at t_x. There are a number of reasons for growing this buffer layer. First of all, during the growth of this buffer layer, the effusion cell temperature of the composition determining element can be ramped and stabilized to the temperature required to grow the next composition. Secondly, optical constants can be extracted from the buffer layer growth (using a growth-rate analysis). If the material quality remains good and the temperature stays at t_x, the optical constants for each buffer layer should be identical. This provides a good self-consistency check of the temperature stability and determined optical constant accuracy. And lastly, the buffer layer provides 'optical contrast' to ensure that the growth of the next composition generates interference oscillations in the ellipsometric data.
4. Repeat steps 2 and 3 for the number of compositions desired.
5. Repeat steps 2-4 for the number of temperatures desired

≈ 400Å buffer layer at temperature t_2
≈ 1000Å layer, composition c_3, temp. t_2
≈ 1000Å buffer layer at temperature t_2
≈ 1000Å layer, composition c_2, temp. t_2
≈ 1000Å buffer layer at temperature t_2
≈ 1000Å layer, composition c_1, temp. t_2
≈ 1000Å buffer layer at temperature t_2
≈ 1000Å layer, composition c_3, temp. t_1
≈ 1000Å buffer layer at temperature t_1
≈ 1000Å layer, composition c_2, temp. t_1
≈ 1000Å buffer layer at temperature t_1
≈ 1000Å layer, composition c_1, temp. t_1
≈1 μm buffer layer at temperature t_1
Substrate

Figure 5.23. Proposed structure to measure optical constant spectra at 2growth temperatures and 3 compositions.

Advantages

1. It can be used with almost any lattice matched ternary semiconductor system, independent of the growth technique (MBE, MOVPE, etc.). A few simple modifications may be required for lattice mis-matched semiconductor systems (smaller layer thicknesses may have to be used to prevent the structure from relaxing). Also, for some material systems and growth technologies, it may not be possible to grow a binary buffer layer between each composition, but many of the benefits of the method can still be maintained even without the inclusion of the buffer layers in the growth structure.
2. The entire library of optical constants is determined on the same wafer and in the same experiment. This eliminates errors in wafer angle of incidence reproducibility, and minimizes errors in temperature reproducibility.
3. The procedure is simple enough (a single 1-3 hour growth run) that it could easily be performed on different growth chambers to account for small differences in window effects, material quality, growth methods, etc. At this point, there is no guarantee that the measured optical constant library would be universally applicable for insitu growth control on other chambers, although this would certainly be a desirable goal.
4. Determining the optical constants of the material during growth is far more accurate (and useful) than measuring the optical constants of a static surface.

Multi-layer MCT / HgTe 'Optical Constant' Structure

The multi-layer HgCdTe/HgTe structure shown in Table 5.3 was grown to extract $Hg_{1-x}Cd_xTe$ optical constants as a function of composition. The multiple HgTe buffer layers served a couple of purposes:

1) They verified that the surface quality (from an optical standpoint) remained constant throughout growth (by observing the exact same optical constants for all HgTe layers)

2) They provided optical contrast such that the interference oscillations from the growth of subsequent MCT layers could be used to determine growth rates.

Two MCT layers were also grown at the exact same nominal composition to verify that the accuracy and/or reproducibility of the MCT optical constants was not influenced by the HgTe buffer layers.

With the current technology, high quality MBE growth of HgCdTe can only occur in a very narrow temperature window (180 - 190° C). The temperature dependence of material optical constants is often smaller than the composition dependence. Since ideally HgCdTe is grown only within this narrow temperature window, it was decided to determine compositionally dependent optical constants only at a single typical growth temperature. It would be difficult to systematically vary the temperature during HgCdTe growth anyway, as with current MBE technology, it is hard enough to keep the temperature 'somewhere' within the acceptable window. The results presented in the next chapter demonstrate that for MBE growth of HgCdTe, a composition dependent optical constant library acquired at a single growth temperature is adequate.

Nominal Layer Composition	Nominal Layer Thickness (Å)	CdTe Cell Temperature	Ellipsometer Growth Rate (Å/sec)
MCT x=.32	10000	644	4.28
HgTe	2000	-	3.03
MCT x=.27	10000	638	4.12
HgTe	2000	-	3.05
MCT x=.17	10000	626	3.71
HgTe	2000	-	3.06
MCT x=.22	10000	632	3.92
HgTe	2000	-	3.09
MCT x=.22	10000	632	3.94
CdZnTe Substrate	-	-	-

Table 5.3. Multi-layer HgTe / MCT structure grown to determine HgCdTe composition-dependent optical constant library at a single growth temperature.

Figure 5.24 shows a portion of the raw ellipsometric data from the multi-layer growth run. Each time a new layer is grown, pronounced interference oscillations are apparent in the data. The nominal layer thickness (1 μm) of the MCT layers were large enough such that they became optically thick. This large thickness was chosen such than exsitu EDX measurements could be performed on a cleaved edge of the wafer. Thinner thicknesses (2000Å) were used for the HgTe buffer layers, to minimize any potential degradation in the crystalline quality of the structure caused by the slightly lattice mis-matched HgTe layers.

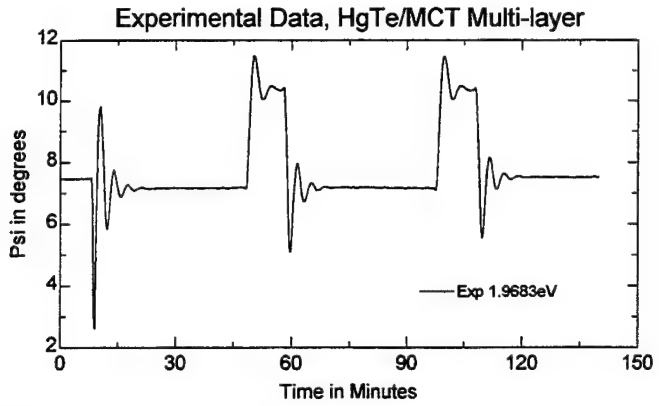

Figure 5.24. Insitu ellipsometric data at a single wavelength during the first half of the multi-layer growth structure of Table 5.3.

The growth rates reported in Table 5.3 were extracted from a growth-rate analysis of the ellipsometric data, as will be described in the next section. However, the reported MCT growth rates are somewhat of an approximation, depending on which time range was used to extract the growth rate (the growth rate appeared to be slightly higher when each MCT layer growth was initiated, possibly due to flux transient effects from the CdTe effusion cell).

For continuity, the optical constants which were extracted from the multi-layer MCT / HgTe growth structure will be presented next (a discussion of the growth-rate analysis is deferred to the following section). The very nice systematic curves extracted for the MCT optical constants (at growth temperature) vs. composition are shown in Figure 5.25 and 5.26.

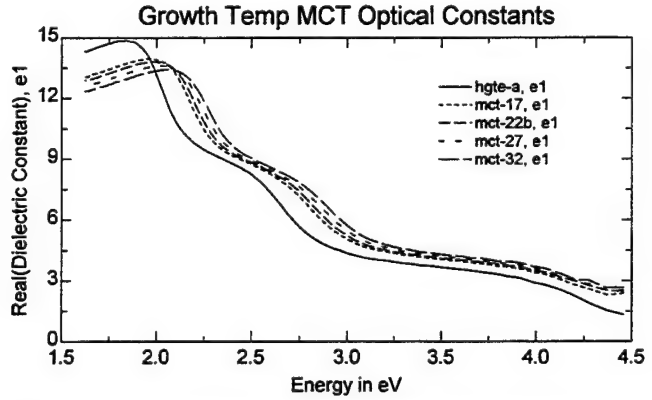

Figure 5.25. Real part of the $Hg_{1-x}Cd_xTe$ dielectric constant at 180°C.

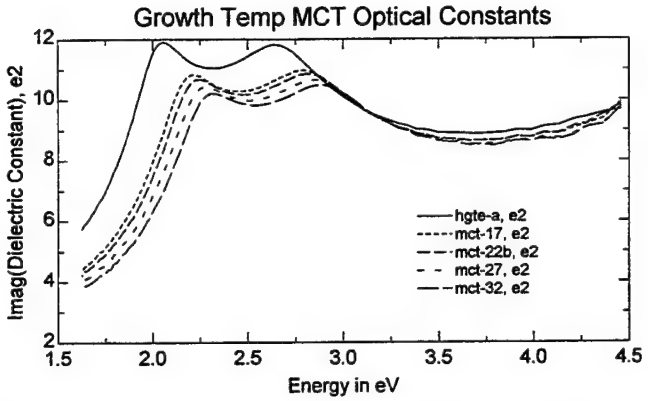

Figure 5.26. Imaginary part of the $Hg_{1-x}Cd_xTe$ dielectric constant at 180°C.

While it was possible to extract these optical constants from a growth rate analysis of the dynamic SE data, for the optically thick MCT layers a simple bulk model was used instead. This is same the multiple spectroscopic timeslice approach which was used to extract the temperature-dependent optical constants of the CdZnTe substrate. For each composition, the multiple timeslices were spaced throughout the optically thick region of the MCT film growth. Optical constants derived in this manner more closely mimic the nature of the insitu SE data which is observed throughout most MCT growth runs, which consist of 4-10 hour runs at a single constant composition (for >90% of the run, the layer is optically thick).

These graphs shown in Figures 5.27 and 5.28 verify the optical quality and reproducibility of the different layers throughout the growth of the entire multi-layer structure, thereby providing a very useful self-consistency check on the extracted optical constant spectra. The HgTe optical constants were extracted from a growth-rate analysis of the dynamic SE data acquiring during the each of the 4 HgTe buffer layers.

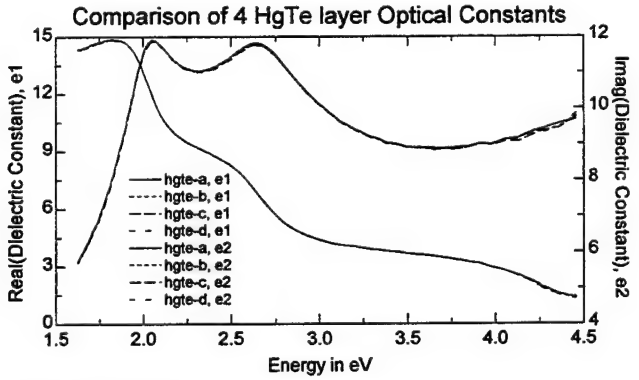

Figure 5.27. Reproducibility of the HgTe optical constants throughout the growth of the multi-layer structure.

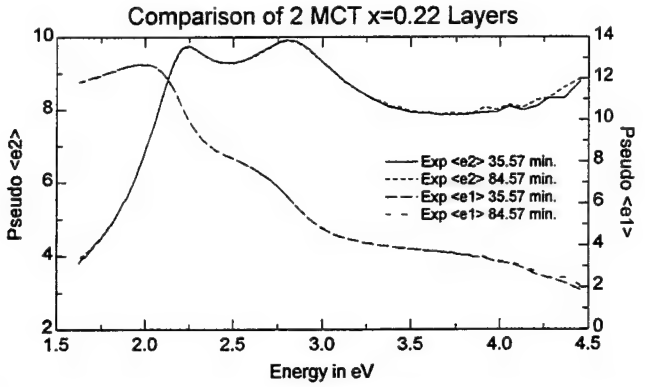

Figure 5.28. Reproducibility of the two MCT layers with the same nominal composition.

Composition-Dependent Optical Constant Library

In a manner similar to the CdZnTe substrate temperature-dependent library, the MCT optical constant spectra shown in the previous section can also be easily assembled into a composition-dependent optical constant library. The procedure is the same, and the syntax ASCII file format is only slightly different, as shown in Table 5.4.

Alloy File Listing	Comments
HgCdTe, from Run1004	comment line
ALLOY	'ALLOY' keyword denotes comp. library
eV	wavelength units used in this file
NK	optical constants specified in 'n' and 'k'
5	number of optical constant sets
0 .17 .22 .27 .32	compositions of optical constant sets
0	# of 'critical points' for shifting interp.
	<blank line>
5 2.548 2.1361	optical constant data at x=0,
4.99 2.9298 1.7164	column format: eV n k
4.98 2.4409 2.1853	
... ...	etc. for rest of x=0 opt. const. list
	<blank line>
4.4572 2.5553 1.6301	optical constant data at x=0.17
4.3662 2.5227 1.5927	
4.2759 2.5981 1.6162	
... ...	etc. for rest of x=0.17 opt. const. list
	<blank line>
4.4572 2.5555 1.7518	optical constant data at x=0.22
4.3662 2.5717 1.702	
4.2759 2.6566 1.6945	
... ...	etc. for rest of x=0.22 opt. const. list
and so on. for the rest of the compositions ...	

Table 5.4. File format for WVASE32 composition dependent optical constant library.

'Global' Parameterization of the MCT optical constants

For the same reasons it was performed with CdZnTe, global parameterization was also performed on the MCT optical constants. In this case, however, optical constant spectra as a function of both temperature and composition was included in the global parameterization. In addition to the MCT growth temperature optical constants at x

= 0, 0.17, 0.22, 0.27, and 0.32 (nominal) from the preceding section, room temperature MCT optical constants at x = 0 and 0.20 (from literature data by Aspnes) were included in the global fit. To simplify the optical constant parameterization, only the 1.8 - 3.4 eV spectral range data was included in the fit, as this region contains the critical point structures which are most sensitive to composition.

For this fit, assumptions still had to be made about the compositions which should be assigned to the optical constant spectra extracted from the growth of the multi-layer MCT/HgTe structure. The Table 5.5 shows the available composition values; except for one EDX composition, all of the values in the table are in systematic agreement with each other. The 'Growth Rate' compositions were calculated assuming unity sticking coefficients for the group II atoms, and the SE determined growth rates from Table 5.3 ($x = (R_{MCT} - R_{HgTe}) / R_{MCT}$). However, since the unity sticking coefficient assumption is not completely valid for HgCdTe growth, it is still difficult to conclusively say that the 'Growth Rate' compositions are more *accurate* than the EDX compositions. For the purposes of setting up the parameterized optical constant fit, the nominal composition for the first MCT layers (x=0.22) was assumed to be accurate (some previous FTIR data confirmed this assumption, and the 'Growth Rate' composition is also in good agreement). The composition of the other layers was then assumed to scale in multiples of 0.04, i.e., x = 0.18, 0.22, 0.26, and 0.30. These compositions are close to those extracted from the ellipsometer 'growth rates', and are still in reasonable agreement with both the nominal and EDX compositions. These *assumed* compositions are corrected in the next chapter by correlating FTIR and ellipsometer compositions from subsequent growth runs.

Nominal Composition	Composition from 'Growth Rates'	EDX Composition
0.32	0.292	0.279
0.27	0.260	0.240
0.17	0.178	0.166
0.22	0.219	0.191
0.22	0.215	0.270

Table 5.5. MCT Compositions from Multi-layer MCT/HgTe Structure

The resulting global parameterization allows WVASE32 to generate MCT optical constants at any temperature and composition (realistically, for T=0-250 C and x=0-0.35). It is then possible to simultaneously fit for the MCT composition and temperature (assuming that they are *uncorrelated*), and thereby by study the potential effects of temperature/composition interaction on the ellipsometric data analysis, which is also done in the next chapter. The graphs in Figures 5.29 and 5.30 show MCT optical constants that were generated from the global parametric model, illustrating the ability of the model to calculate very systematic curves even when extrapolating far outside the nominal temperature and composition values.

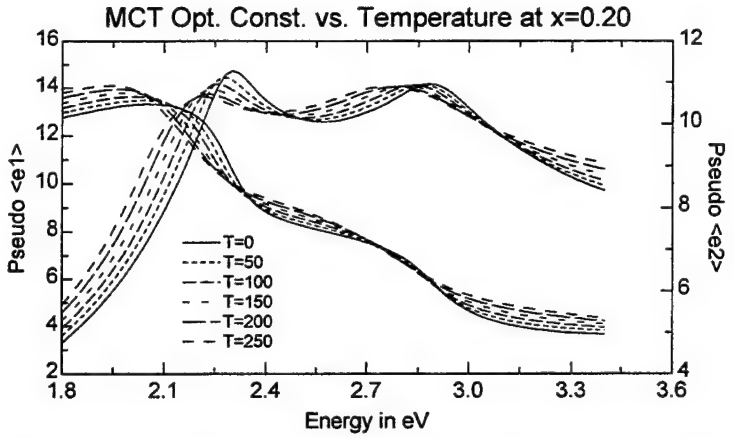

Figure 5.28. Calculated HgCdTe optical constants vs. temperature (at x=0.20) from the global parametric model.

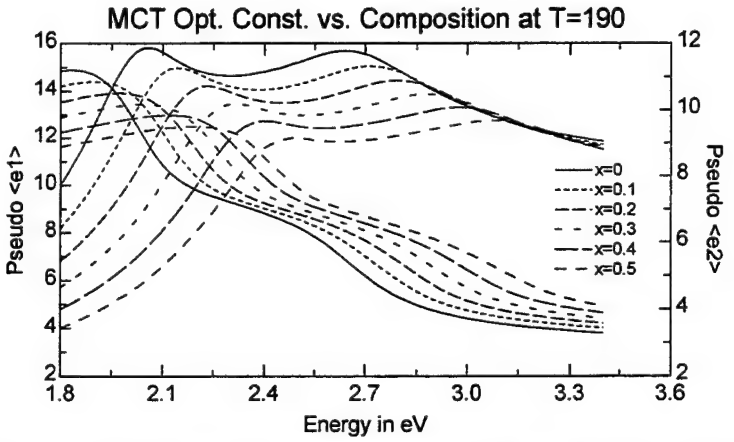

Figure 5.29. Calculated HgCdTe optical constants vs. composition (at T=190) from the global parametric model.

Growth-Rate Analysis of Dynamic Data

As mentioned earlier in this chapter, a more sophisticated data analysis approach is required to extract optical constants from SE data acquired during film growth in which interference oscillations are present. Consider for example the data shown in Figure 5.30. In this graph, the data before the vertical line at time=108 minutes are acquired during the growth of a HgTe buffer layer, and the data after the line are for the 3rd MCT layer (nominal composition = 0.17).

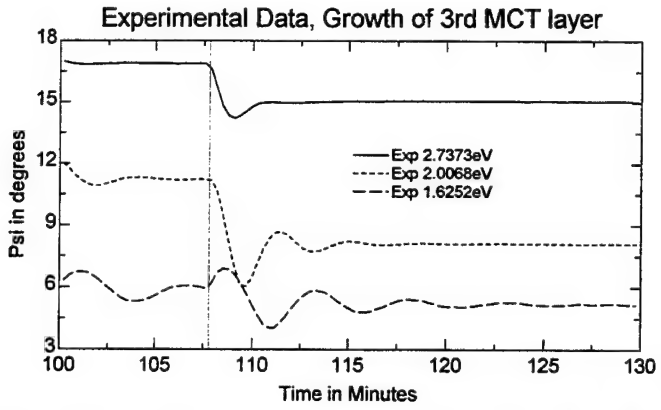

Figure 5.30. Dynamic SE data at 3 wavelengths from the growth of the 3rd MCT layer of the structure shown in Table 5.3.

Virtual Interface Approximation

Since the HgTe buffer layer is not optically thick, it is not possible to model this data set with a single MCT film grown on a HgTe substrate. However, the other alternative of building an optical model with all of the previously grown layers is not very attractive either, from a modeling complexity standpoint. To simplify the data analysis, the 'Virtual Interface' approximation is employed, as is schematically represented in Figure 5.31.

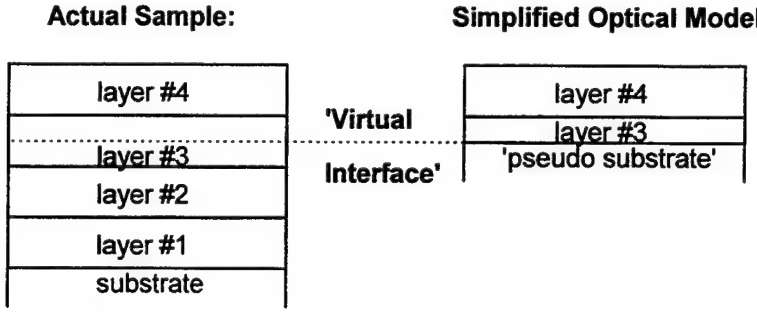

Figure 5.31. Schematic of the 'Virtual Interface' approximation.

In the 'Virtual Interface' (VI) approximation, the previous growth history of a sample is encapsulated into a single 'pseudo substrate'. This 'pseudo substrate' can be defined anywhere within the sample, and does not have to correspond an actual interface in the structure, hence the term 'Virtual' interface. For example, to determine the thickness of the 21st layer which is being grown on top of a 20 layer stack, a virtual interface could be 'dropped' after the growth of the 20th layer, and a simple optical model consisting of the 'pseudo substrate' defined at the virtual interface with a single layer could be used to extract the top layer thickness. This is certainly much easier than building a 21 layer optical model and fitting for the top layer thickness, which would be both computationally inefficient and potentially inaccurate, as any errors in the layer thicknesses and/or optical constants of the bottom 20 layers could directly propagate into errors in the top layer thickness.

The optical constants for the 'pseudo substrate' are found by directly transforming the Psi and Delta values measured at the growth time corresponding to the position of the virtual interface, using equation (2.8). (Actually since a RAE ellipsometer does not measure the 'handedness' of the ellipsometric Delta parameter, there is an ambiguity in the sign of the <e2> value; the WVASE32 software numerically

resolves this ambiguity by trying both roots, and picking the solution which best fits the data.) At least for semiconductor structures, the 'pseudo substrate' optical constants obtained in this manner very accurately encapsulate the optical behavior of all previously grown layers. The VI approximation is nearly exact when all of the materials in a layer stack have high and relatively similar indices of refraction (such as compound semiconductor structures). However, the approximation completely breaks down for lower index materials (such as multi-layer dielectric film stacks). The accuracy of the VI approximation can be numerically verified by performing multi-layer model simulations in the WVASE32 software.

While the term 'Virtual Interface' only recently appeared in the literature, the VI approximation has been widely used (possibly unknowingly or unwittingly) for a much longer time. When measuring multi-layer film stacks (poly Si on oxide on Si, for example) in Si technology with the single wavelength ellipsometer systems which are prevalent in most fabs, it is common for technicians to measure ellipsometric data after two layers have been deposited, and invert this data into an 'n' and 'k' for an 'effective' substrate. After the 3rd layer is deposited, the wafer is remeasured and the thickness of the 3rd layer extracted from a simple *one* layer optical model using the 'effective' substrate optical constants from the first ellipsometric measurement. This procedure, which works to varying degrees of accuracy depending on the optical constants and thicknesses of the constituent layers in the structure, implicitly makes use of the VI approximation.

FastDyn Analysis Layer

In the WVASE32 analysis software, there are two ways to define a virtual interface for use in modeling dynamic SE data. The first approach is to build a model using the 'VIRTUAL.MAT' layer as the substrate combined with a 'DELAY.MAT' layer to specify when the layer growth begins. This approach, while still supported in WVASE, has been supplanted by the 'FASTDYN.MAT' dynamic data analysis layer. In addition to more conveniently implementing the virtual interface approximation, the FastDyn layer provides highly optimized routines for modeling in real-time the growth of semiconductor layers.

While some researchers are convinced that the real-time analysis of ellipsometric data at even a single wavelength requires special data processing algorithms running on exotic microprocessor hardware or 'neural networks', the commercially available WVASE32 FastDyn analysis layer proves them all completely **wrong**. With the highly optimized FastDyn routines, dynamic SE data with 88 wavelengths at 10's of timeslices, i.e. 1000's of Ψ-Δ experimental data point pairs, can be simultaneously analyzed (using the same L-M regression algorithm techniques discuss in chapter 2) in a few seconds on a standard Pentium-class personal computer system.

The FastDyn analysis is still subject to the caveats of the L-M regression algorithm, most notably, poor initial starting values may lead to inaccurate determination of the model parameters. However, in the reasonably well controlled MBE growth environment, the initial starting values for model fit parameters such as growth rate and composition must be known (within 10-40% at the very least, which is close enough for the regression algorithm) if material of good quality is to be grown.

The main advantage of the FastDyn algorithm is that it can extract the optimum composition, temperature, and/or layer growth rate which provides the best fit to *all* of the available dynamic SE data. To optimize the fit sensitivity to specific parameters such as composition, it is certainly possible to use restricted spectral and time ranges of ellipsometric data in the FastDyn analysis. This can further reduce the calculation time of the algorithm, such that sample parameters with excellent precision can be extracted in less than 1 second. This time is less than the SE data

acquisition time in most MBE environments, and is completely adequate for real-time monitoring and control in most semiconductor growth applications.

The layer dialog box for the WVASE32 'FastDyn' layer is shown in Figure 5.32. To use this layer in WVASE32, build a model where 'FASTDYN.MAT' is the substrate, and the layer on top of the substrate specifies the optical constants of the growing film (the top line in the 'FastDyn' dialog box displays the name of this file for reference), as shown in Figure 5.33. The thickness of the top layer is not used in the FastDyn analysis algorithm.

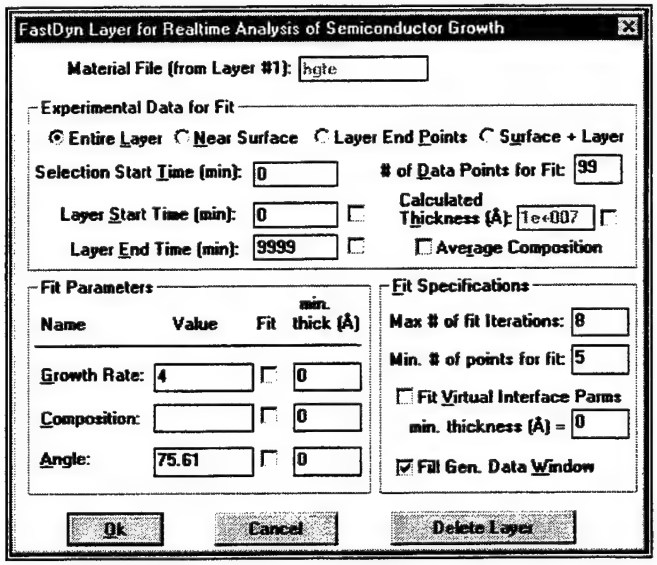

Figure 5.32. Dialog box for the WVASE32 FastDyn analysis layer.

1	hgte	0 Å
0	fastdyn	1 mm

Figure 5.33. WVASE32 model for using the FastDyn analysis layer.

While the appearance of Figure 5.32 is daunting, using the FastDyn layer to analyze dynamic SE data is fairly straightforward. The first step in performing a FastDyn analysis is to specify which data will be used in the fit. This specification is done using a combination of the WVASE32 'Experimental' window's *Range Select* menu option (see Figure 4.14), and the FastDyn layer dialog box itself. Since the FastDyn analysis is geared exclusively towards dynamic data, it is important to disable the 'Spectroscopic mode' checkbox in the *Range Select* dialog box.

The other important things to specify in the *Range Select* dialog box are the time range for the selected data, and the wavelength ranges for fitting and graphing the data. When fitting for layer optical constants, all of the available wavelengths are usually selected 'For Data Fitting'. When using an existing optical constant library, it is common to select a wavelength range for fitting which has the highest sensitivity to the parameter of interest (for example, the 1.8 - 3.4 eV spectral range is more sensitive to HgCdTe composition). When selecting the 'For Graphing Only' wavelengths, is best to highlight a few discrete wavelengths which are evenly spaced across the fitting wavelength spectral range. Next, specify the time range which contains the subset of dynamic data to be analyzed.

When analyzing layer growth, it is important to consider the possibility of non-uniform growth rates and/or composition. Since FastDyn assumes a constant layer

growth rate and optical constants, any variation in these values during the time period of the analysis will degrade the fit. This is not really a limitation of FastDyn, it simply means that a smaller time range of data should be selected for the analysis. In fact, performing the analysis with different time ranges of data is a good way to verify the uniformity of the layer growth. *When selecting a time range for extracting optical constants, it is especially important to stay away from the growth initiation interfaces, as K-cell flux transients, interface mixing, and/or surface roughening, which can occur at these interfaces can degrade the FastDyn fit and corrupt resulting optical constants and growth rates.*

The FastDyn analysis layer adds another level of data selection on top of the basic time and spectral ranges specified in the *Range Select* dialog box; these options are found in the 'Experimental Data for Fit' section of the FastDyn dialog box. The most important value in this section is the '# of Data Points for Fit:' entry. This number specifies the maximum number of timeslices of SE data that will be used in the analysis (keep in mind that even though the dynamic data is *displayed* at only a few wavelengths, *all* of the selected wavelengths are still used for *fitting*). The distribution of the timeslices with respect to the selected experimental data set is determined by highlighting the appropriate 'radio' button (Figure 5.34 graphically illustrates the different FastDyn data selection criteria):

- **Entire Layer**: The timeslices are equally distributed across the selected experimental data range. This is useful for modeling the growth of an entire layer.
- **Near Surface**: The timeslices are consecutively chosen at the end of the selected time range. In this manner, the data for the analysis comes only from the 'Near Surface' of the growing layer
- **Layer End Points**: In this mode, half of the data points are consecutively chosen starting at the beginning of the selected time range, and the other half are chosen at the end of the time range. This may be useful when the growth rate is not constant throughout the whole layer.
- **Surface + Layer**: FastDyn will perform two separate data fits in each analysis, one using the 'Entire Layer' mode (which provides a more accurate growth rate), and another using the 'Near Surface' mode (which provides the near surface composition, but using the more accurately determined growth rate from the 'Entire Layer' mode fit). If the 'Average Composition' box is checked, FastDyn will also return the average composition value from the 'Entire Layer' fit.

At the first timeslice in the selected data set, a virtual interface is implicitly defined and calculated by the FastDyn analysis algorithm.

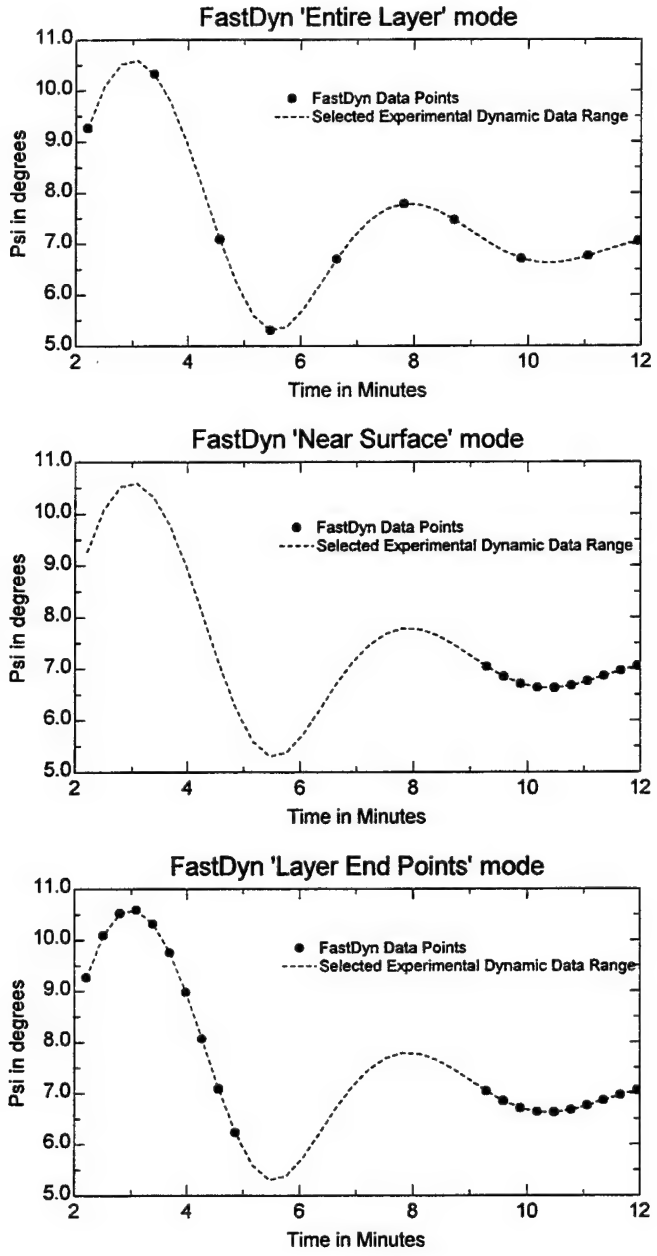

Figure 5.34. FastDyn data selection modes, with the '# of Data Points for Fit:' = 10.

The 'Selection Start Time (min):' entry can override the time range of the dynamic data which is defined using the *Range Select* command. If this entry is set to a time greater than the starting time of the displayed dynamic data, only data points with times greater than (or equal to) the 'Selection Start Time' will be used in the FastDyn fit (if the 'Selection Start Time' is less than the starting time of the displayed data, the entry is not used by FastDyn). In this way, the user can view a larger portion of the dynamic data set (by setting the *Range Select* appropriately), while at the same time FastDyn can analyze a desired subset of the displayed data.

The 'Layer Start Time (min):' and 'Layer End Time (min):' specify the starting and ending times for the layer growth. If the layer is growing throughout the duration of the specified experimental time range, leave these entries at their defaults values of '0' and '9999' respectively. This options are useful for precisely quantifying the

thickness of a grown layer, and should be used with the FastDyn 'Entire Layer' mode. The 'Calculated Thickness (Å)' entry is calculated by multiplying the FastDyn determined growth rate times the difference between the Start and End layer times (or the last time in the selected experimental data range and the Start time, if the End Time is not within the selected range). This thickness is a parameter which is *derived* from the growth rate fit; however, for the purposes of reporting this value to the user and/or other external programs, it can also be defined as a pseudo fit parameter by checking the adjacent box. FastDyn assumes that the material interfaces at the beginning and end of the layer growth are abrupt and ideal. Figure 5.35 illustrates the use of these entries on a typical ellipsometric layer growth trajectory. These parameters can also be defined as fit parameters, such that FastDyn can accurately determine the layer growth starting and ending times by fitting to the experimental data.

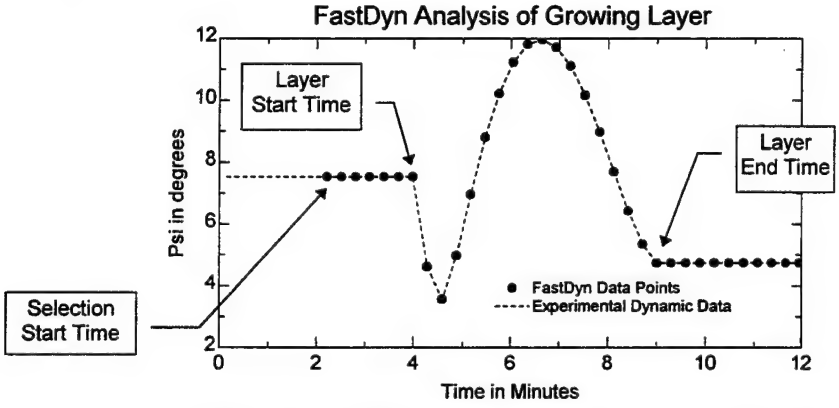

Figure 5.35. FastDyn settings to describe the growth of a layer.

The 'Fit Parameters' section of the FastDyn layer dialog box defines which layer parameters will be fit during the FastDyn analysis. Starting values for the Growth Rate, Composition (if the material file specified for layer #1 is an ALLOY or ALLOY-TEMP file), and Angle (of incidence) can be entered in the corresponding boxes, and fit parameters can be defined by clicking on the adjacent boxes. The 'min. thick (Å)' boxes specify the minimum layer thickness which is required before FastDyn will actually fit the parameter. For example, if the layer is too thin, there will not be much sensitivity to the composition of the layer, such that fitting for the composition may not provide acceptable accuracy (or even worse, it may cause the composition parameter to wander off to an unphysical value which prevents the fit from converging to the correct value in subsequent fits). If the 'min. thick (Å)' value is set to 100, the composition will actually be 'fit' only when the layer thickness (as calculated by the previous FastDyn analysis) exceeds 100Å.

The 'Fit Specifications' section determines how the L-M regression analysis operates for the FastDyn analysis of the data. The 'Max # of fit Iterations:' specifies how many iterations the L-M algorithm will perform before returning the fit results. When fitting dynamic data, the initial parameter starting values are usually quite close to the final best fit values, such that a lower number for the 'Max Iterations' (in the 4 - 10 range, for example) is usually acceptable. Lower numbers also reduce the FastDyn analysis time as well. The 'Min. # of points for fit:' number works in a manner similar to the 'min. thick' settings found in the 'Fit Parameters' section: FastDyn will not actually perform a fit until the number of selected timeslices equals or exceeds the 'Min. # of points for fit' value. This is very helpful when analyzing dynamic data in real-time. A appropriate FastDyn model can be built, and the fit can be started at the same time the layer growth is initiated. The FastDyn analysis will

not begin fitting the data until enough information exists (i.e., the 'Min. # of points' are available, and the 'min. thick' has been reached) to robustly extract the desired parameters. The 'Fit Virtual Interface Parms' checkbox can be used to define the pseudo substrate optical constants (which are normally directly inverted from the Psi and Delta values at the virtual interface) as fitting parameters. This slightly increases the FastDyn analysis time, but it can increase the accuracy of the fit somewhat by minimizing the effect of noise in the experimental Psi and Delta data on the virtual interface calculation. The 'Fill Gen. Data Window' checkbox tells FastDyn to fill the WVASE32 'Generated Data' window with ellipsometric data calculated from the best fit model. This data is subsequently displayed in the 'Graph' window, where the quality of the FastDyn fit can be visually inspected. Normally this option is left on, but to slightly reduce the FastDyn analysis time, it can be turned off.

Extracting Optical Constants with FastDyn

The FastDyn analysis algorithm will now be used to extract optical constants of the layers grown in the MCT / HgTe structure. Before proceeding, it is important to verify that the WVASE32 software has enough memory allocated to perform the analysis. In the WVASE32 *Global* | *Defaults* menu option, click on the 'Memory Allocation' button. The resulting dialog box in Figure 5.36 shows the appropriate memory allocation values which should be used for the FastDyn analysis of optical constants with data acquired by an M-88 system.

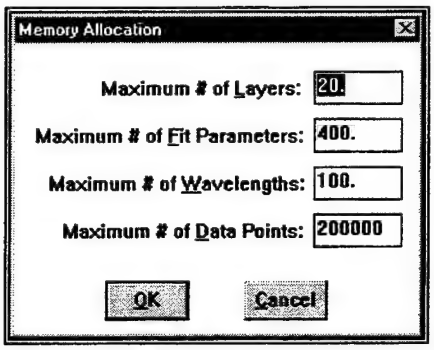

Figure 5.36. Typical 'Memory Allocation' settings for FastDyn optical constant analysis.

The general strategy when extracting optical constants for a growing layer is to start with an optical constant file which is fairly similar to the growing material. Fixing the growth rate at its nominal value, the optical constants are first fit over a very limited time range. The time range of dynamic data is then incrementally increased in subsequent fits, and the growth rate is also added as a fit parameter. Finally, the selected time range is set to include most of the dynamic data acquired during the layer growth, and the resulting FastDyn analysis (in which the virtual interface parameters are also fit) returns the best optical constants and growth rate which represent the entire grown layer. This procedure helps the L-M regression algorithm to 'lock on' to the correct branch for the optical constants. If you try to start the FastDyn optical constant fit using the full layer growth time range with even slightly wrong starting optical constants or growth rate, the L-M algorithm will probably 'get lost' and return a poor data fit and unphysical optical constant values.

Consider once again the 3rd MCT layer growth shown in Figure 5.30. A step-by-step procedure for extracting the optical constants of this layer is as follows:

1. *Range Select* a small time range of data near (but not too close to) the beginning of the layer growth, for example t = 110 - 112 minutes. Build a WVASE32 model as shown in Figure 5.33, and set up the

FastDyn parameters as shown in Figure 5.32. The 'hgte' optical constant file is from the standard WVASE32 optical constant library, and contains room temperature HgTe optical constants. These will serve as 'reasonable' starting values for the growth temperature optical constants of the MCT layer. To define the optical constants of the growing layer as fitting parameters, click on the 'n' and 'k' boxes in the 'Opt Const Fit' section of the 'hgte' layer dialog box. In the FastDyn layer, the growth rate is fixed at a nominal value of 4 Å/second. The Angle of incidence was fixed at a value of 75.61° (which was determined by a substrate data fit), and held *fixed* throughout the subsequent optical constants analysis. Using these settings, perform a *Normal Fit* in the WVASE32 'Fit' window.

2. Next, extend the selected time range to t = 110 - 115 minutes. Add the FastDyn Growth Rate as a fit parameter, and again perform a *Normal Fit.*

3. Finally, select the t = 110 - 130 time range. Add the 'Virtual interface' parameters to the fit, and perform a *Normal Fit.* The resulting data fit is shown in Figure 5.37, and the extracted optical constants from the fit are shown in Figure 5.38. The growth rate from this fit was 3.7905±0.00609 Å/second.

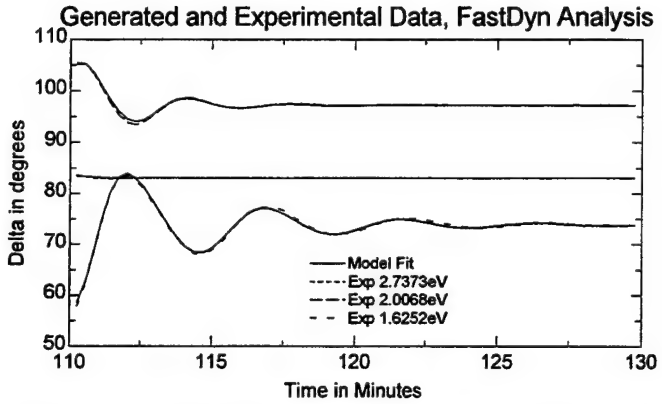

Figure 5.37. Data fit from FastDyn analysis of MCT layer growth.

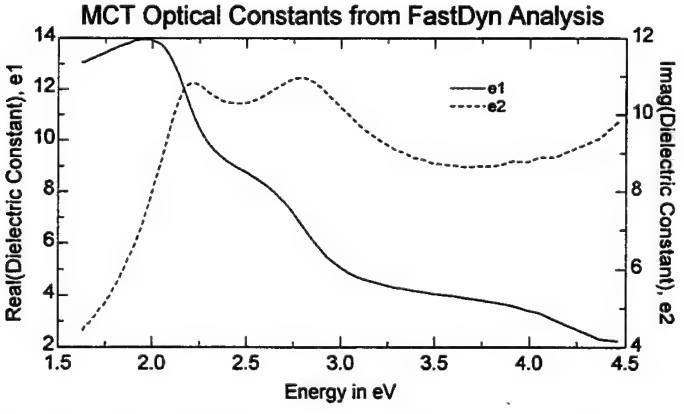

Figure 5.38. MCT optical constants from FastDyn analysis of layer growth.

After successfully completing the above procedure, the optical constants can be saved, and the procedure repeated for another film in the multi-layer MCT / HgTe structure.

A close examination of Figure 5.37 reveals that the fit is not perfect near the starting time. This effect, which is studied more thoroughly in the next chapter, is due to non-uniformity in the initial layer growth rate and/or composition. It should also be noted that the growth rate from the above analysis, 3.79 Å/second, is slightly higher than the 3.71 Å/second value listed in Table 5.3 for the 3rd MCT layer. This is because the growth rates in Table 5.3 were extracted using data which was far enough (> 5 - 10 minutes) from the interface such that the growth rate had settled to its equilibrium value.

6. Data Analysis Results

In this chapter, the optical constant libraries from the previous chapter are used to analyze the insitu SE data acquired during typical HgCdTe growth runs. These results are much easier to assimilate than the previous chapter's 'determination of optical constants' tutorial: it is fairly straightforward to use an existing optical constant library to analyze SE data.

Monitoring the CdZnTe substrate 'Heat-Clean'

Ellipsometric Model

To analyze the insitu SE data acquired during the CdZnTe substrate heat-clean procedure, the WVASE32 model shown in Figure 6.1 was built. While the 'CZT-NV' is actually a WVASE32 ALLOY-TEMP file, the composition value has no effect on the optical constants calculated by this layer. The 'srough' layer is a 50% mixture of the underlying CZT-NV optical constants and void (which has an index of refraction = 1); this is the traditional ellipsometric model for surface roughness. The actual overlayer on the CdZnTe substrate is certainly more complex than this. However, it is difficult using insitu SE alone to determine the true nature of the overlayer. From a monitoring standpoint, the thickness of the surface roughness layer is a good relative gauge of the CdZnTe surface quality.

1	srough	0 Å
0	czt-nv x=0.000 T=100	1 mm

Figure 6.1. Model for CdZnTe substrate during the heat-clean procedure.

The fit parameters which were defined for this analysis were: substrate temperature, angle of incidence, and surface roughness thickness. By going to the WVASE32 'Fit' window and selecting the *Edit Parms* menu option (shown in Figure 6.2), the surface roughness parameter was allowed to go 'negative' (this dialog box can also be used to set lower and upper limits on any defined fit parameter, which can be useful in preventing the L-M analysis algorithm from getting 'lost'). While a negative surface roughness parameter may seem unphysical, a negative value simply means that the current surface is 'cleaner' than the surface on which the optical constant library was derived (keep in mind that it is impossible to determine the absolute quality of the substrate interface from SE data alone).

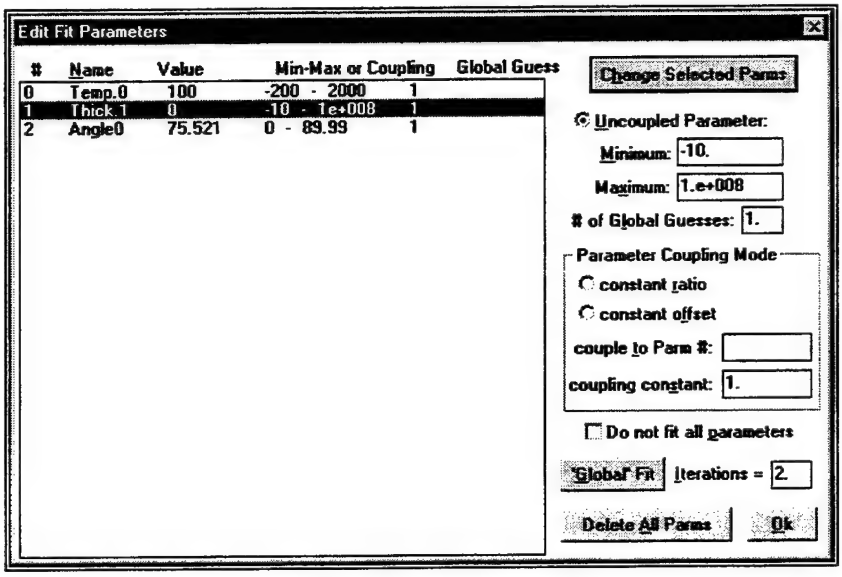

Figure 6.2. WVASE32 'Edit Parameters' dialog box.

When selecting ellipsometric data for the following fits, a spectral range of 2.8-3.8 eV was chosen to enhance the sensitivity of the temperature fitting (see Figures 4.16 and 5.22). To visualize the quality of the data fit using this model, a spectroscopic timeslice was selected at the beginning of the growth run (before the substrate heat-clean procedure), and a *Normal Fit* was performed on the spectroscopic data. The resulting data fit is shown in Figure 6.3, and the fit parameters are listed in Table 6.1.

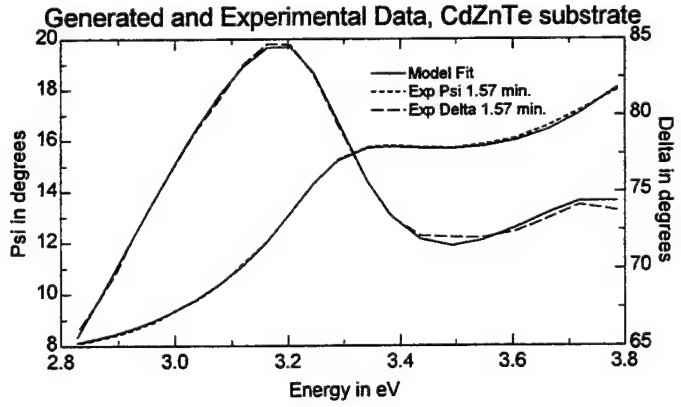

Figure 6.3. Data fit on CdZnTe substrate before heat-clean procedure.

Parameter	Value
MSE	0.4076
Temperature, °C	153.47±3.25
Surface Roughness, Å	25.948±0.337
Angle of incidence, °	75.446±0.0113

Table 6.1. Fit parameters from CdZnTe substrate fit before heat-clean procedure.

Point-by-Point Data Fit

To monitor how these parameters evolve throughout the heat-clean procedure, the *Range Select* command is first used to select the SE data acquired during the time range corresponding to the heat-clean, and the data is displayed in the 'dynamic' mode (see Figure 4.14). Using the same model (as shown in Figure 6.1), the data is analyzed at each point in selected time range by using the *Pt by Pt* command found in the WVASE32 'Fit' window. This is simulates what the ellipsometer would see in real-time if such a model were fit to each experimental SE spectra as it was being acquired. Figure 6.4 shows the resulting fit to the dynamic ellipsometric data during the substrate heat-clean procedure.

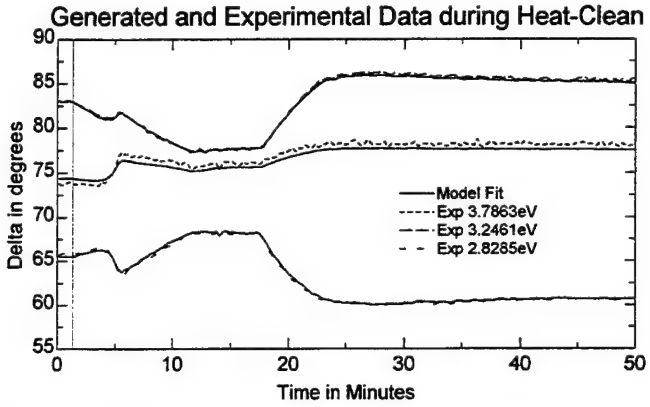

Figure 6.4. SE data fit vs. time during the substrate heat-clean procedure.

To plot the resulting fit parameters from the point-by-point fit vs. time, select the *Data | Point by Point Fit Parms* menu option in the WVASE32 'Graph' window. This brings up a dialog box (shown in Figure 6.5) which allow the user to select a parameter to graph, and specify whether to plot the 'Error bars' (which are actually the 90% confidence limits extracted from the L-M regression statistics) with the parameter values. Figures 6.6 and 6.7 show the Point by Point fit parameter graphs for temperature and thickness which correspond to the data fit of Figure 6.4.

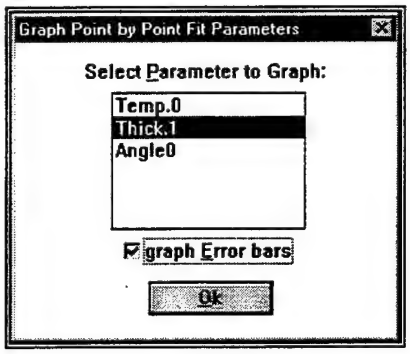

Figure 6.5. Graph Point by Point Fit Parameters dialog box.

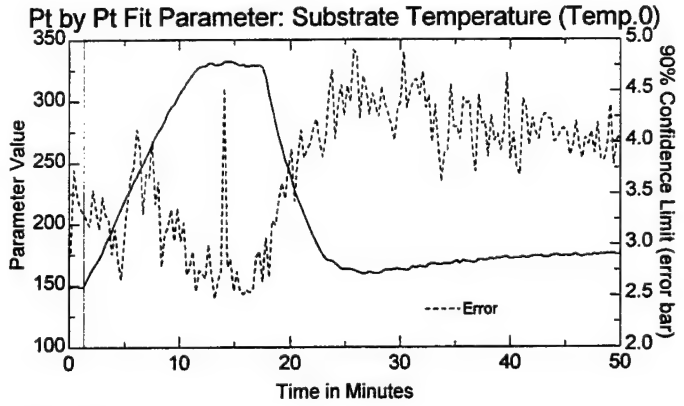

Figure 6.6. Pt by pt fit parameter graph of substrate temperature during the heat-clean.

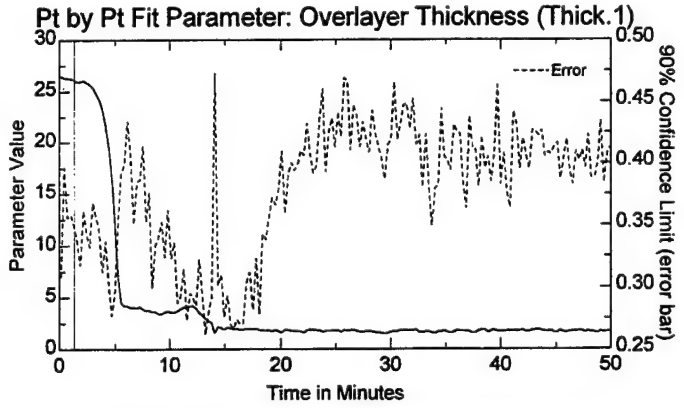

Figure 6.7. Pt by pt fit parameter graph of overlayer thickness during the heat-clean.

Comparing Multiple Runs

Typical graphs of the substrate temperature and overlayer thickness vs. time during the heat-clean procedure of multiple growth runs are shown in Figures 6.8 - 6.12. Qualitatively, the curves look very similar from run to run. The differing amounts of noise in the curves is probably due to differences in beam wobble from run to run. The final substrate temperature and overlayer thickness from run to run are close, but not exactly the same (the substrate temperature was adjust such that the insitu pyrometer temperature was stabilized at 180° C before growth). This may be a real effect, or it may be an artifact caused by variations in the CdZnTe substrate composition or surface quality. Nonetheless, the ellipsometer still can be used to provide relative temperature and overlayer thickness information before the growth.

The droop and slow rise in substrate temperature after the overlayer desorption, which is seen in all of the runs, is also confirmed by insitu pyrometer data. It is very important to wait until the substrate temperature stabilizes before initiating the HgCdTe growth, and monitoring the SE measured temperature value in real-time is an excellent way to observe this (sometimes it takes >30 minutes to stabilize the substrate temperature).

The large initial drop in overlayer thickness, which is seen in only one of the runs, is due to the desorption of some more volatile constituent of the surface overlayer (possibly amorphous Te) which occurs at a lower temperature than the oxide desorption. Most of the samples were inserted into the chamber and stabilized at a

higher substrate temperature (200° C), such that this volatile component of the overlayer was already gone before the ellipsometric monitoring was started; the large drop in overlayer thickness is not observed during the heat-clean of these samples. When the smaller overlayer component is desorbed, it is interesting that most of the curves show a slight increase before the dropping to the 'final' overlayer thickness value.

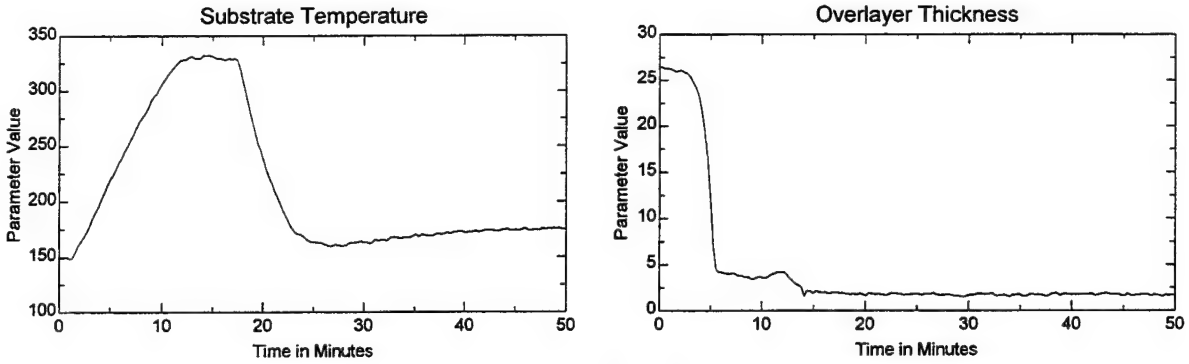

Figure 6.8. Substrate properties during heat-clean for Run #050996

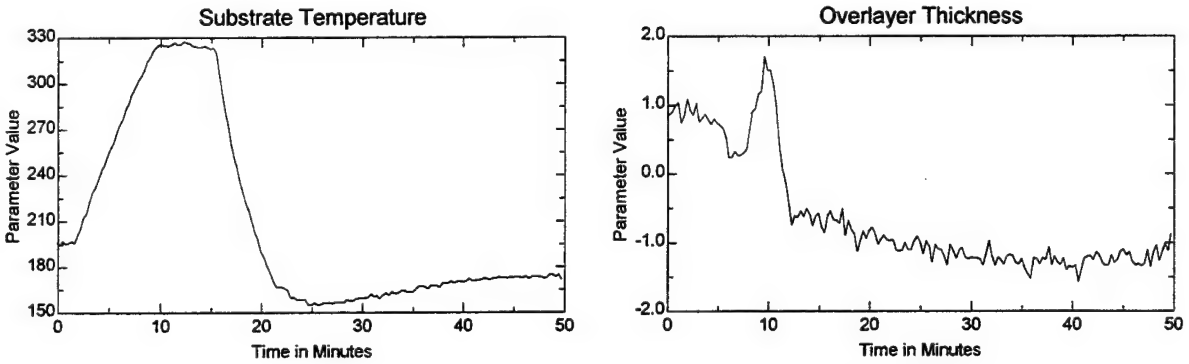

Figure 6.9. Substrate properties during heat-clean for Run #041796

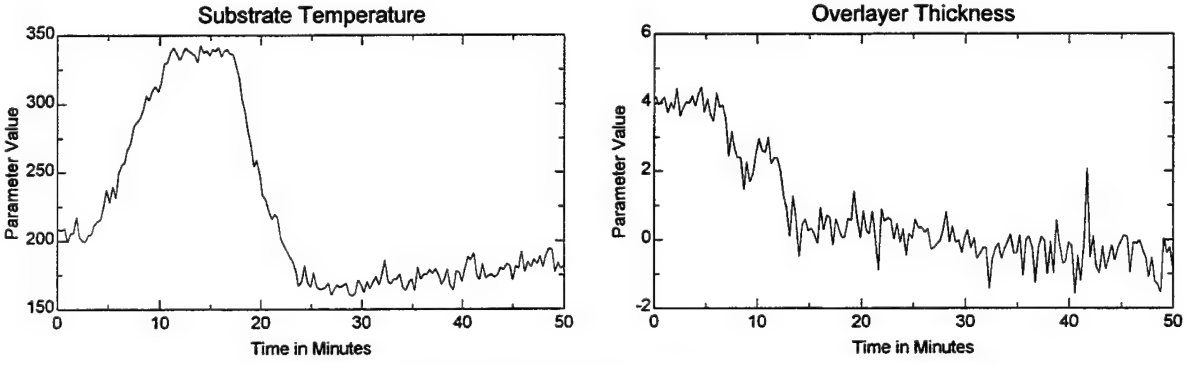

Figure 6.10. Substrate properties during heat-clean for Run #040296

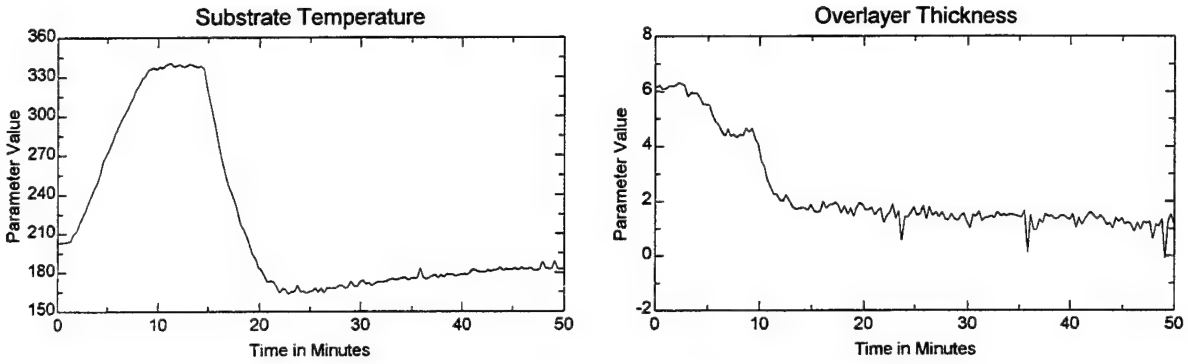

Figure 6.11. Substrate properties during heat-clean for Run #040196

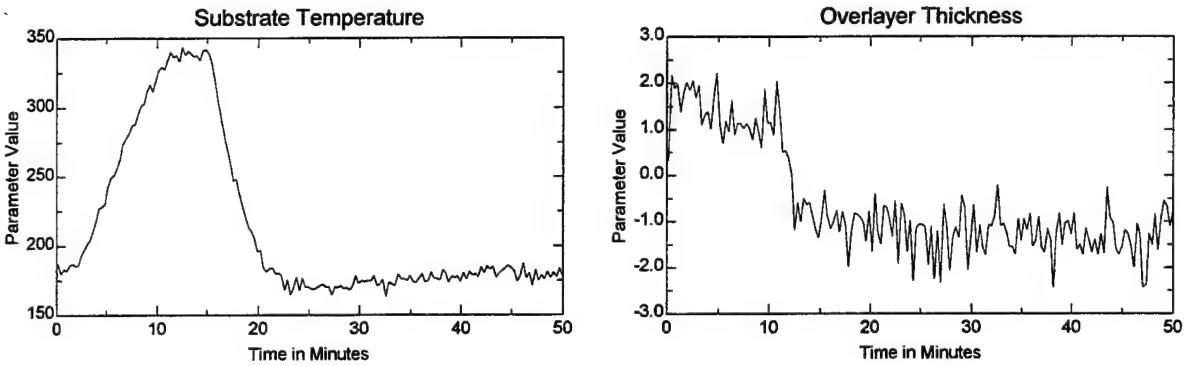

Figure 6.12. Substrate properties during heat-clean for Run #032896

Initiation of HgCdTe Film Growth

Though the most important aspect of the SE monitoring in this contract was to determine the HgCdTe layer composition during growth, understanding how the HgCdTe film growth initiates is also important from a crystal grower's standpoint. The next sections illustrate the sensitivity of SE to some potential non-idealities in HgCdTe film growth. Since the focus in this contract was on composition monitoring, these effects were not pursued, i.e., no attempt was made to systematically adjust the growth conditions to minimize these effects. The SE methodology for observing and quantifying the non-ideal growth effects is given here; correlating such results with the layer quality as determined by other exsitu characterization techniques would be an interesting topic for future work.

Surface Roughening at CdZnTe interface

In theory, when the effusion cell shutters are opened and HgCdTe film growth is initiated on the CdZnTe substrate surface, an ideal and abrupt HgCdTe/CdZnTe interface is formed and the HgCdTe growth front advances in an atomically smooth manner. Insitu SE is quite sensitive to the ideal (or non-ideal) nature of the interface during growth initiation. To study the HgCdTe film growth process, a FastDyn model (which assumes an ideal interface and growth mode) was first built to analyze the SE data acquired during the growth initiation. The WVASE32 model and FastDyn layer settings are shown in Figures 6.13 and 6.14. The data fits from the analysis are shown in Figure 6.15. While the fits are fairly good, small yet significant

discrepancies in the fit can be observed near t=55 minutes when the HgCdTe layer growth was initiated.

1	mct-nv x=0.243 T=22	0 Å
0	fastdyn	0.00022782 mm

Figure 6.13. FastDyn model to study HgCdTe growth process.

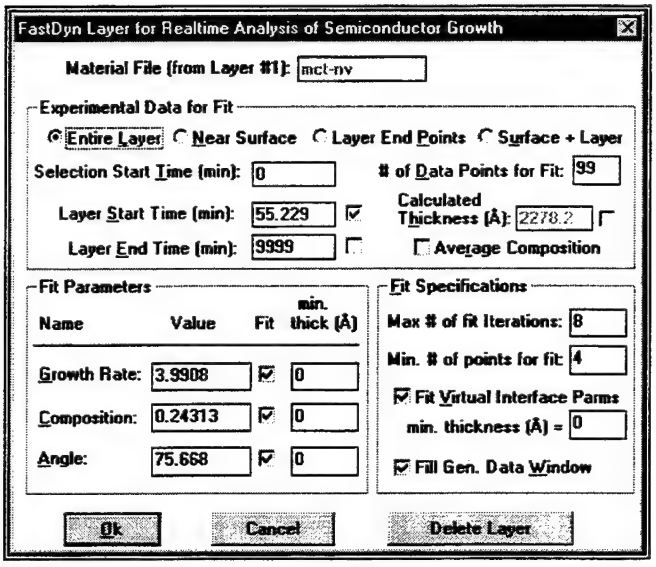

Figure 6.14. FastDyn layer settings for HgCdTe growth initiation analysis.

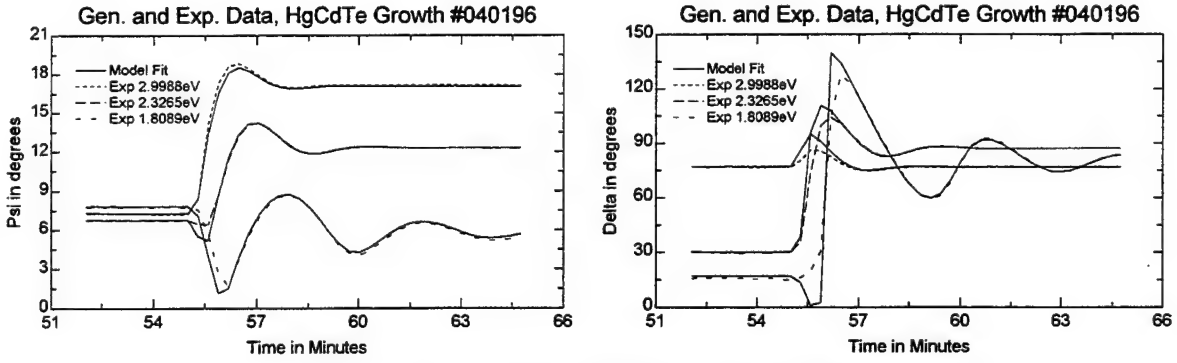

Figure 6.15. FastDyn data fits from HgCdTe film growth on CdZnTe substrate.

Multiple Timeslice Analysis

Surface roughness was suspected as the main reason for the discrepancies observed in the data fits. Unfortunately, at the current time (but it will in the future), the FastDyn analysis algorithm does not support the modeling of surface roughness. To further study this effect, another more sophisticated analysis approach was tried. The first step in this analysis was to define multiple spectroscopic timeslices distributed across the HgCdTe growth initiation process (see Figure 6.16). The 'Spectroscopic' display mode was then enabled, yielding the spectra seen in Figure 6.19. The model shown in Figure 6.17 was built, and the MCT and surface roughness thicknesses, MCT composition, and angle of incidence were defined as fit parameters.

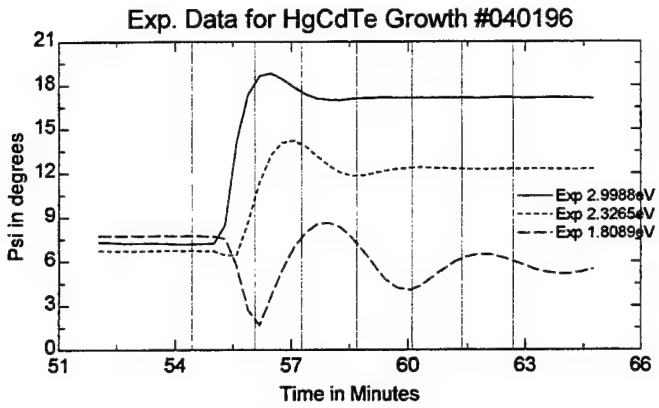

Figure 6.16. Specification of multiple spectroscopic timeslices spaced across the HgCdTe growth initiation process.

2	srough	0 Å
1	mct-nv x=0.240 T=22	0 Å
0	czt-nv x=0.000 T=180	1 mm

Figure 6.17. WVASE32 model to study film roughness during HgCdTe growth initiation.

When multiple timeslices of dynamic data are displayed in the spectroscopic mode, 'right-clicking' the mouse button on the WVASE32 'Model' window (or hitting the 'Backspace' key with the 'Model' window active) will bring up the dialog box shown in Figure 6.18. This complicated dialog box allows the user to individually specify model parameters for each timeslice of the experimental data. Parameters can also be declared as 'global' by clicking the checkbox adjacent to the parameter name. In Figure 6.18, the 'Angle0' and 'Alloy.1' parameters have been declared global, such that the same value of these parameters will be used in modeling each timeslice. The 'Thick.2' (surface roughness) and 'Thick.1' (MCT layer thickness) will be individually fit at each timeslice. Starting values for these parameters at each timeslice can be conveniently defined by clicking the corresponding 'set values' button. After setting up the multi-model analysis as described, a *Normal Fit* was performed, resulting in the data fits shown in Figure 6.19. The model parameters determined from the fit for each timeslice are shown in Figure 6.20.

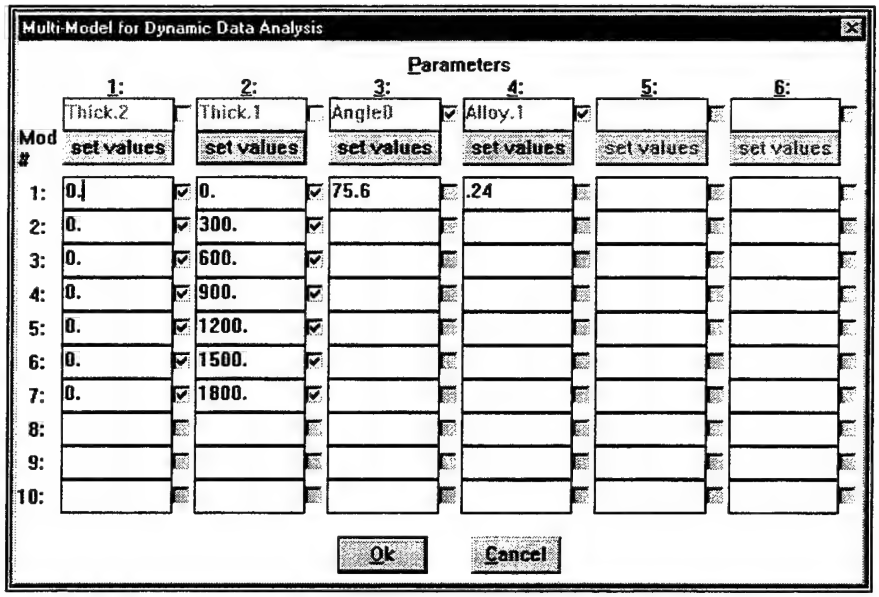

Figure 6.18. WVASE32 Multi-model dialog box for dynamic data analysis.

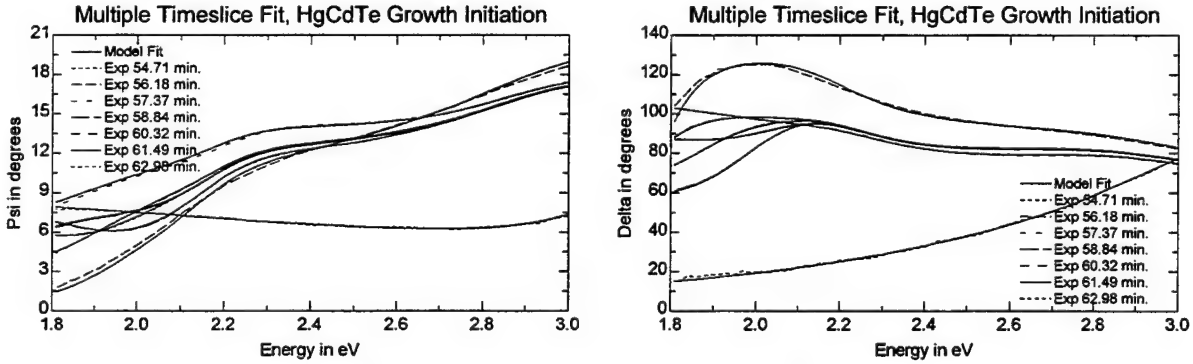

Figure 6.19. Multiple spectroscopic timeslice fit for HgCdTe growth initiation.

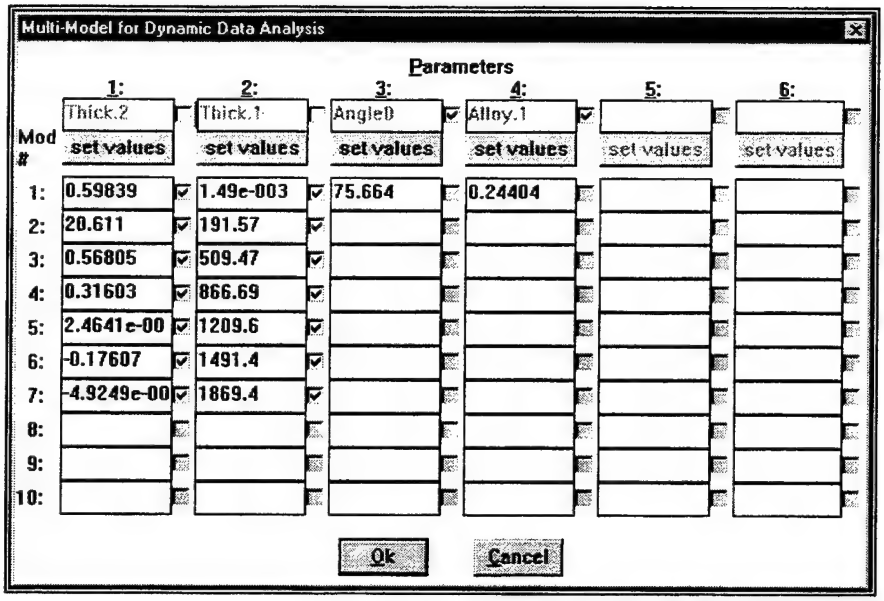

Figure 6.20. Fit parameters determined from multiple timeslice fit of HgCdTe growth.

Surface Roughness vs. Time

The preceding multiple timeslice fit was performed to extract the best average growth values for the angle of incidence and MCT layer composition in the presence of a potentially varying surface roughness. These model parameters were then fixed at their 'best average' values, and a point-by-point fit of the dynamic growth data was performed, fitting only for the MCT and surface roughness thicknesses. The resulting data fits are shown in Figure 6.21; these graphs demonstrate a noticeably better data fit than the ideal FastDyn analysis shown in Figure 6.15. The resulting point-by-point fit parameters are shown in Figure 6.22. A dramatic increase (30Å) in surface roughness is observed during the initial HgCdTe growth. However, by the time the film is 500Å thick, the surface has completely recovered. Since the data fits with the surface roughness model are so good, it can be concluded that at least from an optical standpoint, the CdZnTe / HgCdTe interface must be abrupt, and that surface roughness is a dominant factor in the initial part of HgCdTe growth.

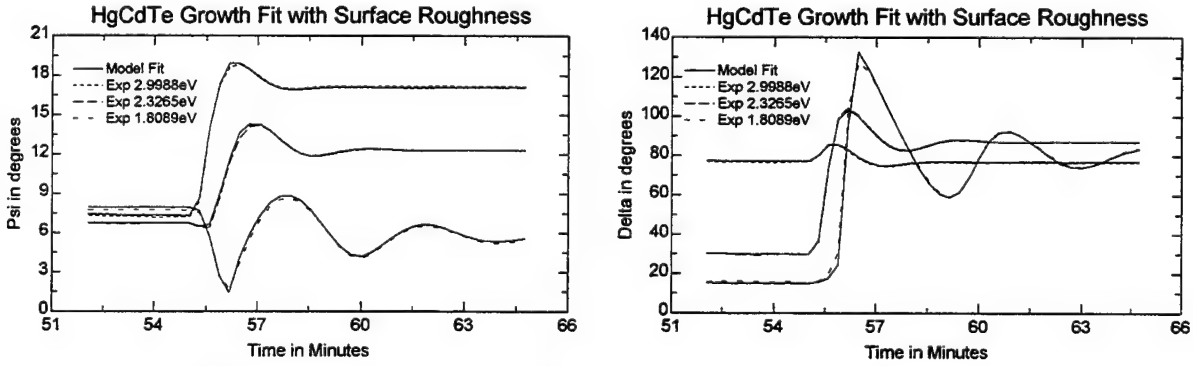

Figure 6.21. Point-by-Point fits of HgCdTe growth with surface roughness model.

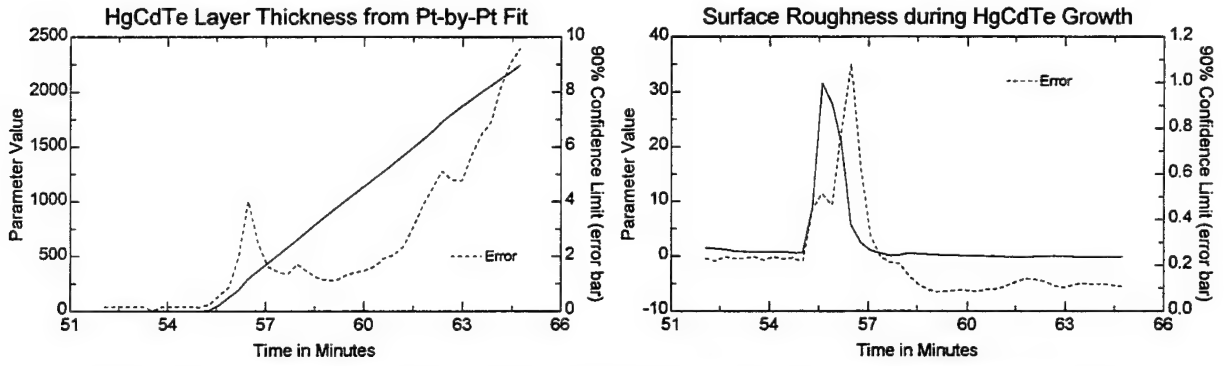

Figure 6.22. Parameters from Point-by-Point fit of HgCdTe growth #040196 with surface roughness model.

The same modeling procedure was applied to some of the insitu SE data acquired during other HgCdTe growth runs. The results of these analysis are shown in Figures 6.23 - 6.26; all of the growth runs seem to exhibit the same surface roughening phenomena during the initial phase of HgCdTe growth. The limited time resolution of the insitu SE data makes it difficult to quantify the true height of the surface roughness peak. However, in Table 6.2 an interesting qualitative comparison is made between the surface roughness of the CdZnTe substrate immediately before growth and the peak surface roughness during the initial layer growth of HgCdTe. While there is certainly not enough data to make conclusive statements about the relationship, a trend is observed which does merit further investigation.

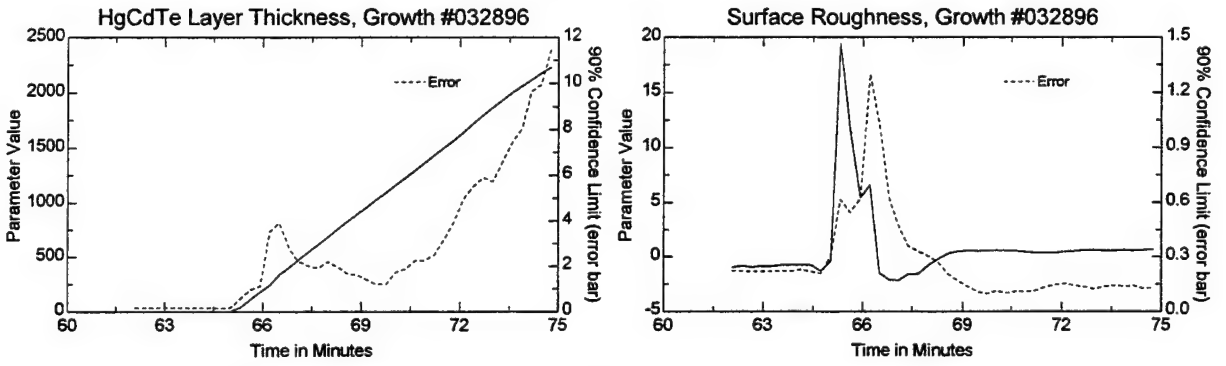

Figure 6.23. Parameters from Point-by-Point fit of HgCdTe growth #032896 with surface roughness model.

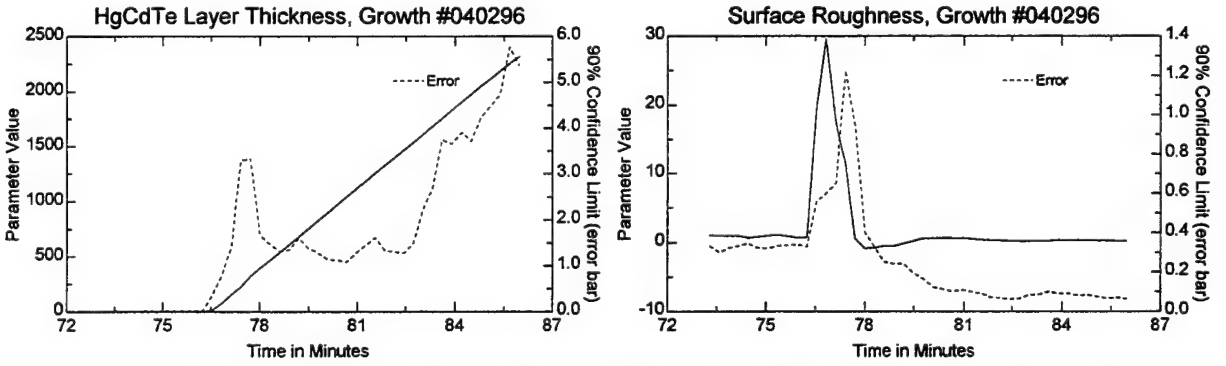

Figure 6.24. Parameters from Point-by-Point fit of HgCdTe growth #040296 with surface roughness model.

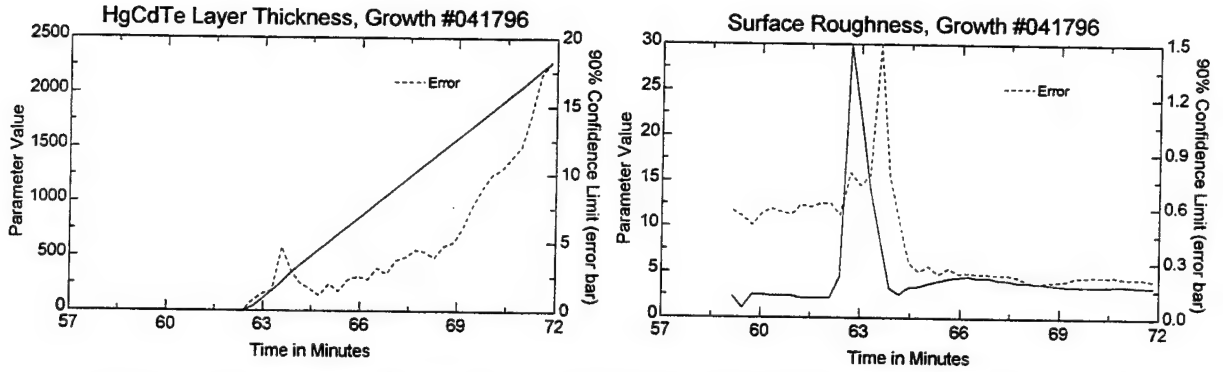

Figure 6.25. Parameters from Point-by-Point fit of HgCdTe growth #041796 with surface roughness model.

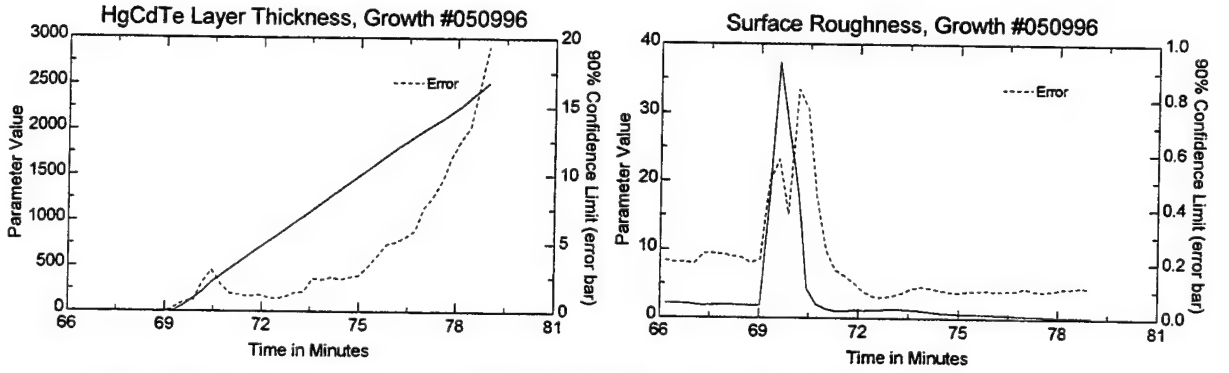

Figure 6.26. Parameters from Point-by-Point fit of HgCdTe growth #050996 with surface roughness model.

Run #	CdZnTe substrate 'roughness' (Å)	HgCdTe growth roughness (Å)
050996	2	37
040196	1	31
040296	-0.5	30
041796	-1	30
032896	-1.5	19

Table 6.2. Comparison of CdZnTe substrate roughness vs. HgCdTe growth roughness.

Flux Transient Effects

Another non-ideal MBE growth effect was observed when extracting the optical constants and growth rates from the multi-layer MCT / HgTe structure of Table 5.3. In the growth of this structure, a HgTe buffer layer was grown while the CdTe effusion cell shutter was closed. To grow the MCT layers, the CdTe effusion cell shutter was then opened. Since the CdTe shutter was closed for a number of minutes during the HgTe layer growth, the opening of the shutter caused 'flux transient' in the CdTe species. This effect is common in most MBE systems, and can be detected by a close analysis of the insitu SE data.

The data set which was used to demonstrate the flux transient effect is shown in Figure 5.30. A FastDyn model was built, using the settings shown in Figure 6.27. To explore how the growing layer's composition and growth rate varied due to the

flux transient, a Point-by-Point near-surface FastDyn fit was done on the dynamic data from t=108-117 minutes. Figure 6.28 illustrates how the FastDyn 'near-surface' data selection mode 'tracks' the last 5 experimental data points throughout the point-by-point fit. The resulting layer growth rate and composition are shown in Figures 6.29 and 6.30. Due to the limited number (and close spacing) of data points, there is not a lot of sensitivity to growth rate in a near-surface mode fit. However, Figure 6.29 still does show the trend of decreasing growth rate with time, which is consistent with a flux transient effect. Figure 6.30 dramatically shows the effect of the CdTe flux transient on HgCdTe composition: it takes almost 10 minutes for the composition to stabilize at its equilibrium value.

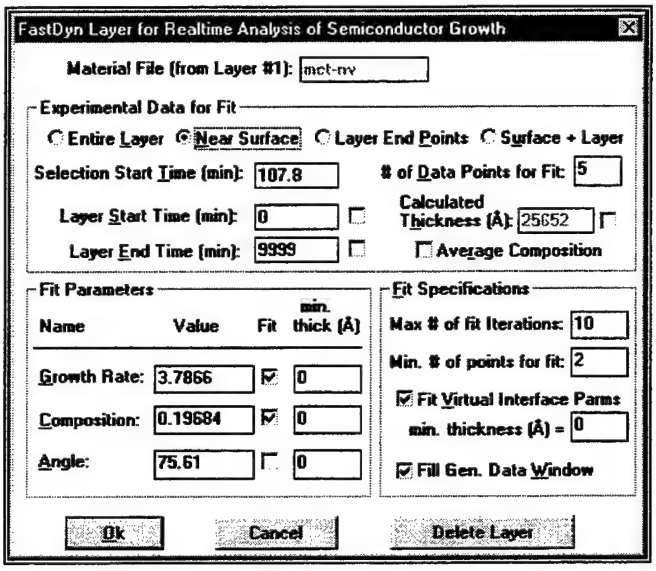

Figure 6.27. FastDyn settings to analyze flux transient data.

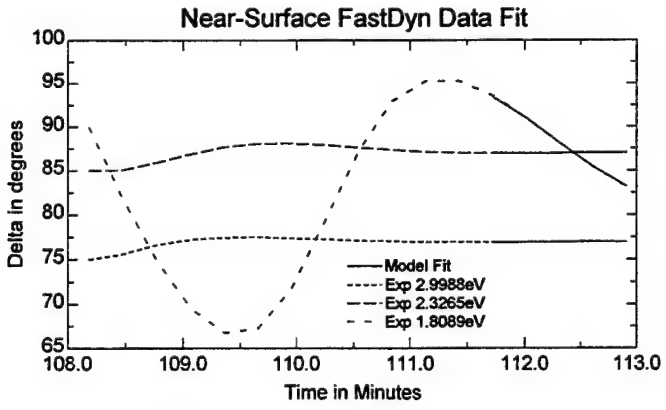

Figure 6.28. Near-Surface FastDyn data fit.

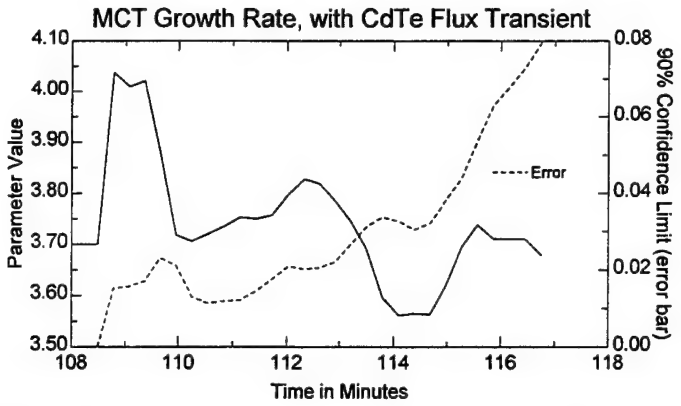

Figure 6.29. MCT growth rate from a near-surface FastDyn analysis, in the presence of the CdTe flux transient.

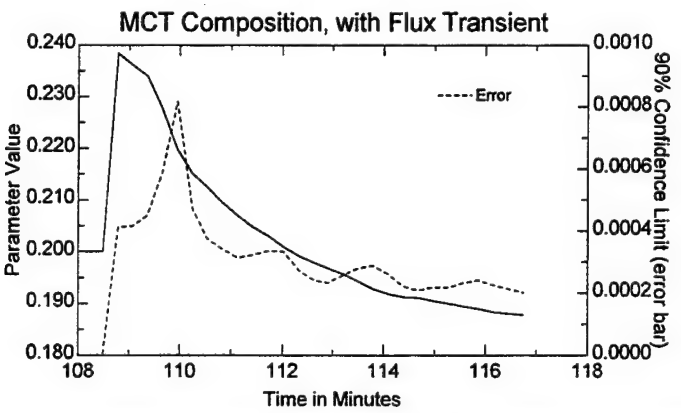

Figure 6.30. MCT composition from a near-surface FastDyn analysis, in the presence of the CdTe flux transient.

Monitoring HgCdTe Composition

The most important goal of this contract was to quantitatively extract in real-time the HgCdTe composition throughout an MBE growth run. The previous section showed analysis results for insitu SE data acquired during the growth initiation of a HgCdTe layer. While these results focused on some of the non-ideal growth effects which were extracted from the SE analysis, HgCdTe compositions were also returned as part of the analysis. The accuracy of these compositions, however, may be adversely affected by the non-idealities which were present and had to be simultaneously accounted for in the model.

Fortunately, the growth initiation phase represents only a small fraction of the total growth time for a typical HgCdTe MBE run. For most of the 4 - 10 hour growth run, the HgCdTe film is optically thick, and can therefore be optically modeled as a bulk material. (It only takes a few thousand Angstroms for a HgCdTe film to become optically thick, or less than 20 minutes at a typical 4 Å/second growth rate.) This greatly simplifies the SE data analysis, as each spectra can be independently modeled (there are no interference oscillations, so FastDyn analysis is not required). Surface roughness is also much easier to account for on a bulk substrate.

While using a bulk model to analyze the SE data does greatly simplify the extraction of the HgCdTe layer composition, it does not guarantee that the resulting compositions will be accurate. In this section, a very careful and systematic analysis of the insitu SE data acquired across multiple MBE growth runs is described. The purpose of this multiple growth run analysis is to correlate the insitu ellipsometer composition for each run with the FTIR composition for each sample measured exsitu. Since the FTIR measured composition directly relates to the bandedge of the HgCdTe film (which is the most important parameter for an IR photo-detector device), it is very important that the ellipsometer composition is in agreement with this value.

Determining the Best Model

Very early in the analysis of the insitu SE data, it became apparent that the ellipsometer determined MCT composition drifted throughout the growth run (examples of this will be shown in a later section). To objectively extract a single composition value which could be compared with the FTIR data, a single data fit was performed (with each prospective model) for each growth run, using 9 spectroscopic timeslices of data which were equally distributed across the optically thick growth time of the run. Figure 6.31 illustrates this data selection paradigm, and the corresponding spectroscopic timeslices are shown in Figure 6.32. Since the data fits were performed with the 'spectroscopic' display mode enabled, to extract average parameter values from the multiple timeslices it was necessary to define all the fit parameters as 'global' in the multiple model dialog box (see Figure 6.33; this dialog box is brought up by right-clicking the mouse on the 'Model' window).

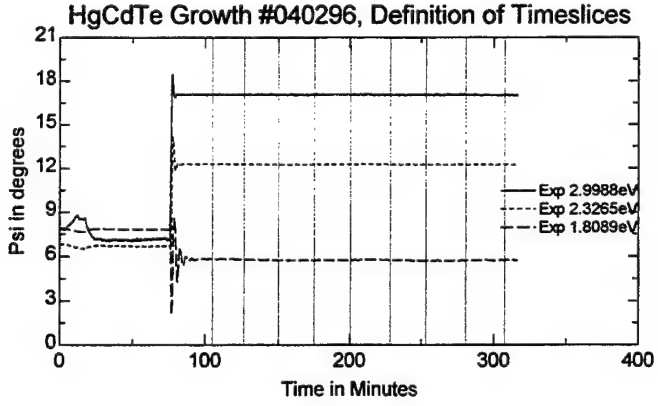

Figure 6.31. Definition of spectroscopic timeslices for HgCdTe growth run #040296.

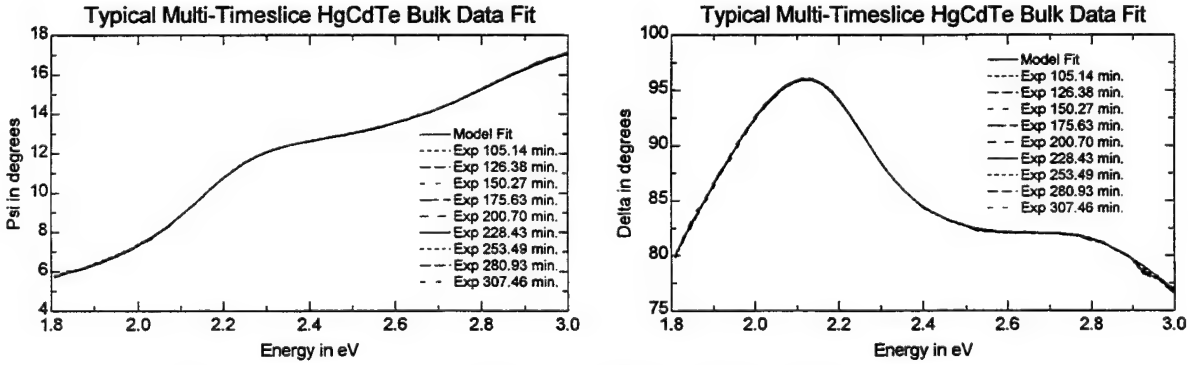

Figure 6.32. Typical multiple spectroscopic timeslice data fit on HgCdTe Growth #040296.

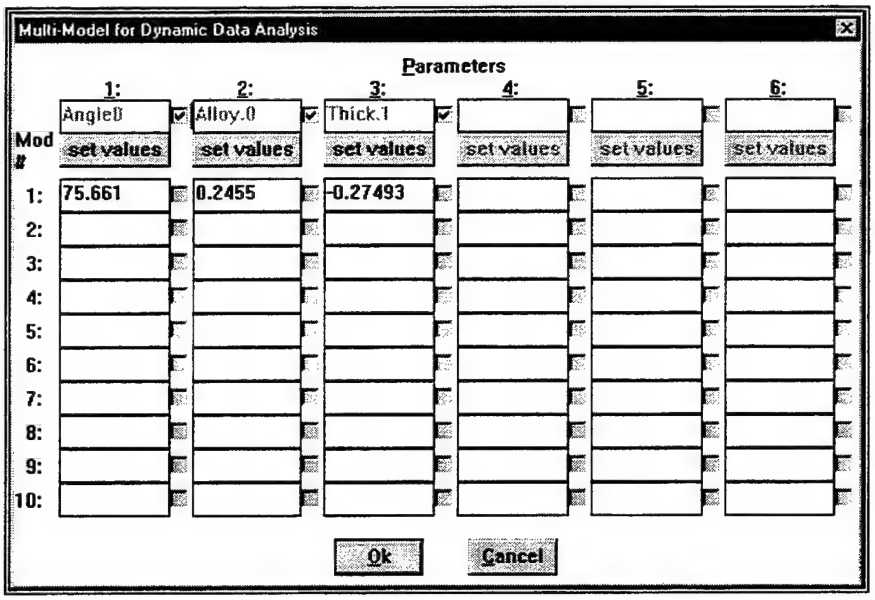

Figure 6.33. Multiple model dialog box; parameters are defined 'global' by checking the box to the right of the parameter name.

A number of different models were considered, all of which were based on the simple bulk model shown in Figure 6.34. The main difference between the models were in which parameters were fit. However, variations of the parametric MCT optical constant library were also experimented with, and various spectral ranges for the experimental data were also considered in an effort to find a modeling approach which yielded the best correlation with the FTIR composition values. The composition results for a few representative models which were tried are summarized the Table 6.3. These results are presented graphically in Figure 6.35.

1	srough	0 Å
0	mct-nv x=0.220 T=22	1 mm

Figure 6.34. Bulk model used to extract HgCdTe composition.

Growth Run	FTIR Comp.	Fit Parms #1: comp, temp, angle, roughness	Fit Parms #2: comp, angle, roughness	Fit Parms #3: comp, angle	Fit Parms #4: comp, angle (Psi only fit)
032196	.230	.223	.229	.223	.222
032896 (#1011)	.242	.228	.232	.230	.230
040196 (#1013)	.249	.235	.242	.244	.245
040296 (#1014)	.247	.237	.240	.241	.241
040396 (#1016)	.191	.182	.182	.192	.195
040596 (#1018)	.211	.217	.198	.181	.178

Table 6.3. Ellipsometer MCT Compositions, extracted using different analysis models.

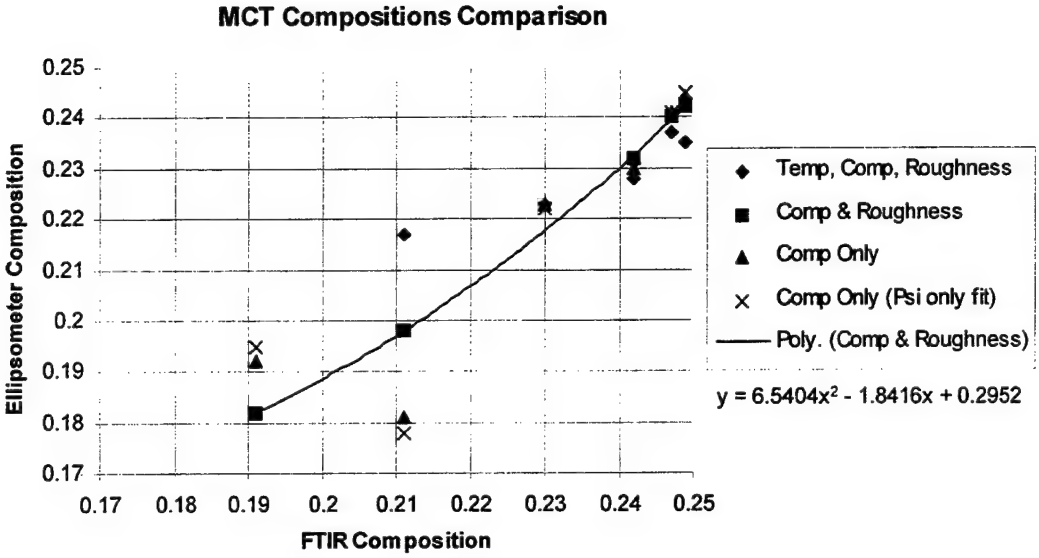

Figure 6.35. Correlation between ellipsometer and FTIR compositions for various models.

The main conclusion of the different modeling approaches is: only model #2, which fits for the composition, *surface roughness*, and angle of incidence yields a systematic correlation between the FTIR and ellipsometer compositions across 5 different growth runs *(the data point from run 032196 had to be thrown out, as it was not in agreement with the other runs; however, this data was acquired with a different M-88 detector unit)*. The other models did not provide ellipsometer compositions that were systematic with the FTIR compositions. These issues are explored in the next sections.

Why Didn't Fitting for the Temperature Help?

To explore this issue, a series of model fits were performed, in which both the composition *and* temperature were fit, and then the composition only was fit (at different fixed the temperatures). The data for run 032896 (shown in Table 6.4) clearly exhibits correlation: The MSE (Mean Square Error) from the fit barely changes when the temperature is moved from 170 to 180 degrees. This basically implies that we do not have not have enough sensitivity to fit for both the temperature and composition (although the composition and surface roughness values do change as a function of the assumed temperature). Since good quality MCT will grow only in a narrow temperature window anyway, it is better to fix the temperature at its nominal value.

Temp.	Comp.	MSE	Roughness (Å)
175 (Fit)	.228	.12	.14
170 (Fixed)	.224	.13	-.23
180 (Fixed)	.231	.13	.49
190 (Fixed)	.239	.19	1.22

Table 6.4. Temperature and Composition fits from HgCdTe Growth run #032896.

Fitting the data from run 040596 results in an unreasonably high temperature, as illustrated in Table 6.5. When the temperature is fixed at the nominal value, the resulting composition value is in much better agreement with the FTIR composition.

Fitting for the temperature enables the ellipsometric model to 'fudge' a better fit, but in this case it does so at the expense of the composition accuracy.

Temp.	Comp.	MSE	Roughness (Å)
208 (Fit)	.221	.63	5.14
180 (Fixed)	.200	.74	3.01

Table 6.5. Temperature and Composition fits for HgCdTe growth run #040596

What justifies throwing out a data point?

The data for run #032196 was acquired with a different M-88 detector unit. In theory, any ellipsometer system should acquire the exact same Psi and Delta data. However, in practice small variations will exist, and these variations can become significant when we are trying to monitor MCT composition with ultra high accuracy. Table 6.6 shows what happens to the MCT composition extracted from the ellipsometer data for very small assumed wavelength shifts in the ellipsometer detector. From detector to detector, wavelength shifts of up to 1 nm may be possible; this may explain part of the observed discrepancy in composition.

Assumed Wavelength Shift (nm)	Fit MCT composition
0	.233
0.5	.230
1.0	.228
1.5	.226
2.0	.223

Table 6.6. Fit MCT composition in the presence of a ellipsometer wavelength shift.

Reassigning the Nominal Composition Values

The graph in Figure 6.36 shows the systematic agreement between the ellipsometer and FTIR compositions when the ellipsometric model fits for both composition and surface roughness (the angle of incidence was also a fit parameter in all of the models that were tried). Except for the data point from run 032196, a simple 2^{nd} order polynomial curve can describe the relationship nicely. Of course, what is really desired is an exact correspondence between the ellipsometer and FTIR compositions. The reason that this is not the case is that *assumed nominal* compositions were used in the construction of the optical constant library (FTIR data could not be obtained for each layer in the multi-layer MCT/HgTe structure, and the EDX data was not accurate enough). From the graph below, it appears that the assumed compositions were about 0.01 low. To correct this offset, the composition values in the optical constant library file were simply replaced with values derived from the polynomial fit (actually, the equation shown in the graph had to be inverted to obtain the correct FTIR composition as a function of the assumed ellipsometer composition). Subsequent analysis results presented in this report are performed with this 'composition corrected' MCT file. This file has been 'optimized' to work only at the MCT growth temperature (nominally 180C), and over a limited spectral range (1.8-3.0 eV) and composition range (x=0.15-0.30).

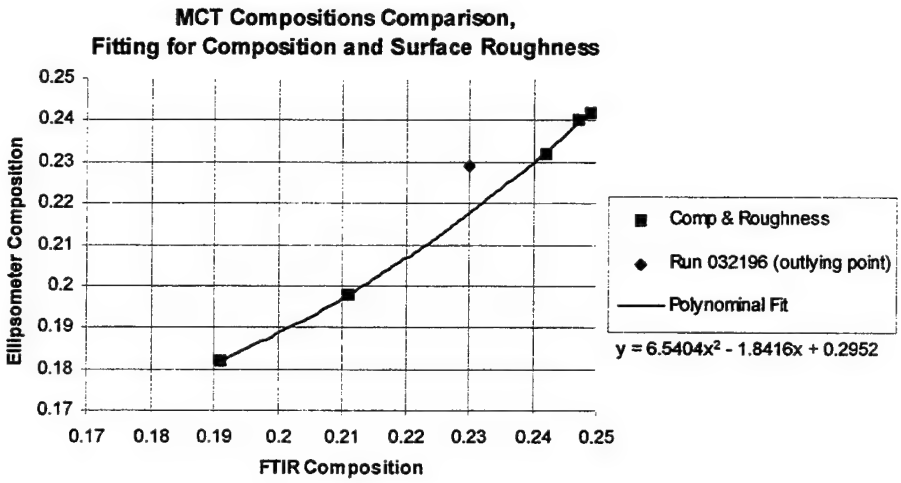

Figure 6.36. Correlation between ellipsometer and FTIR compositions for the best fit model.

Detailed Run by Run SE Data Analysis Results

Using the optimized and composition corrected MCT optical constant library (which is stored in a WVASE temp-alloy file named MCT-NV.MAT), all of the recent MCT growth runs were refit, using a point-by-point analysis of the SE data acquired during the optically thick region of growth. Only experimental data in the 1.8 - 3.0 eV spectral range was included in the fit. The results, which are subsequently shown in Figures 6.37 - 6.41, illustrate the following points:

1. Very good quality in the data fits is observed from run to run. This indicates that the insitu SE ellipsometer system reproducibly acquires accurate data, and that the MCT-NV optical constant library can be used to precisely fit this data over a range of compositions.
2. Changes in ellipsometer composition, surface roughness, and angle are observed throughout the growth run, which may or may not be real.
3. The signal to noise in the fit parameters varies from run to run; however, with a little bit of data smoothing, the precision in the MCT composition is near the target value of 0.001.

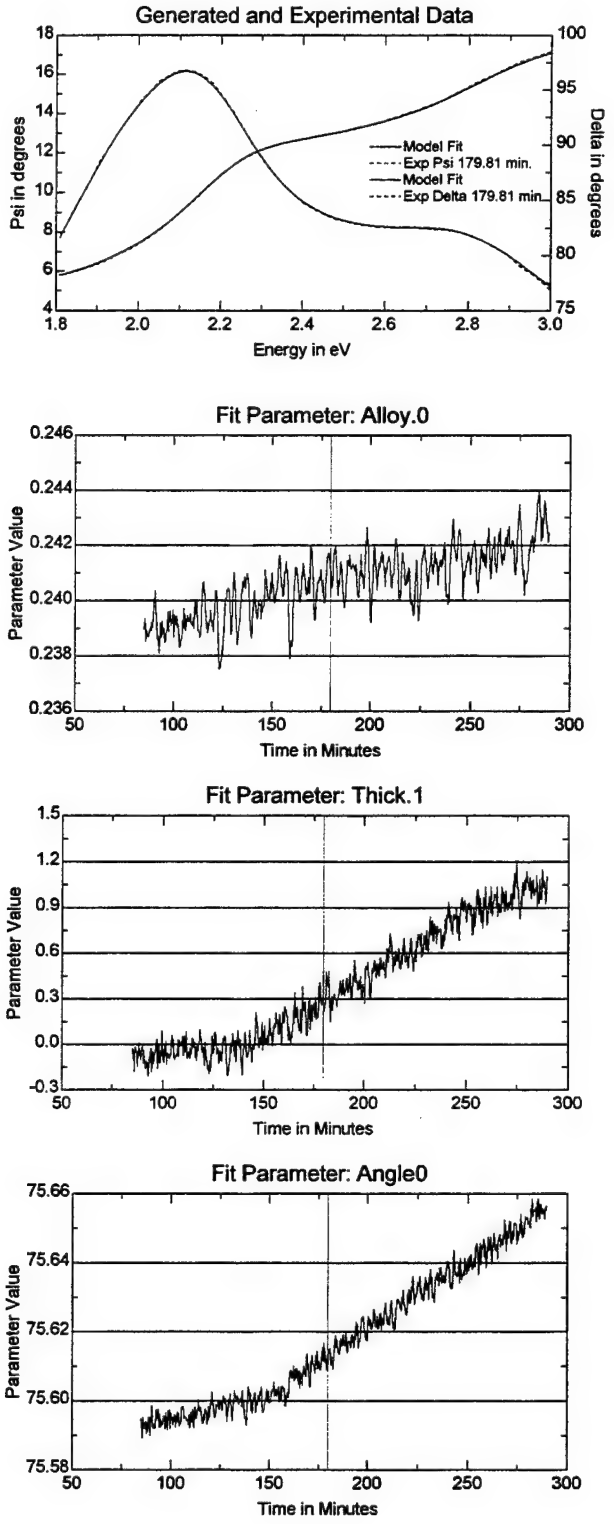

Figure 6.37. Results for Run 032896 (#1011), FTIR x=0.242.

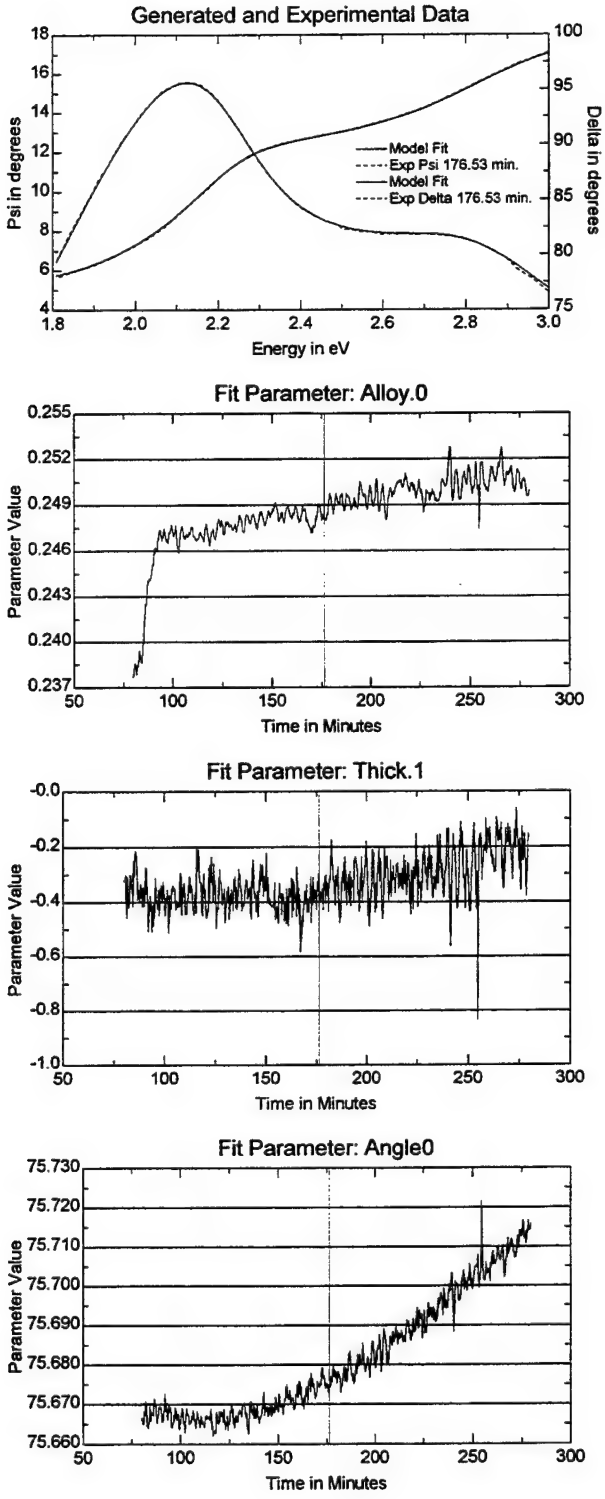

Figure 6.38. Results for Run 040196 (#1013), FTIR x=0.249.

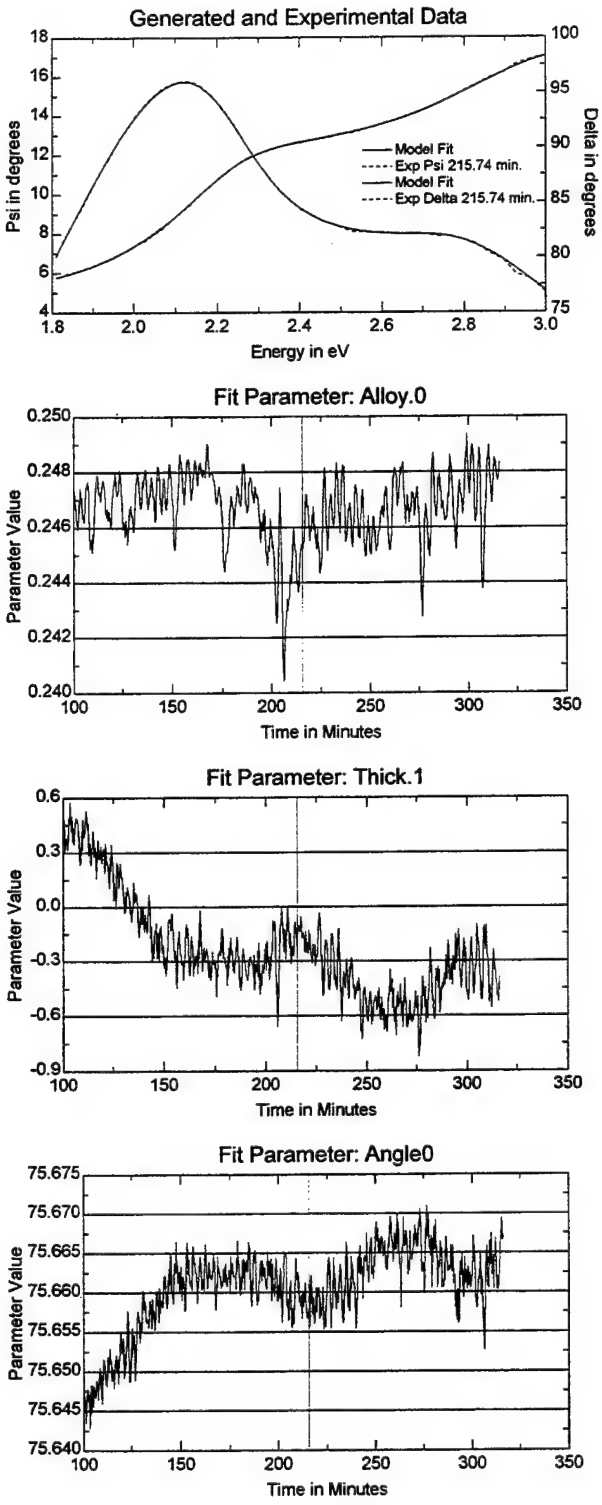

Figure 6.39. Results for Run 040296 (#1014), FTIR x=0.247.

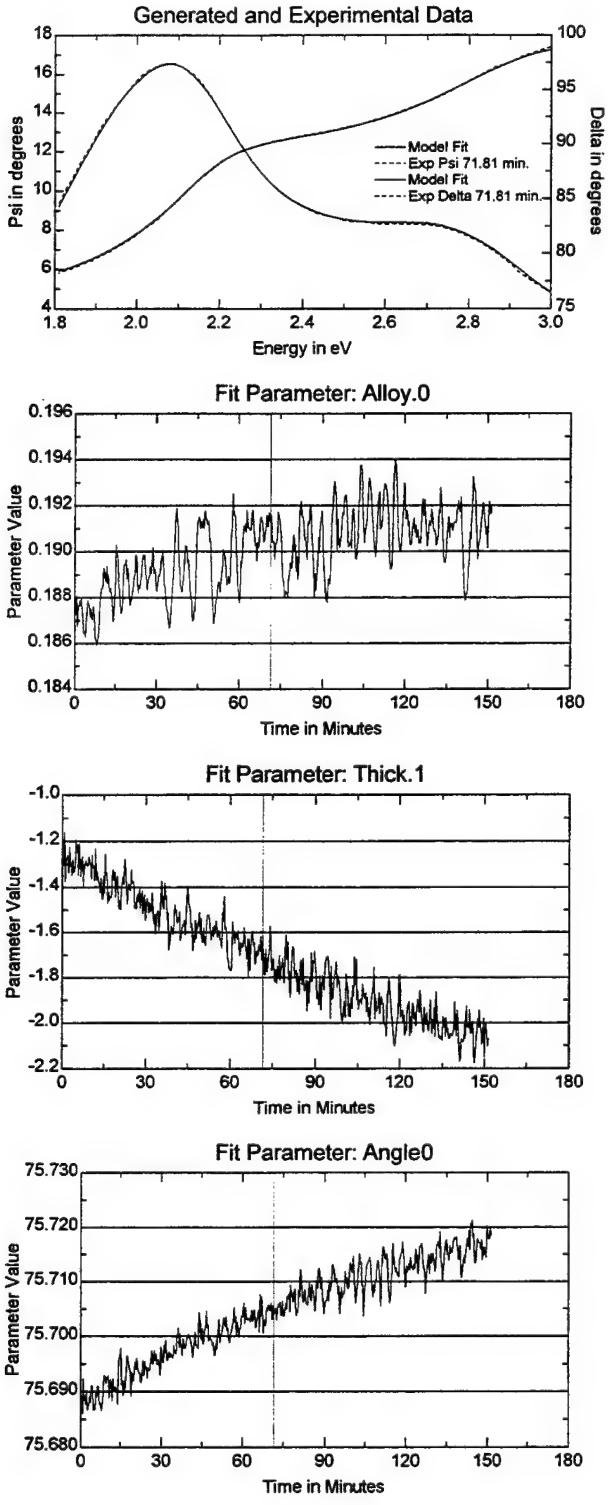

Figure 6.40. Results for Run 040396 (#1016), FTIR x=0.191.

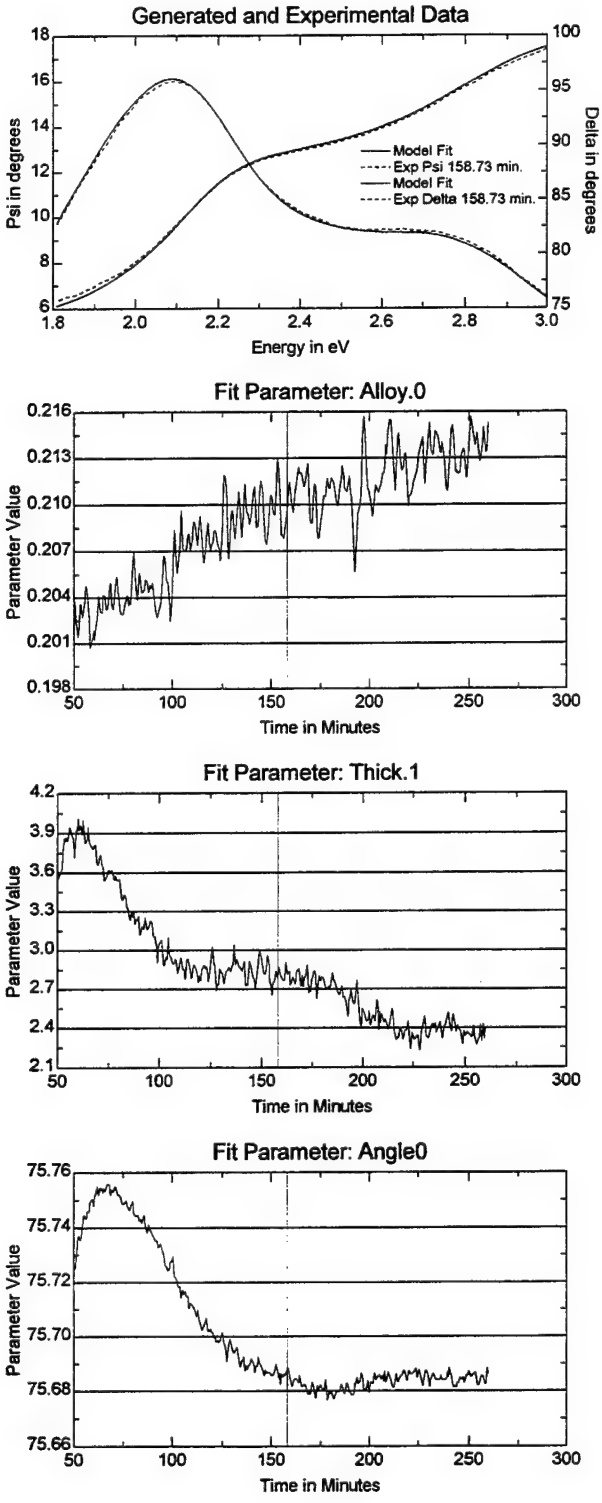

Figure 6.41. Results for Run 040596 (#1018), FTIR x=0.211.

The data from this run does not fit as well as the other runs. Likewise, the surface roughness and angle graphs exhibit behavior that is not seen in the other growth runs.

Summary of Final SE Composition Results

A final 'average' composition analysis of the multiple HgCdTe growth runs was performed, using the best fit model which included surface roughness and the final MCT optical constant library. The multiple spectroscopic timeslice approach which was described earlier was used to obtain objective average composition values for the grown HgCdTe layers. The results are summarized in Table 6.7 and Figure 6.42. Excellent composition reproducibility and accuracy is achieved: for all 6 growth runs which were performed over a one month period, the insitu ellipsometer determined compositions were with ±0.001 of the FTIR composition values. This level of composition accuracy adequately satisfies the requirements of current IR detector technology.

Growth Run	FTIR Comp.	Ellipsometer Comp.	Surface Roughness (Å)	MSE
#1011	0.242	0.241	0.4	0.38
#1013	0.249	0.249	-0.3	0.55
#1014	0.247	0.246	-0.2	0.21
#1016	0.191	0.19	-1.7	0.34
#1018	0.211	0.209	2.9	0.82
#1024	0.253	0.252	3.3	0.39

Table 6.7. Final insitu SE composition results.

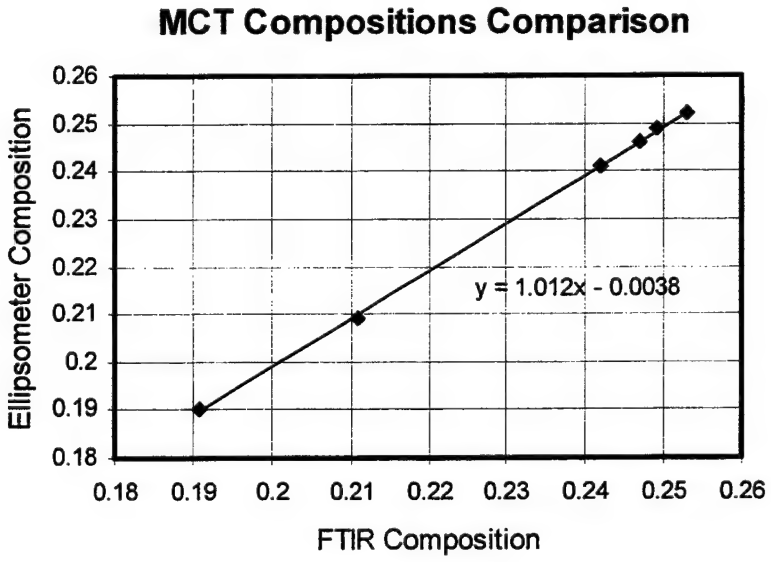

Figure 6.42. Correlation between ellipsometer and FTIR compositions, using best fit model which included surface roughness and the final MCT optical constant library.

SE Sensitivity to HgCdTe Growth Parameters

Using the best fit model and final optical constant library, a sensitivity analysis of the insitu SE data to the HgCdTe growth parameters was performed. The results of this analysis are shown in Figures 6.43 and 6.44. The purpose of this analysis is to demonstrate the stringent levels of ellipsometric data precision and accuracy which are required to achieve acceptable composition accuracy.

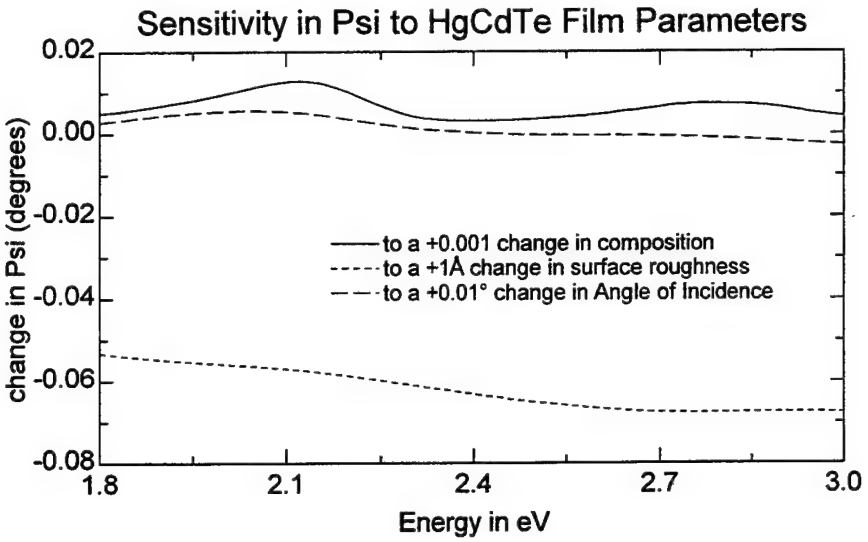

Figure 6.43. Sensitivity in the ellipsometric Psi data to the HgCdTe film parameters

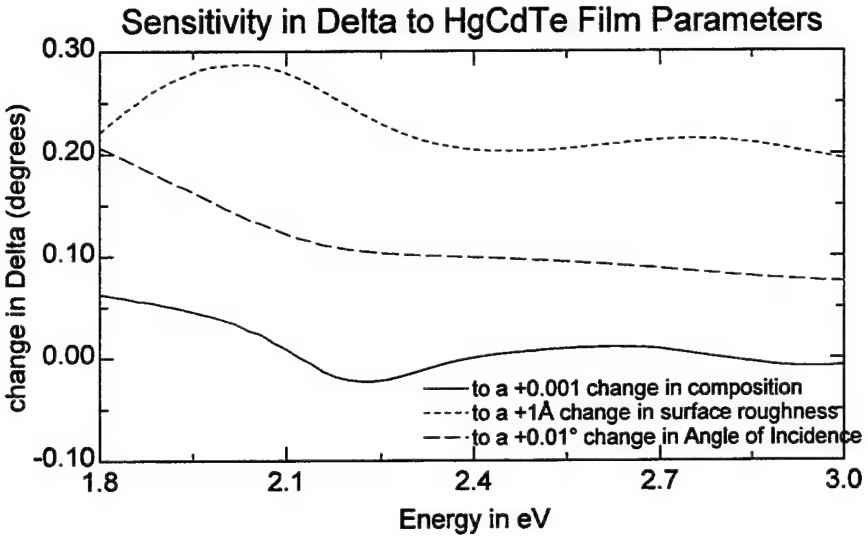

Figure 6.43. Sensitivity in the ellipsometric Delta data to the HgCdTe film parameters.

To accurately determine the composition (±0.001 in x) of a HgCdTe film, the ellipsometric Psi and Delta data must be measured insitu to accuracies of ≈0.01° and ≈0.05° respectively. Since the average measured values for Psi and Delta are ≈15° and ≈100°, this implies that the ellipsometer system needs to be accurate to 1 part in 2000. This level of accuracy can be difficult to achieve with an exsitu ellipsometer system, but it is even more difficult to achieve under insitu conditions, in which the data must be acquired through vacuum windows and on small, rotating samples.

From the preceding section, it is clear that the J.A. Woollam Co. M-88 ellipsometer technology is capable of meeting these data accuracy requirements, at least over a one month period of time. However, further work is required to determine the long term system and composition accuracy, and the applicability of results to M-88 instruments which may be installed on other MBE chambers.

7. Growth Manager Software

The Growth Manager (GMan) Software was developed to provide an easy to use, customizable interface to the insitu ellipsometer system. Another design goal of the Growth Manager program was to provide seamless integration of the ellipsometer system with other components (sensors, control computers, etc.) in the deposition system. Throughout the term of this contract, numerous versions (at least four major releases, and several minor ones) of such software were developed and tested at NVESD. While in each version of the program the user interface evolved and matured, it wasn't until the final iteration that the name 'Growth Manager' was adopted, and true customizability was incorporated into the program. This 'customizability' enables the software to operate in a variety of deposition environments: in addition to the NVESD HgCdTe MBE chamber, 'Custom' versions of GMan have been successfully integrated with other insitu SE systems used in MOCVD and MBE environments for III-V semiconductor growth.

One of the capabilities which was provided in earlier versions of the software, the ability to monitor and control the substrate temperature using the NTM1 Bandedge temperature sensor, is no longer directly supported in the latest GMan software. Currently, NVESD is not using the NTM1 temperature sensor in the HgCdTe MBE growth process, and instead relies on a low temperature pyrometer for substrate temperature measurements. However, the customizable nature of GMan makes it possible to add support for the NTM1, or any other sensor system, by writing a simple GMan-compatible Object module.

Overview of the Growth Manager (GMan) Program

Main Features / Program Architecture

The Growth Manager (GMan) software greatly simplifies the operation of an insitu spectroscopic ellipsometer (SE) system. Figure 7.1 schematically shows how the GMan program interacts with the other software and hardware components in the ellipsometer / deposition system environment. The WVASE32 software is still used to align and calibrate the insitu SE hardware, acquire ellipsometric data, and perform the data analysis. However, the GMan software automates and controls these operations via a Windows Dynamic Data Exchange (DDE) communication link to the WVASE32 program. All of the operational parameters which are required by the ellipsometer system can be specified and saved in the GMan configuration files, such

that the day to day operation of the ellipsometer system is as easy as pressing a button.

The GMan software also automatically logs all of the ellipsometric data, acquisition conditions, and real-time growth parameters for each run. This historical log can be useful in documenting the run-to-run reproducibility of the material growth, and in diagnosing deposition and/or ellipsometer system problems.

An external communication link makes it possible for GMan to communicate with and/or be controlled by other computers and sensors in the deposition system. This link can be made using an RS-232 serial interface, or a TCP/IP network link.

The Growth Manager software itself can be customized and extended by adding custom analysis and/or interface object modules. These custom modules are small OLE objects (the Windows acronym for 'Object Linking and Embedding') which are written in Visual Basic. The GMan programming manual provides detailed information on how to program such objects. The basic analysis object modules required for the real-time monitoring of semiconductor growth are supplied with the software. These object modules can be optimally configured by the user for each material system and device structure that will be grown.

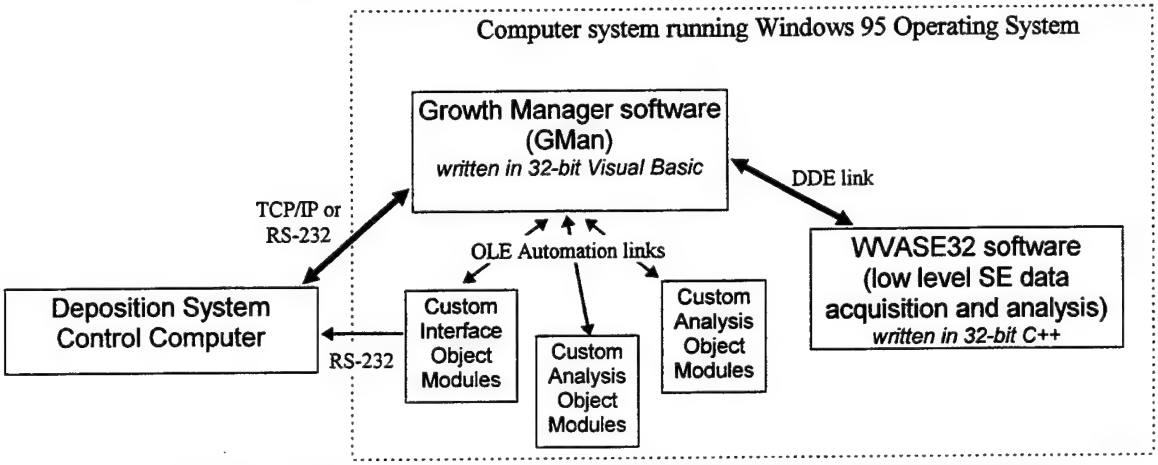

Figure 7.1. Inter-program and system communication architecture for the Growth Manager program.

Program Setup

The default directory structure used by the Growth Manager program is shown in Figure 7.2. The Growth Manager 'Setup' program (which is run by inserting Setup Disk #1 into the floppy drive and running *A:SETUP.EXE)* automatically creates the subdirectory structure shown in this figure. The Growth Manager software *requires* the Windows 95 operating system. It is important to copy the optical constant library files which are required for the real-time analysis of the SE data into the GMan 'MAT' subdirectory.

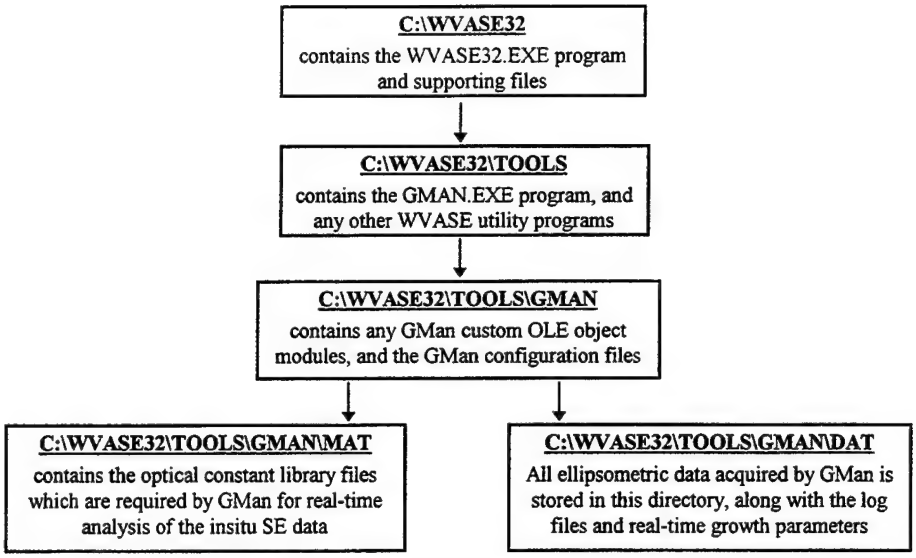

Figure 7.2. Growth Manager directory structure.

The default GMan directory structure shown in Figure 7.2 is completely adequate for most installations. However, for cases in which the insitu SE system is used for multiple applications (for example, the system is moved between an MBE reactor and an etching chamber), it is useful to maintain a separate GMan directory structure for each application. To specify a different path for the GMan MAT and DAT directories, pass a command line argument to the GMAN.EXE program which specifies the desired 'GMAN' path (the GMan program will automatically create the MAT and DAT subdirectories under this path). In Windows 95, this is done by right-clicking on the GMan icon to edit its 'Properties', and changing the 'Target' of the shortcut to specify a command line argument for the GMAN.EXE program that contains the desired data path. Figure 7.2b shows an example of this. This capability allows the user to have multiple GMan configurations, along with associated DAT and MAT directories, on a single hard drive. Multiple GMan icons can be created on the Desktop to provide easy access to the different GMan directories.

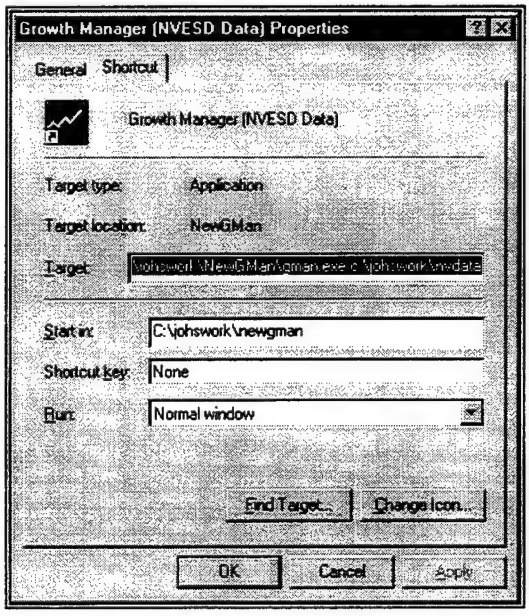

Figure 7.2b. Specifying a different data path for the GMan program.

Front Panel Description

Figure 7.3 shows the front panel which appears when the Growth Manager program is started. An overview of the key elements on this screen are given below; more detailed descriptions are given in the following section of the manual.

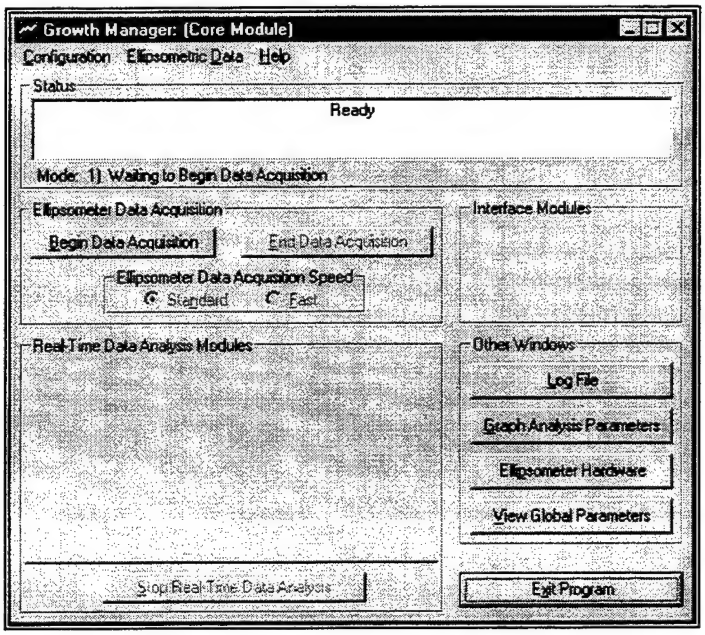

Figure 7.3. Growth Manager front panel (without any customization).

Menu Bar

There are three main headings on the Growth Manager front panel menu bar: *Configuration*, *Ellipsometric Data*, and *Help*. The *Configuration* option allows the user the completely customize (and save) all the configuration settings for the GMan program. With the *Ellipsometric Data* option, the user can choose the display mode for the 'raw' ellipsometric data which is being acquired in real-time. The *Help* option is used to display the online help file, and an 'About' box which lists the version number of the current GMan program.

'Status' area

The 'Status' area of the front panel displays the current status of the GMan program. The large message box may contain the results of real-time data analysis, the current status of the ellipsometer hardware, or other descriptive information about the system, depending on the current GMan mode, which is specified by the *Mode:* entry in the status area. There are five modes which the GMan program can be in:

1. **Waiting to Begin Data Acquisition** - This is the mode which Growth Manager starts up in. If GMan is configured to use the TCP/IP or Serial port communication links, the 'Status' box will display appropriate information about the communication link during this mode.

2. **Preparing for Data Acquisition** - This mode is entered when the 'BeginDataAcquisition' command is initiated. During this mode, the ellipsometer hardware is aligned (which may require user intervention) and calibrated.

3. **Acquiring Data** - After the ellipsometer hardware is successfully calibrated, the ellipsometer will begin acquiring ellipsometric data, and the GMan Mode box will display this message.
4. **Changing Data Analysis** - This mode is entered when a 'Real-Time Data Analysis Module' is selected. Growth Manager stays in this mode until the selected Analysis Module is successfully loaded.
5. **Real-Time Data Analysis: xxxxx** - The 'xxxxx' string describes the Data Analysis module which is currently active. The 'Status' box contains the results of the real-time data analysis.

'Ellipsometer Data Acquisition' area

The *Begin Data Acquisition* and *End Data Acquisition* buttons are used to start and stop the ellipsometer data acquisition. The *Ellipsometer Data Acquisition Speed* can be set to 'Standard' or 'Fast' by clicking the desired radio button. (It may be useful to switch to the 'Fast' acquisition speed when monitoring the growth of thin layers, for example.)

'Real-Time Data Analysis Modules' area

This area displays the available data analysis modules which can be accessed. The number, names, and functionality of these buttons are custom defined in the GMan *Configuration* settings. After data acquisition has been started, the user can click one of the available buttons to initiate the real-time analysis of the SE data. The currently active real-time analysis can be canceled hitting the *Stop Real-Time Data Analysis* button. It is also possible to switch real-time analysis modes by simply clicking a different analysis button (it is not necessary to *Stop* the current analysis before switching modes).

'Interface Modules' area

This area displays any custom-defined interface modules, which are specified in the GMan *Configuration* settings. Interface modules can be used to directly communicate with the deposition system, and thereby provide the capability to implement real-time feedback control of the deposition from within the GMan software. For GMan to directly provide feedback control of a given deposition system, however, an interface module must be custom programmed (as a Visual Basic OLE object).

'Other Windows' area

The buttons in this area bring up GMan windows which provide additional functionality and information to the user:

- **Log File:** GMan automatically logs relevant information about the growth into a log file, which is displayed by clicking on this button. The user can also add descriptive information about the growth run into this file; GMan will 'timestamp' any user entries into the log file such that growth events can be associated with the ellipsometer times in the archived data files.
- **Graph Analysis Parameters:** This button brings up a window which plots the analysis parameters in real-time. This is useful for visualizing how the sample properties (such as temperature, composition, thickness, etc.) are changing throughout the growth run.

- **Ellipsometer Hardware:** The ellipsometer hardware can be manually aligned and/or calibrated by accessing this button; this is useful when the ellipsometer system is first mounted on the chamber.
- **View Global Parameters:** A list of 'Global' parameters which describe the current state of GMan and the latest data analysis results can be accessed via this button.

'Exit' button

The Growth Manager program can be exited by pressing this button. GMan will not allow the user to exit the program if the ellipsometer is currently acquiring data; in this case, the user must hit the *End Data Acquisition* button before clicking on the *Exit* button.

Customizing the GMan Program

The *Configuration* menu option is the starting point for all GMan customization. Figure 7.4 shows the menu sub-options which are accessible under the *Configuration* heading. The sub-options which are listed under the *Custom Modules* heading are dependent on the current GMan configuration.

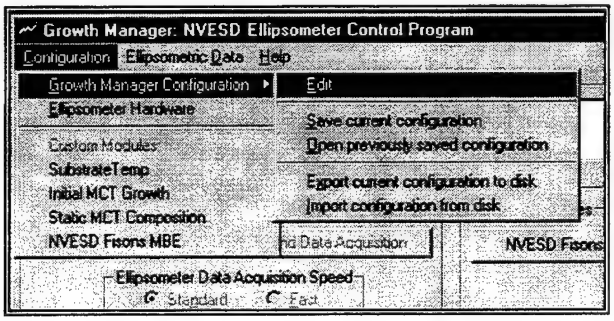

Figure 7.4. The Growth Manager Configuration menu options.

Growth Manager Configuration

To edit the main GMan configuration file, select the *Configuration* | *Growth Manager Configuration* | *Edit* menu option. Upon selecting this option, the dialog box shown in Figure 7.5 will appear. Since inadvertent changes to the GMan Configuration File can drastically affect the operation of the GMan program, user confirmation is required before the configuration file can be edited. It may also be advisable to SAVE the current configuration before any major changes are made.

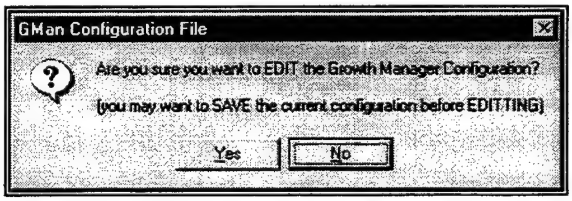

Figure 7.5. Confirmation box for editing the GMan Configuration File.

Figure 7.6 shows the dialog box which is used to edit configuration settings in the Growth Manager program. A configuration setting is selected for editing by highlighting the desired entry in the 'Current Settings' list. A description of the selected configuration setting will appear in the 'Description' box. The configuration

setting can be changed in the 'Selected Option' area. To reset the entry to its default value, click on the *Default Value(s)* button. If a 'heading' entry is selected in the 'Current Settings' list (in Figure 7.6, 'General' and 'Custom Modules' are heading entries), clicking on the *Default Value(s)* button will reset the settings of all the configuration entries which are indented under the selected 'heading'.

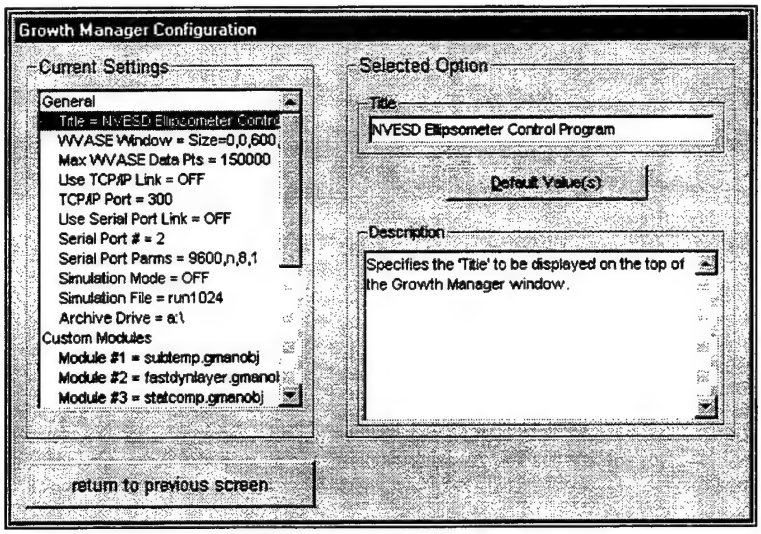

Figure 7.6. Standard Growth Manager configuration dialog box.

When you are done editing the configuration settings, hit the *return to previous screen* button. If changes have been made to the configuration file, the message box shown in Figure 7.7 will appear. To save the changes, answer 'Yes'; to ignore the changes and revert to the original configuration settings, select 'No'.

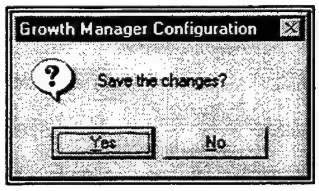

Figure 7.7. Confirmation message for saving changes to the GMan Configuration file.

A brief description of the entries found in the Growth Manager Configuration file is given in Table 7.1. For most of the entries in this table, the 'description' field adequately defines the functionality of the corresponding settings. *The 'Custom Modules' and 'Custom Interface' settings, however, are extremely important in the customization of the GMan program, as they determine the number and layout of the 'custom' buttons on the GMan front panel.* Note that for many of the entries to 'take effect' (especially the communication-related settings), it is necessary to exit and restart the GMan program.

Setting Name	Description
General	
Title	Specifies the 'Title' to be displayed on the top of the Growth Manager window.
WVASE Window	Specifies the size of the background WVASE program window; should be set to either 'Size=Xpos,Ypos,Width,Heigth' (in pixels), or the

	keyword 'Maximize'
Max WVASE Data Pts	Specifies the maximum number of ellipsometric data points that can be acquired by the program. Make sure that this number is large enough for your application.
Use TCP/IP Link	Enables the TCP/IP network communication link to Growth Manager. You must re-start Growth Manager for this setting to take effect.
TCP/IP Port	TCP/IP port number that Growth Manager will 'Listen' on to establish the TCP/IP socket link.
Use Serial Port Link	Enables the Serial Port communication link to the Growth Manager Program. You must re-start Growth Manager for this setting to take effect.
Serial Port #	Serial Port number to use for the link.
Serial Port Parms	Serial port settings (using the DOS 'mode' command format: baud rate, parity, data bits, stop bits) to use for the link.
Simulation Mode	Enables the 'Simulation Mode' of Growth Manager. In this mode, ellipsometric data will be simulated from an existing data file, instead of actually being acquired by the ellipsometer hardware. This mode is very useful for testing/debugging communication links, and verifying data analysis parameters.
Simulation File	Specifies the filename of the ellipsometric data file (.bdt extension) that will be used for the simulation mode. This file must be stored in the 'DAT' directory under the current GMAN directory.
Archive Drive	Specifies the path for archiving the ellipsometric data.
Custom Modules	Specifies the OLE object names of the custom data analysis modules. These modules show up as custom buttons on the Growth Manager window.
Module #n	
Custom Interface	Specifies the OLE object names of the custom interface modules. These modules show up as custom buttons on the Growth Manager window.
Button #n	
Log	
nRun	Default # for next Growth Run (if not explicitly given a descriptive name)

Table 7.1. Entries in the Growth Manager Configuration File.

To add buttons to the GMan front panel, enter the GMan OLE object name for the desired custom analysis module into a 'Button #n' configuration entry. The currently available GMan custom analysis modules are:

- **SubTemp.GManObj** - extracts the substrate temperature and overlayer thickness
- **FastDynLayer.GManObj** - determines the growth rate, composition, temperature, etc. for a growing semiconductor layer
- **StatComp.GManObj** - determines the composition, temperature, surface roughness, etc. of a static or optically thick semiconductor layer

Upon exiting and saving the Growth Manager Configuration file, the GMan front panel will be updated to display the buttons corresponding to the specified custom analysis modules. If GMan can not load the specified OLE object, the button caption will contain the name of the object as specified in the configuration file; otherwise, the button caption will be accordingly named by the analysis module object. For example, the default button caption for the SubTemp.GManObj module is 'Substrate Temp' (this caption can also be 'customized' by editing the corresponding custom analysis model configuration file).

Ellipsometer Hardware Configuration

This configuration file specifies the parameters which govern the ellipsometer system alignment, calibration, and data acquisition. Table 7.2 lists and describes the entries in this file. For optimum instrument performance, it is important to set these parameters properly for each insitu environment. For example, the 'Acq Time' entries for alignment, calibration, and data acquisition should be set equal to the substrate rotation period (or an integral multiple) for best signal-to-noise.

Setting Name	Description
Alignment	Specifies the alignment parameters. Alignment of the detector box is important when acquiring accurate ellipsometric data.
Acq Time	Signal averaging time for sample alignment, in seconds
Fast Acq Time	Signal averaging time for 'fast' sample alignment, in seconds
Skip Alignment	If this parameter is turned ON, the sample alignment screen will NOT be displayed each time a growth run is started; if the sample alignment is very reproducible, this may be acceptable behavior. However, for most installations, it is a good idea to leave this option OFF such that the alignment can be verified and adjusted if necessary before each run.
Normal Calibration	Specifies the Normal Calibration parameters. Calibration of the ellipsometer is important when acquiring accurate ellipsometric data. The Normal Calibration procedure must be performed each time the ellipsometer system is started up.
Skip Calibration	If this parameter is turned ON, the Normal Calibration procedure will not necessarily be performed each time a growth run is started; this provides the user the opportunity to 'manually' perform the Normal Calibration directly in WVASE. However, for most installations, it is a good idea to leave this option OFF such that the Normal Calibration procedure is automatically performed before each run.
Acq Time	Signal averaging time for each calibration data point, in seconds.
# of Points	Number of data points acquired for calibration
Polarizer Span	Degree span of the polarizer for the calibration data points

Ps Err Limit	Acceptance limit for the Ps (polarizer azimuth) calibration parameter err bar.
As Err Limit	Acceptance limit for the As (analyzer azimuth) calibration parameter err bar.
Fd Err Limit	Acceptance limit for the Fd (detector azimuth) calibration parameter err bar.
Coarse Calibration	Specifies the Coarse Calibration parameters. Coarse Calibration of the ellipsometer system should be performed only when the system is moved to a different location/chamber, or if the Normal Calibration procedure is unable to lock onto acceptable calibration parameters
Acq Time	Signal averaging time for each calibration data point, in seconds.
# of Points	Number of data points acquired for calibration
Polarizer Span	Degree span of the polarizer for the calibration data points
Ps Err Limit	Acceptance limit for the Ps (polarizer azimuth) calibration parameter err bar.
As Err Limit	Acceptance limit for the As (analyzer azimuth) calibration parameter err bar.
Fd Err Limit	Acceptance limit for the Fd (detector azimuth) calibration parameter err bar.
Data Acquisition	Specifies the parameters used for the Ellipsometer Data Acquisition
Angle of Incidence	Nominal angle of incidence for the ellipsometric measurements
StdAcquisition, Acq Time	Signal averaging time for each data point, in seconds.
Polarizer	Azimuthal angle of the polarizer (in degrees); this angle should be chosen near the measured ellipsometric Psi data for optimal data accuracy
High Accuracy	Enables the 'High Accuracy' data acquisition mode; two ellipsometric measurements are taken for each data point (at +P and -P polarizer settings) to 'zone average' the data.
FastAcquisition, Acq Time	Signal averaging time for each data point, in seconds, when the 'FastAcquisition' mode is selected
Graph Update	Enables automatic updating of the raw ellipsometric data graph
Update Period	Specifies how often (in number of data points), the raw ellipsometric data graph should be updated
Acquisition Channels	A string that specifies which channels of ellipsometric data should be acquired. This string must use one of the following formats: 'all', 'skip=n', channel list '0 10 20', and wavelength range '1.8-2.4 eV'. The 'all' keyword will use all of the available data channels, the 'skip=n' keyword (where 'n' is replaced by an integer) will use every n'th channel, the channel list specifies a list of discrete channel numbers (separated by commas), and the wavelength range specifies a range of

	channels (the range must be specified in either eV or nm).
Fit Channels	A string that specifies which channels of ellipsometric data will be used in the data analysis. See the Acquisition Channels entry for details on the format of this string.
Graph Channels	A string that specifies which channels of ellipsometric data will be used for graphing the raw ellipsometric data. See the Acquisition Channels entry for details on the format of this string.
Raw Data Channels	A string that specifies which channels of raw ellipsometric data will be sent back to the Growth Manager program (and can then be accessible by external programs). See the Acquisition Channels entry for details on the format of this string. This entry can be left blank if raw ellipsometric data is not required by your application.
Log Alignment Data	Enables the Logging of Alignment and Intensity data throughout the growth run; this information can be displayed in the Parameter Graph

Table 7.2. Entries in the Ellipsometer Hardware Configuration File.

'Custom Modules:' Configuration

For each custom analysis module which is specified in the Growth Manager Configuration File, a menu option will appear for its corresponding configuration file. These configuration files are edited in a manner similar to the GMan and Ellipsometer Hardware configuration files. For a explanation of the entries in these files, refer to the 'Description' field which appears in the configuration dialog box. Note than for some of the entries to 'take effect', it may be necessary to exit and restart the GMan program.

Saving and Exporting Configurations

The current GMan configuration settings can be saved under a specified name (and subsequently opened) by using the *Save current configuration* and *Open previously saved configuration* menu sub-options which are found under the *Growth Manager Configuration* menu option on the GMan front panel. This capability allows the user to specify multiple 'configuration sets' for the GMan program. For example, one could create (and save) a customized GMan configuration set for growing InGaAs-based materials, and another configuration for growing AlGaAs structures. The *Open previously saved configuration* option could then be used to easily switch between the different custom configurations.

The configuration settings can also be exported and imported onto a floppy disk, using the *Export current configuration to disk* and *Import configuration from disk* menu sub-options. The 'Archive drive' entry in the Growth Manager configuration file specifies the path which is used for the archive (by default, the A: floppy drive is used). Insert a blank floppy disk into the drive before selecting the *Export current configuration to disk* option; likewise, insert the disk containing the archived configuration data into the drive before selecting the *Import configuration from disk* option. These options are useful for transferring a GMan configuration set to another insitu SE installation which is also running the GMan software.

The options described in this section save and/or restore *all* of the GMan configuration settings, including the Growth Manager, Ellipsometer Hardware, and Custom Modules configuration files.

Operation of the GMan Program

Starting Growth Manager

To start the GMan program, click on the corresponding icon on the Windows desktop (if one exists), or select the *Programs \ WVASE 3.0 \ GMan* entry which appears on the 'Start' button menu. It is not necessary to start the WVASE32 program before starting GMan, as GMan will automatically start WVASE32 if it is not already running.

GMan will disable the menus in the WVASE32 program; this is to prevent a novice user from making inadvertent changes in the WVASE32 program while GMan is running. To redisplay the WVASE32 menus (which should not be required for the normal operation of GMan), switch to the WVASE32 program and hit Alt-M.

First Time Operation (SE Hardware diagnostics)

If this is the first time that GMan is being run on a given insitu installation (or if there are problems with the current ellipsometer system which require some diagnostic capabilities), it may be helpful to click the 'Ellipsometer Hardware' button on the front panel. This brings up the dialog box shown in Figure 7.8. From this screen the user can manually perform ellipsometer alignment and calibration.

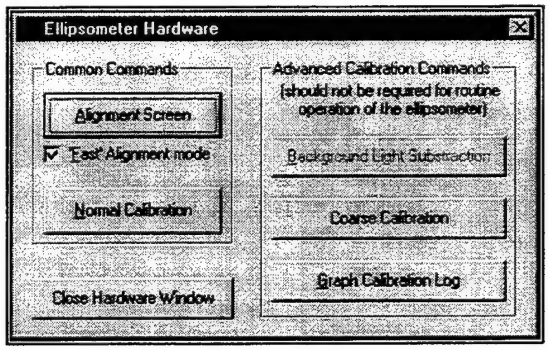

Figure 7.8. Ellipsometer Hardware dialog box (used for initial setup and diagnostics).

Alignment in GMan

The 'Alignment Screen' is used to verify the alignment of the ellipsometer detector box with respect to the beam reflected off the sample. Pressing this button displays the WVASE32 alignment screen: simply adjust the output tilt stage to center the crosshair on the screen. When you are finished, press the 'Esc' key to cancel the alignment screen. The sampling time for the alignment is specified in the Ellipsometer Hardware configuration file. Two alignment acquisition times are specified, one for 'standard' alignment, and one for 'fast' alignment. The 'fast' alignment mode is useful for visualizing how the ellipsometer beam alignment varies throughout the substrate rotation period. The 'standard' alignment gives the *average* beam alignment throughout the substrate rotation period. It is helpful to start by

performing alignment in the 'fast' mode, and then switch to the 'standard' mode for the final beam alignment.

Calibration in GMan

The Ellipsometer Hardware configuration file specifies (to WVASE32) how the ellipsometer system will be calibrated. Separate settings exist for both 'Coarse' calibration (which should only have to be performed the when the system is initially mounted on the chamber, or if the 'Normal' calibration fails), and 'Normal' calibration (which is performed each time a new sample is loaded into the chamber).

If the calibration is not successful, GMan will display an error message containing the calibration parameters, their 'error bars', and the corresponding GMan acceptance (error) limits. To obtain a successful GMan calibration, it may be necessary to either increase the '# of Points' and/or 'Acq Time' settings in the appropriate calibration section(s) of the Ellipsometer Hardware configuration file, or to increase the 'Err Limit' of the corresponding calibration parameter in the same file.

To visualize how the instrument calibration parameters have changed over time, select the 'Graph Calibration Log' button. This runs a separate program (CALVIEW.EXE) which graphically displays the calibration information, as shown in Figure 7.9. To use this program, select the desired entries in one of the list boxes, along with a parameter type to graph from the corresponding drop-down list, and then click on the 'Plot Data' button. The 'WVASE Log File' list contains info from the recent 'Normal' and 'Coarse' calibrations; the 'Detector Polarization Sensitivity' and the 'Electronics Calibration' lists are from the ellipsometer system (straight-through) calibrations, which are performed less frequently.

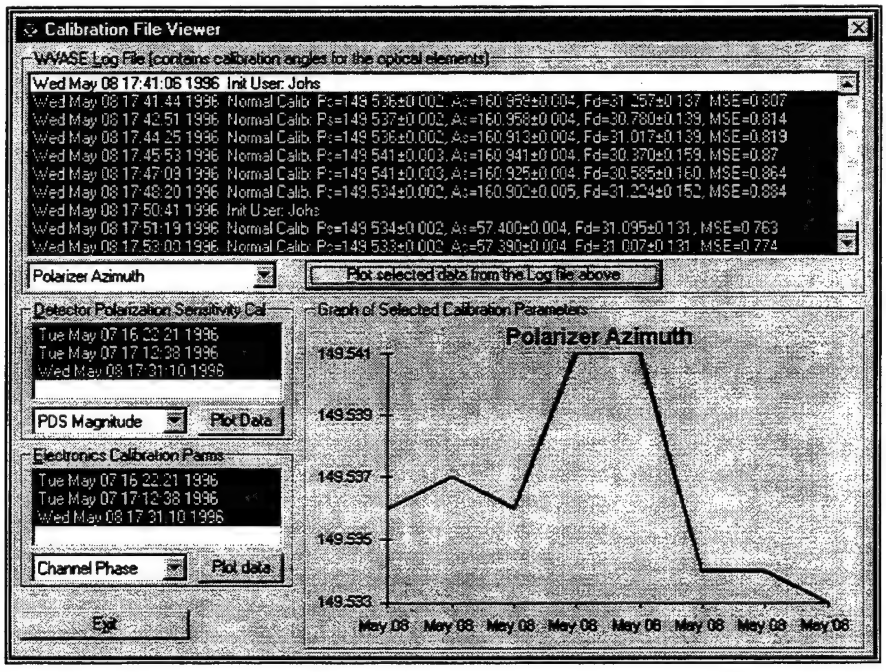

Figure 7.9. CALVIEW program for viewing the calibration parameter log.

Background Light Subtraction

While the optics of the M-XX system normally prevent it, in some circumstances (intense radiation from a plasma, for example), stray background light from the

chamber *can* enter the detector and corrupt the ellipsometric measurement. To correct for the effects of stray light, it is possible to hit the 'Background Light Subtraction' button after the data acquisition process has been started in GMan. (However, this capability has **not** been required for any epitaxial semiconductor growth applications, using both MBE and MOCVD deposition techniques.)

Normal (Daily) Operation

The following sections describe the procedures that should be followed to perform insitu spectroscopic ellipsometry (SE) monitoring of a growth run using the Growth Manager (GMan) program. It is assumed that the GMan configuration files have been set up appropriately *before* the procedures are started.

Begin Data Acquisition

The 'Begin Data Acquisition' button on the GMan front panel initiates the insitu SE monitoring of the growth run. Upon clicking this button, the dialog box shown in Figure 7.10 appears. Enter a descriptive name to save the data files for this growth run (the names of existing data files, from previous growth runs, are shown for reference). The descriptive name can be of arbitrary length and can contain spaces. However, some special symbol characters (such as '\' or '/') are not allowed in name; GMan will *require* the user to enter a valid the filename before continuing. Alternatively, by enabling the 'Use an automatically assigned Run Number ...' checkbox, GMan will assign a unique number to the growth run.

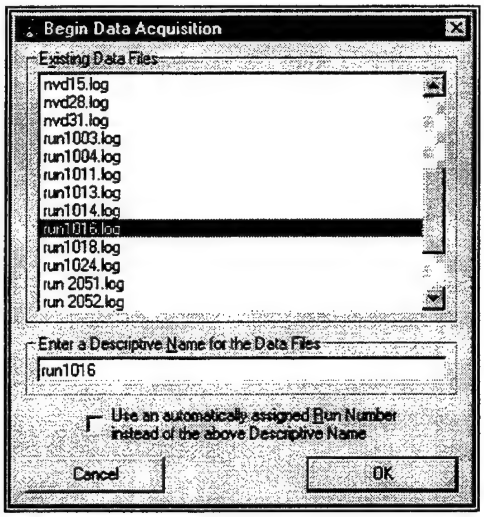

Figure 7.10. Begin Data Acquisition dialog box (enter a descriptive name for the growth run)

After entering a descriptive name (or enabling the checkbox), clicking the 'OK' button on the dialog box (shown in Figure 7.10) will bring up the ellipsometer alignment screen. As described in the 'Alignment in GMan' section above, adjust the output tilt stage to center the crosshair on the screen. Hit the 'Esc' key when you are finished with the alignment process.

After alignment, GMan will initiate a calibration of the ellipsometer system. This may take a while, depending on the calibration settings (# of Points, Acq Time, etc.) in the Ellipsometer Hardware configuration file. A status message indicating that calibration is being performed will appear in the GMan front panel. If the calibration is *successful*, GMan will begin acquiring ellipsometric data, and the 'Mode:' indicator on the front panel will change to '3) Acquiring Data'. If the calibration is

not successful, the 'Mode:' will be set to '1) Waiting to Begin Data Acquisition', and a descriptive error message will be displayed.

Very Important Note: Since the 'Begin Data Acquisition' procedure automatically aligns and calibrates the insitu SE system, it is *absolutely critical* that the sample is both under actual growth conditions (i.e., the substrate is rotating) and the surface is stable (i.e., the temperature is **not** changing, and no films are being deposited) *throughout* the entire alignment and calibration process. This means that an appropriate 'time window' in the growth process must be reserved to perform these procedures, and the 'Begin Data Acquisition' button should not be selected until the sample is in a 'stable' condition. In practice, it is easy to insert a 5-10 minute step into the growth recipe which holds the wafer at a given temperature before continuing with the oxide desorption process. Ideally, the sample temperature during this period would be near the growth temperature, as the ellipsometer beam alignment can change as the substrate temperature is increased from room temperature to growth temperature.

Log File

GMan will automatically enter the results of the insitu SE alignment and calibration into the Log file, which is shown in Figure 7.11. Additional comments can be entered by the user in the 'Log Item:' field; when the 'Add Log Item' button is pressed, the comment will be added to the Log File, along with the current ellipsometer 'Time' (in minutes). This allows the user to associate various events during the growth process (shutters opening, changes in cell temperatures, etc.) with specific times in the ellipsometer data set.

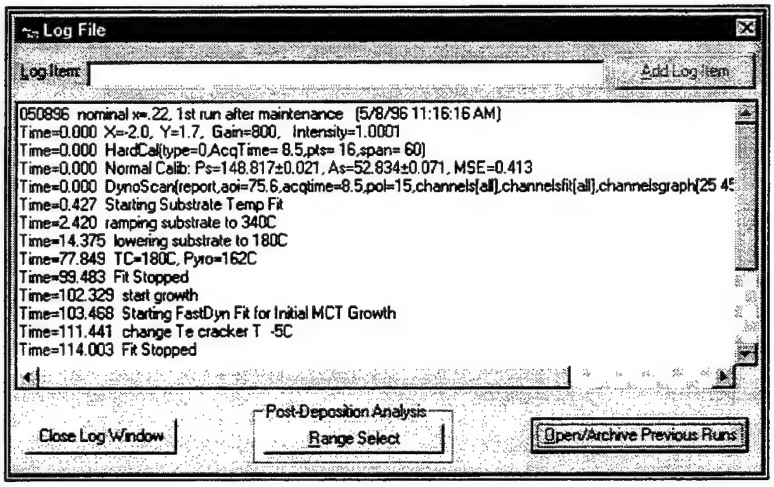

Figure 7.11. The GMan Log File dialog box.

Real-Time Data Analysis

After the data acquisition process has been started in GMan (i.e., the 'Mode:' indicator reads '3) Acquiring Data'), the user can click on one of the 'Real-Time Data Analysis Modules' buttons. The number and names of these buttons are *customized* in the Growth Manager configuration file. Likewise, the resulting behavior of a given button is dependent on the type of analysis object (and its configuration settings) which is associated with the button. In general, however, clicking a Real-Time Data Analysis button will cause the 'Mode:' indicator to switch to '4) Changing Data Analysis'; if the analysis module is successfully loaded, the

'Mode:' will read '5) Real-Time Data Analysis: xxxxx', where 'xxxxx' specifies the name of the current data analysis algorithm.

Most Real-Time Data analysis modules will update the status display on the GMan front panel with current parameters from the real-time analysis of the insitu SE data. Sometimes it takes a few ellipsometer data acquisitions (5 - 60 seconds) before the analysis module can calculate the results.

To cancel the current real-time data analysis, simply hit the 'Stop Real-Time Data Analysis' button. It is also possibly to directly switch to another real-time data analysis module *without* stopping the current analysis.

Graph Analysis Parameters

The results of the real-time data analysis can also be viewed graphically by clicking on the 'Graph Analysis Parameters' button on the GMan front panel. The 'Real-Time Analysis Parameter Graph' screen is shown in Figure 7.12. In this screen, any of the parameters which are extracted from the real-time data analysis can be plotted vs. time. Two Y-axes are available for graphing, and two parameters can be simultaneously graphed on each axis. To select a parameter for graphing, click on one of the drop-down list boxes in the Y1- or Y2-Axis area of the screen. As the mouse pointer is moved within the graph region, the 'x=', 'y1=', and 'y2=' fields on the screen correspond to the current position of the mouse on the graph.

A 'Defined Graph Set' can also be selected in the drop-down list at the top of the screen; these 'graph sets' are convenient groupings (for graphing) of parameters which are defined by the real-time analysis modules. For example, the Substrate Temperature analysis module defines a graph set which displays the 'Temp' and 'TempSmooth' parameters on the Y1-Axis and the 'Oxide' parameter on the Y2-Axis. Another useful 'Defined Graph Set' is the 'Alignment Info' set, which displays the ellipsometer alignment and signal intensity throughout the growth run.

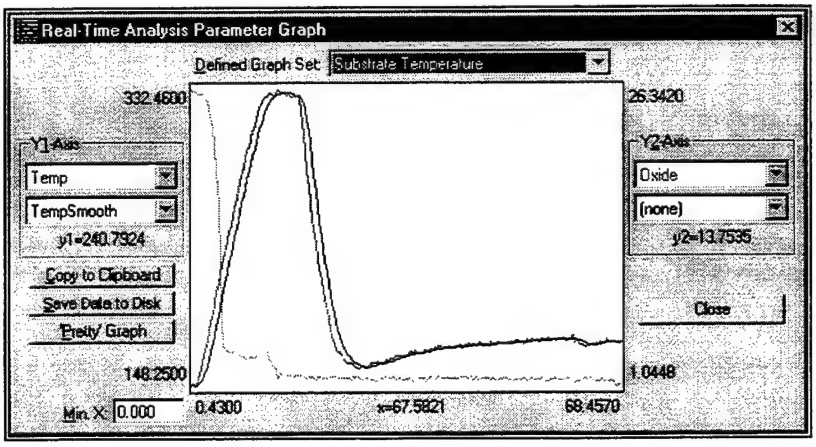

Figure 7.12. The GMan Real-Time Analysis Parameter Graph screen.

The 'Copy to Clipboard' and 'Save to Disk' buttons will output ASCII data from the displayed curves to the clipboard or a disk file respectively. The format of the data is: the 1st line is the name of the 1st graphed parameter, followed by lines with the x (time) and y (parameter value) data for the curve in two tab-delimited columns; the data for the other curves on the graph are specified in the same manner, and are appended to the previous curve data.

The 'Min. X:' field can be used to zoom in on limited time range of the data. The 'Pretty Graph' button can be used to generate (and print or copy to the clipboard) a

more publication-ready version of the graph, as shown in Figure 7.13. To modify, print, or copy the graph shown in this screen, use the pop-up menu which appears by 'right-clicking' the mouse on the graph. Unfortunately, at this time the 'Pretty Graph' option does not support double Y-axis graphs.

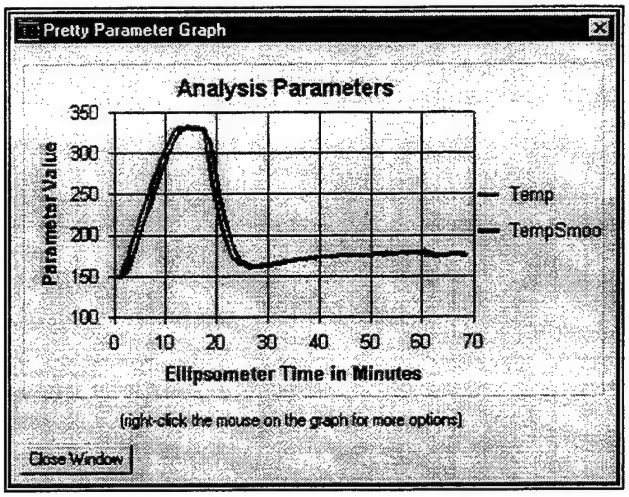

Figure 7.13. 'Pretty' Parameter Graph in GMan.

Viewing the 'Raw' Ellipsometric Data

Much qualitative information about a growth run can be derived from a simple observation of how the 'raw' ellipsometric Psi and Delta parameters change as a function of time. GMan supports the ability to conveniently visualize the raw ellipsometric data in real-time via the *Ellipsometric Data* menu option found on the GMan front panel. The menu options for viewing the ellipsometric data are shown in Figure 7.14.

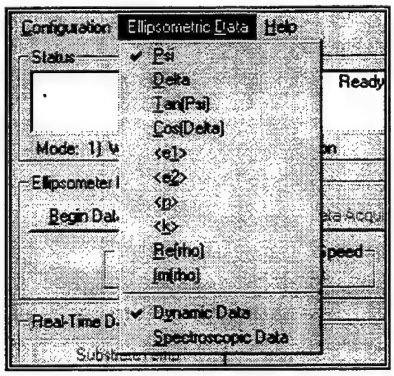

Figure 7.14. Menu options for viewing 'raw' ellipsometric data.

The first set of options in this menu (Psi, Delta, etc.) specify which ellipsometric parameter, or derived quantity, will be graphed. It is a matter of personal preference as to which parameter should be displayed in real-time. For some parts of the growth (the oxide desorption, for example), the ellipsometric 'Delta' parameter may be more sensitive to the growth process, while for other periods (the optically thick regime during the growth of a very thick layer) the pseudo optical constant quantities, such as <e2>, may provide a more direct indicator of the growth quality.

The second set of options in Figure 7.14 allows the user to switch between 'Dynamic' and 'Spectroscopic' display modes. The 'Dynamic' mode plots the raw

ellipsometric data vs. time, as shown in Figure 7.15. After selecting this menu option, GMan will prompt for 'the starting time to display data'; this enables the user to zoom in on the more recent data (enter '0' to view data from the entire growth run). The wavelengths of data which are plotted are specified by the 'Graph Channels' entry in the Ellipsometer Hardware configuration file. The oscillations observed in the dynamic data are due to optical interference effects in a growing film. After an absorbing film becomes 'optically' thick, the interference oscillations are dampened out, and the ellipsometric data vs. time becomes constant (as long as the surface composition, temperature, and morphology also remain constant).

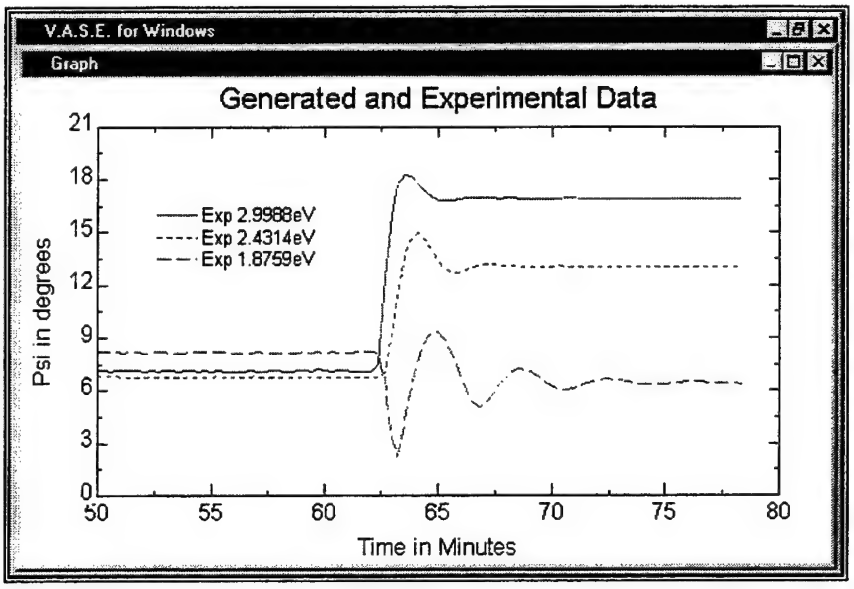

Figure 7.15. Dynamic display mode for insitu SE data.

The 'Spectroscopic' display mode plots the ellipsometric data vs. wavelength, using the most recently acquired timeslice of data. Figure 7.16 shows an example of raw ellipsometric data displayed in the spectroscopic mode. This display mode is useful for visualizing the quality of fit for the substrate temperature and/or static composition real-time data analysis modules, which is evidenced by the agreement of the red 'Model Fit' and green 'Exp Data' curves. (The dynamic mode is better suited for viewing the data fits during the initial growth of a layer, which use the 'FastDyn' real-time data analysis module).

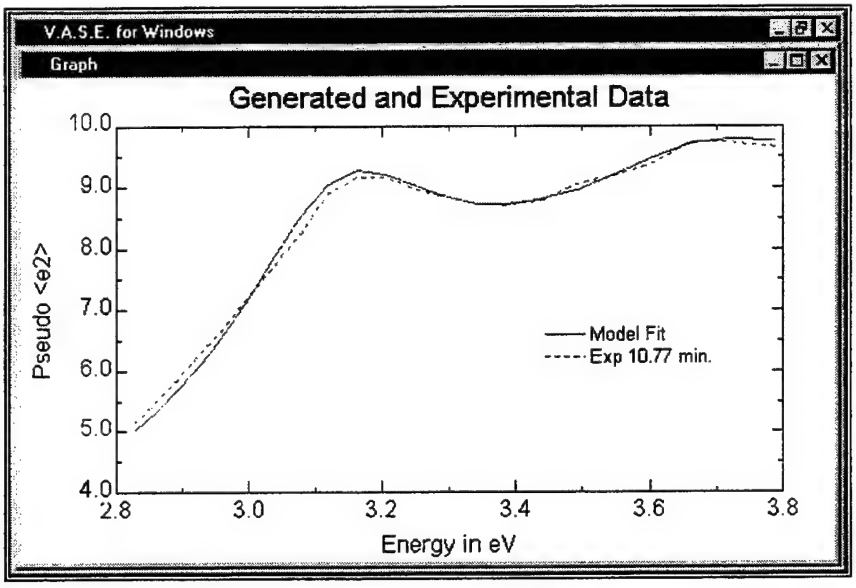

Figure 7.16. Spectroscopic display mode for insitu SE data.

End Data Acquisition

To terminate the insitu SE monitoring, press the *End Data Acquisition* button on the GMan front panel. This will save all of the raw ellipsometric data, the log file, and the real-time analysis parameters into the GMan DAT directory (see Figure 7.2). The save process can take a while; when the process is complete, the 'Mode:' indicator will display '1) Waiting to Begin Data Acquisition'. To prevent the collection of spurious insitu SE data, it is best to end the data acquisition *before* the wafer is removed from the chamber.

Archiving and Retrieving GMan Data

To retrieve the GMan data which was stored in a previous growth run, click the 'Open/Archive Previous Runs' button on the Log File screen (Figure 7.11). This brings up the dialog box which is shown in Figure 7.17. To load data from a previous run, highlight the desired run in the list box, and click the 'Open Selected Run' button. GMan will then load the log file and real-time analysis parameters corresponding to the selected run. If the 'Load raw data in WVASE' button is checked, GMan will also load the raw ellipsometric data into the WVASE32 program.

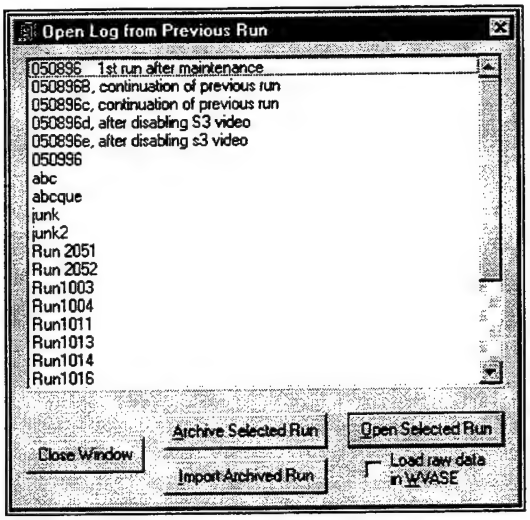

Figure 7.17. Open / Archive / Import GMan data from previous run dialog box.

The 'Archive Selected Run' button allows the user to export the GMan data from the selected run onto floppy disk. The program will automatically split large data files across multiple disks as necessary. The 'Import Archived Run' will read an archived GMan data file from a floppy disk(s). These capabilities are useful for transferring the large amounts of GMan data from one system to another.

Running GMan in *Simulation Mode*

When designing a custom GMan configuration, it is would be desirable to 'test' the real-time data analysis modules (and try different configuration settings to optimize the analysis results) *without* actually having to acquire insitu SE data. It would also be nice to test/debug external communication links to the GMan program without having to run the SE hardware. These capabilities are provided by the GMan simulation mode. To enable the GMan simulation mode, turn the 'Simulation Mode' entry in the Growth Manager configuration file to 'ON', and specify the name of an existing ellipsometric data file (without the .BDT extension) in the 'Simulation File' entry (this file must be stored in the GMan DAT directory). Exit and save the configuration settings; the 'Simulation Mode' indicator will appear in red on the GMan front panel, as shown in Figure 7.18.

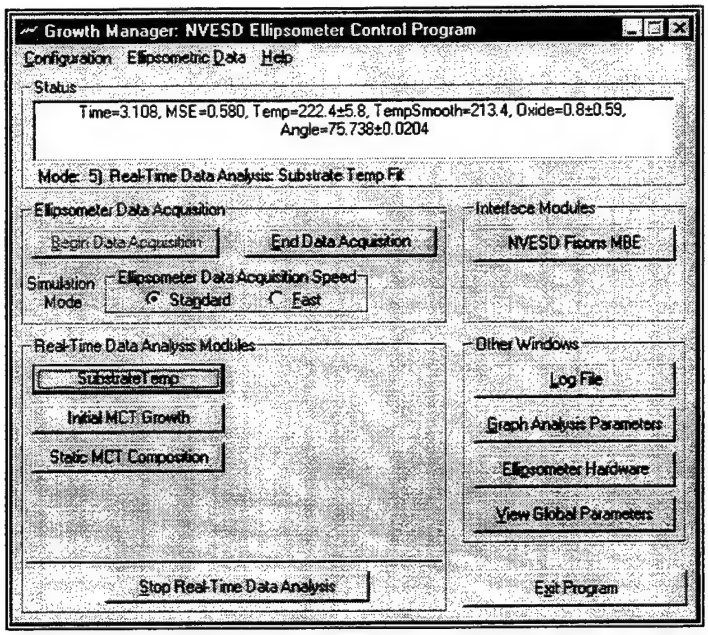

Figure 7.18. The GMan program in 'Simulation Mode'.

Now when the *Begin Data Acquisition* is pressed, the WVASE32 program will 'pretend' to acquire ellipsometric data: instead of initializing the SE hardware and actually acquiring data, it will use the raw ellipsometric data from the existing file. All of the GMan capabilities are supported in simulation mode, including the Fast / Slow modes of data acquisition (which is useful for quickly skipping through data in the simulation), the Real-Time Data Analysis Modules, the Graphing of Analysis Parameters, the Log File, viewing the raw ellipsometric data, and the external communication interface.

Use of GMan at NVESD

Custom Configuration

The NVESD customized version of the GMan program is shown in Figure 7.19. Three Real-Time Data Analysis Modules are defined:

- **SubstrateTemp** - This button is used during the substrate heat-clean procedure to monitor the CdZnTe substrate temperature and overlayer thickness before the HgCdTe growth is initiated.
- **Initial MCT Growth** - This button extracts the HgCdTe growth rate and composition during the initial part of growth (the first ≈ 10 - 20 minutes). It should be pressed 30-60 seconds after the growth is initiated.
- **Static MCT Composition** - This button should be pressed during the optically thick regime (after ≈ 20 minutes of growth) of the HgCdTe film growth to extract the HgCdTe composition.

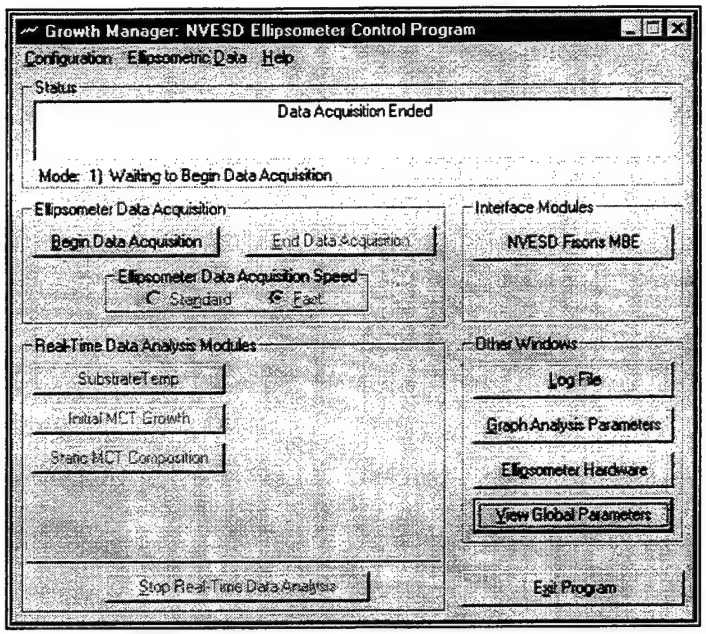

Figure 7.19. NVESD 'Customized' GMan Front Panel layout.

The NVESD Fisons MBE 'Interface Module' is used to provide a link to the Fisons MBE control computer, which is used for feedback control of the HgCdTe growth. This button is described in more detail in the next section.

Examples of using the three Real-Time Data analysis buttons throughout the phases of the HgCdTe growth process are shown in the Figures 7.20 - 7.22.

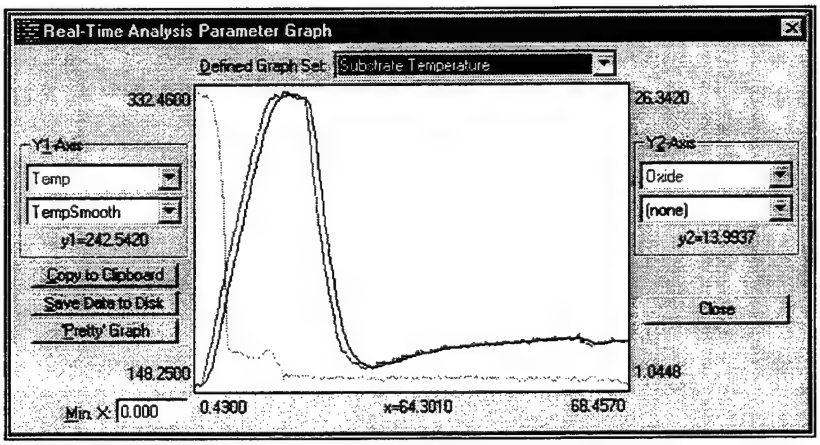

Figure 7.20. Real-Time analysis parameters during the CdZnTe heat-clean procedure.

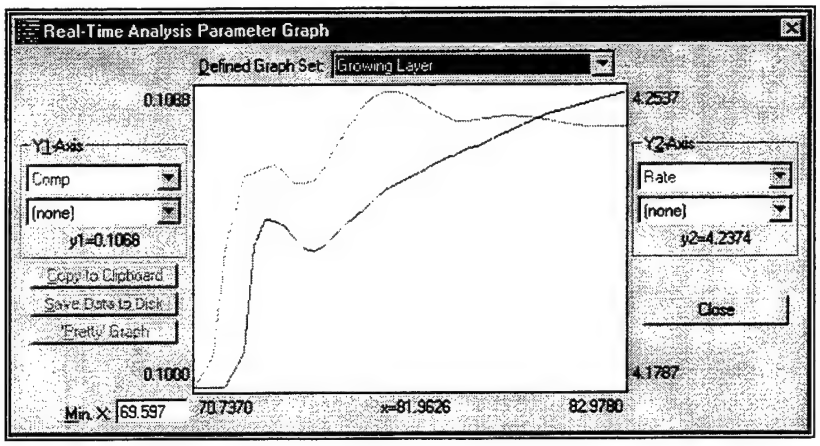

Figure 7.21. Real-Time composition and growth rate during initial MCT growth.

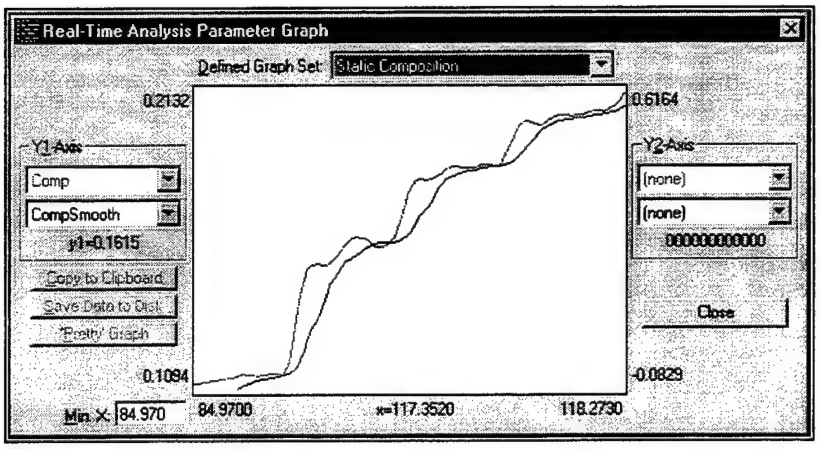

Figure 7.22. MCT composition during optically thick region of growth (the CdTe cell temperature was intentionally changed during this run, and therefore the composition is changing accordingly).

For reference purposes, the contents of the various GMan configuration files at the NVESD installation are listed below:

NVESD Growth Manager Configuration File

```
[General]
Title=NVESD Ellipsometer Control Program
Use TCP/IP Link=OFF
TCP/IP Port=300
Simulation Mode=OFF
Archive Drive=a:\
Hide WVASE=OFF
Max WVASE Data Pts=150000
Simulation File=run1024
Mat/Dat Path=
WVASE Window=Size=0,0,600,400
Use Serial Port Link=OFF
Serial Port #=2
Serial Port Parms=9600,n,8,1

[Custom Modules]
Module #1=subtemp.gmanobj
Module #2=fastdynlayer.gmanobj
```

```
Module #3=statcomp.gmanobj
Module #4=
Module #5=
Module #6=
Module #7=
Module #8=
Module #9=
Module #10=

[Custom Interface]
Button #1=nvesd.gmanobj
Button #2=

[Log]
nRun=2051
```

NVESD Ellipsometer Hardware Configuration File

```
[General]
[Alignment]
# of Revs=50
Skip Alignment=OFF
Acq Time=8.5
Fast Acq Time=0.2

[Normal Calibration]
Skip Calibration=OFF
# of Revs=30
# of Points=30
Polarizer Span=180
Acceptance Limit=2
Acq Time=8.5
Ps Err Limit=0.1
As Err Limit=0.5
Fd Err Limit=2

[Coarse Calibration]
# of Revs=5
# of Points=60
Polarizer Span=180
Acceptance Limit=0.5
Acq Time=3
Ps Err Limit=0.05
As Err Limit=0.2
Fd Err Limit=1

[Data Acquisition]
# of Revs=20
Polarizer=15
High Accuracy=ON
Graph Update=ON
Update Period=1
Acquisition Channels=all
Fit Channels=all
Graph Channels=25 45 70
StdAcquisition, # of Revs=60
FastAcquisition, # of Revs=5
Angle of Incidence=75.6
StdAcquisition, Acq Time=8.5
FastAcquisition, Acq Time=0.5
```

```
Log Alignment Data=ON
Raw Data Channels=
```

NVESD Substrate Temp Configuration File

```
[Substrate]
Temp File=czt-nv
Oxide File=srough
Fit Wvls=2.8-3.8 eV
Smoothing=8
Nominal Temp=180
```

NVESD Initial MCT Growth Configuration File

```
[General]
Name=Initial MCT Growth
Opt Const File=mct-nv
Nominal Comp=0.225
Nominal Rate=4
Fit Type=0
Interface Time=0.5
Num Points=50
Min Points=3
Max Iter=8
Fill Gen Data=ON
Fit Wvls=1.8-3 eV
Nominal Temp=180

[Fit Parms]
Fit Comp=ON
Comp Bounds=.1 .4
Comp Min Thick=50
Fit Rate=ON
Rate Bounds=2.5 6
Rate Min Thick=10
Fit Angle=ON
Angle Bounds=74 77
Angle Min Thick=50
Fit VI=ON
VI Min Thick=50
Fit Temp=OFF
Temp Bounds=200 700
```

NVESD Static MCT Composition Configuration File

```
[Parms]
Name=Static MCT Composition
Comp File=mct-nv
Surface Roughness=ON
Fit Wvls=1.8-3 eV
Smoothing=10
Nominal Comp=0.25
Nominal Temp=180
```

Interfacing with the Fisons Control Computer

To interface with the Fisons control computer, a GMan custom interface module was programmed (NVESDOBJ.EXE; its OLE object name is NVESD.GManObj). Pressing this button brings up the dialog box shown in Figure 7.23.

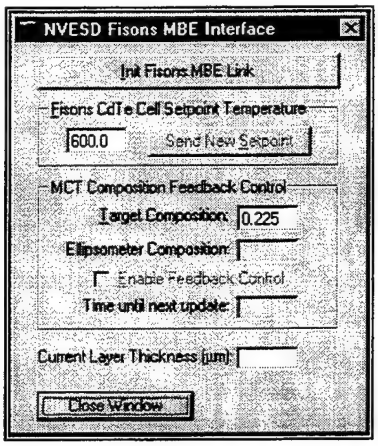

Figure 7.23. GMan NVESD Fisons MBE Interface control box.

To complete the Fisons-GMan communication link, it is also necessary to run the COMKEY.EXE program on the Fisons OS/2 computer. (This program was installed into the 'startup' folder of the Fisons computer, such that it should be automatically run each time the computer is restarted.) COMKEY.EXE was written in the VX-REXX programming language, and is used to convert characters sent over the serial link into emulated keystrokes that can be used to indirectly control the Fisons MBE control software. This is not a very elegant or robust way to implement inter-system communication, but it was fairly simple and does not interfere with or disable the standard operation of the Fisons MBE control software.

To initialize / test the GMan-Fisons communication link, click on the 'Init Fisons MBE Link' button, and follow the on-screen prompts. If the link is successfully initialized, a new CdTe setpoint temperature can be entered and sent to the Fisons MBE control computer (using the 'Send New Setpoint' button).

During the optically thick regime of the HgCdTe growth in which GMan is in the 'Static MCT Composition' Real-Time Analysis mode, the 'Enable Feedback Control' box can be checked. When feedback control is enabled, the NVESD Fisons MBE Interface object will compare the 'Target Composition' with the 'Ellipsometer Composition', and periodically update the Fisons MBE CdTe cell setpoint temperature to bring the ellipsometer composition closer to the target value. A simple proportional feedback algorithm is used. The feedback constants are set in the configuration file, which is listed below.

The 'Current Layer Thickness (μm):' field at the bottom of the box calculates the current (extrapolated) HgCdTe layer thickness, based on the SE growth rate determined during the initial MCT layer growth, and the total layer growth time.

NVESD Fisons MBE Interface Module Configuration File

NVESD Configuration Entry / Default Value	Description
[MCT Feedback Settings]	
Update Rate=8	Specifies how often (in minutes) the CdTe setpoint will be updated to provide feedback control
Feedback Constant=210	Determines the CdTe cell temperature correction for feedback control: NewTemp = OldTemp + (TargetComp-CurrentComp)*FeedbackConstant
Min CdTe Temp=500	Protection Limits for the CdTe effusion cell
Max CdTe Temp=700	Protection Limits for the CdTe effusion cell
[MBE Link Settings]	Specifies how to connect to the Fisons MBE machine. IMPORTANT NOTE: The 'COMKEY.EXE' program MUST be

	installed and running on the Fisons OS/2 Computer for the communication link to work.
Serial Port=1	Specifies which serial port to use for the MBE communication link.
Port Settings=1200,n,8,1	Specifies the serial port settings: baud rate, parity, data bits, stop bits.
Init String={alt}lm	Keystokes to 'initialize' the communication link
CdTe String #1={alt}lt	Keystrokes to send the first part of the CdTe temperature update message
CdTe String #2={down}{down}{down}{down}{tab}	Keystrokes to send the second part of the CdTe temperature update message
CdTe String #3={Enter}	Keystrokes to send the third part of the CdTe temperature update message
Delay Time=300	Delay (in milliseconds) between sending keystroke strings to the Fisons computer

HgCdTe Feedback Control results

Using the GMan-Fisons custom interface module described in the preceding section, a HgCdTe SE feedback control experiment was performed. The real-time analysis parameters resulting from the control experiment are shown in Figure 7.24 ('pretty' graphs from this experiment are shown in Figure 7.25). The initial target composition was x=0.225, however, as shown in the parameter graph, the actual HgCdTe composition (as determined by insitu SE) was much lower ($x \approx 0.10$). The NVESD GMan - Fisons feedback loop was used to automatically change the CdTe cell temperature under SE control to achieve the target composition of x=0.225. Due to the non-optimal feedback constant, this process took almost 1 ½ hours. In the next phase of the experiment, a target composition of x=0.28 was chosen. The feedback constant was also increased in an effort to achieve faster convergence in the controlled composition. This did indeed work, as illustrated by the nicely dampened composition response curve near the middle of figure. Finally, the feedback constant was again increased, and the target composition was dropped to x=0.20. In this case, the feedback loop was under-dampened, as evidenced by the oscillations in the measured composition and CdTe setpoint temperature.

This experiment conclusively demonstrates that the feedback loop actually does work, albeit in a non-optimal manner. Improved control could be obtained by adding integral or derivative information to the feedback algorithm, i.e., performing PID control. However, in HgCdTe growth, the composition is normally quite close to the target value anyway, such that a sophisticated control algorithm should not required to achieve adequate control.

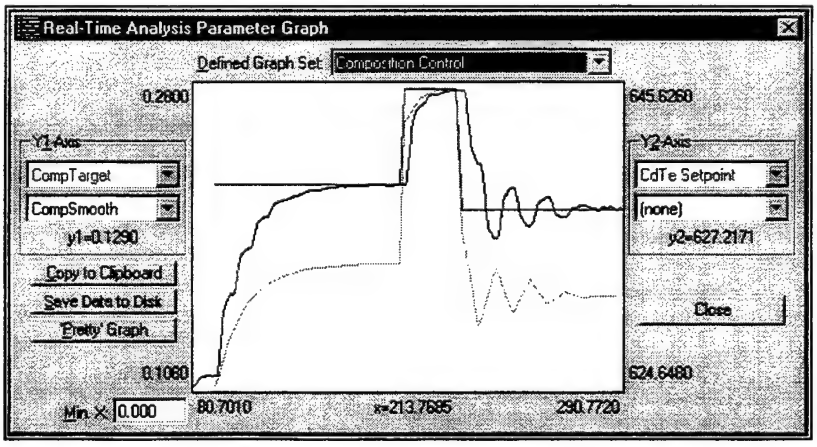

Figure 7.24. Real-time analysis parameters for HgCdTe feedback control experiment.

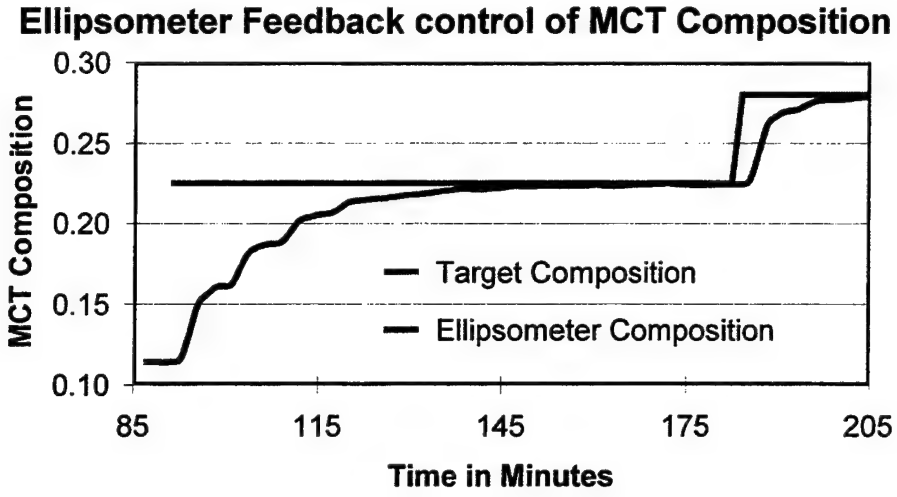

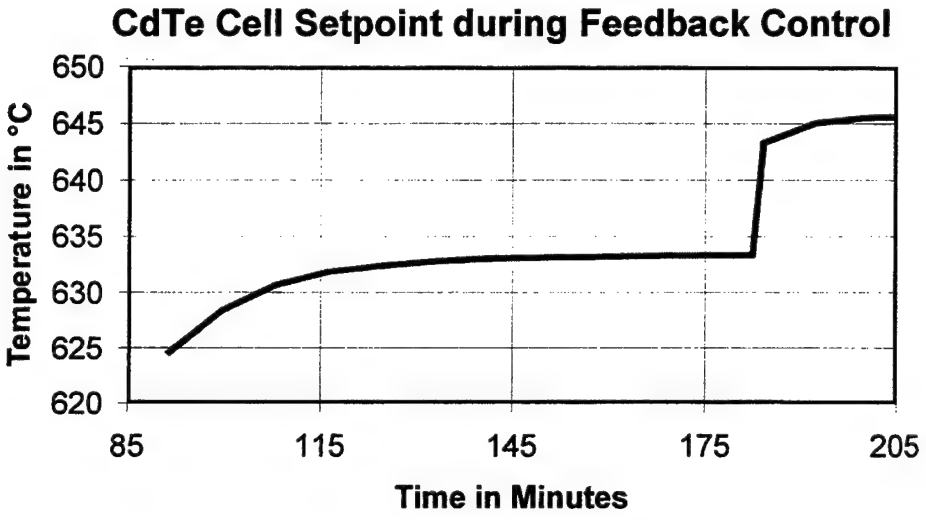

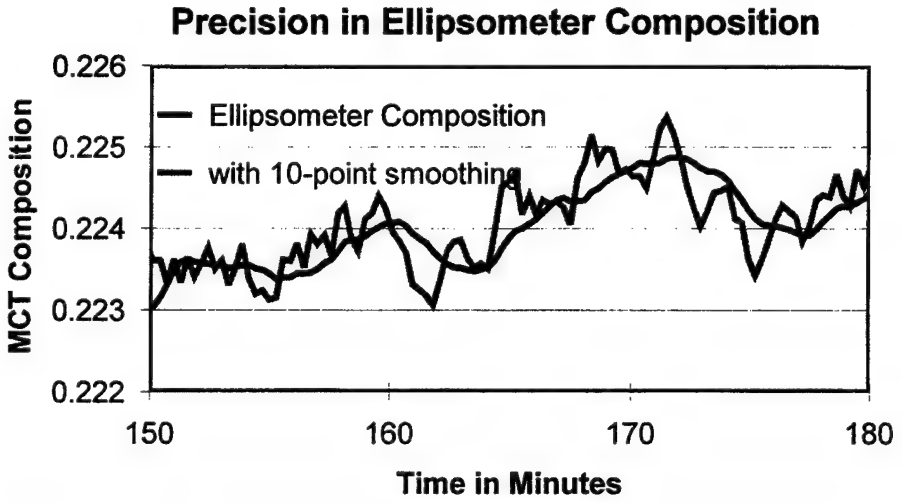

Figure 7.25. 'Pretty' parameter graphs from the HgCdTe feedback control experiment.

External Communication Protocol

Overview

The Growth Manager (GMan) program provides a high level user-friendly interface which hides the complex details of acquiring and analyzing real-time ellipsometric data. The 'front panel' functionality of Growth Manager is also available to external systems via the external communication protocol described in this document. This protocol can be run either over a TCP/IP network, or an RS-232 serial link. The physical communication link (TCP/IP or Serial) is specified in the Growth Manager Configuration menu option; other details about the link (such as TCP/IP port number, or Serial Baud rate) are also specified in this menu option.

General Protocol Specifications

The GMan external communication protocol is an ASCII-based messaging protocol. ASCII command strings are sent from the external system to GMan, and GMan will then send a response back to the external system. In current computer systems terminology, GMan would be the 'server' and the external system would be the 'client'. All ASCII commands which can be sent by the external system must be terminated with a carriage return / line feed sequence (the CR and LF characters, or Chr$(13)+Chr$(10) in BASIC lingo). Likewise, all responses from GMan will be terminated with the CR + LF characters.

'Classes' of GMan Commands:

- *Basic communication commands:* query the state of the GMan program
- *Standard control commands:* control the standard operations of GMan
- *Custom commands:* user-customizable commands for real-time ellipsometric data analysis

Basic GMan Communication Commands

Command Name: Mode

Returns the string displayed in the 'Mode: ' window of the Growth Manager program; this string describes the current operation mode of the ellipsometer. The external system should send this command (and continuously poll, if necessary) to determine the current state of GMan and the ellipsometer system. The supported GMan 'Mode' strings are listed below; throughout this document the GMan mode is referenced by the number in the mode string.

1. **Waiting to Begin Data Acquisition** - This is the mode which Growth Manager starts up in. If GMan is configured to use the TCP/IP or Serial port communication links, the 'Status' box will display appropriate information about the communication link during this mode.
2. **Preparing for Data Acquisition** - This mode is entered when the 'BeginDataAcquisition' command is initiated. During this mode, the ellipsometer hardware is aligned (which may require user intervention) and calibrated.

3. **Acquiring Data** - After the ellipsometer hardware is successfully calibrated, the ellipsometer will begin acquiring ellipsometric data, and the GMan Mode box will display this message.
4. **Changing Data Analysis** - This mode is entered when a 'Real-Time Data Analysis Module' is selected. Growth Manager stays in this mode until the selected Analysis Module is successfully loaded.
5. **Real-Time Data Analysis: xxxxx** - The 'xxxxx' string describes the Data Analysis module which is currently active. The 'Status' box contains the results of the real-time data analysis.

Command Name: Status

Returns the string displayed in the 'Status: ' window of the Growth Manager program; the contents of this string depends on the current operation mode of the ellipsometer. When the status information contains numeric information, the general format of this string will be (the *Error Bar* information may not be available for all parameters):

ParmName1=ParmValue1±ParmErrorBar1,
ParmName2=ParmValue2±ParmErrorBar2, etc.

After a growth run has been started (via the BeginDataAcquisition command) and GMan is in Mode 3, the Status command will return a string with the following format,

Time=2.342, RawData[0: 13.23 153.23 10: 32.24 140.97 20: 35.46 135.64]

where the *Time* parameter is the current ellipsometer time in minutes, and the *RawData* parameter lists raw ellipsometric data at the channels specified in the Growth Manager configuration file. The raw data string is enclosed in square brackets [ ], and uses the following format:

[ChannelNumber0: Psi0 Delta0 ChannelNumber1: Psi1 Delta1 etc.]

Command Name: Error

Returns a string describing the current error condition of GMan, or 'OK' if no error is present. GMan will automatically clear the 'Error' string when a command other than 'Mode', 'Status', or 'Error' is sent.

Standard GMan Control Commands

Notes:

If GMan does not recognize a command, or the syntax for the command is not valid, it will return a string 'Error: xxx', where 'xxx' provides descriptive information about the error. If GMan can successfully parse the command, it will return an 'OK' string and begin processing the command.

If any of the commands below are sent while GMan is processing a previous command, a 'BUSY' string will be returned from GMan. To query the current state of GMan while a command is being processed, use the 'Mode', 'Status', or 'Error' commands described in the previous section.

Most of the GMan external commands have the same name and functionality as the corresponding buttons on the GMan front panel. Familiarity with the operation of the GMan program will simplify the process of controlling GMan via the external command interface.

Command Name: BeginDataAcquisition

Equivalent to hitting the 'Begin Data Acquisition' button in Growth Manager; this initiates the ellipsometer alignment and calibration procedure, and then starts the ellipsometer data acquisition process. *It is very important that the surface and temperature of the wafer are stable throughout the execution of this command.* To specify a name for the growth run, add the 'Comment=' argument to the command, for example:

BeginGrowthRun(Comment=InGaAs growth run EM96-1)

If a name is not specified using the 'Comment=' argument, GMan will assign a unique sequential number to the growth run.

Immediately after this command is sent, GMan will switch to Mode '2' (see the 'Mode' command description). If the ellipsometer alignment and calibration is successful, GMan will then switch to Mode '3' and begin acquiring ellipsometric data. If for some reason GMan can not begin the ellipsometric data acquisition, the Mode will be set back to '1', and a descriptive error string can be obtained using the 'Error' command. Therefore, after the external system sends the BeginDataAcquisition command, it should repeatedly send Mode commands (the user may also have to manually adjust the ellipsometer alignment during this time) until GMan enters Mode 3; at this point, the external system can then proceed with the growth.

Command Name: EndDataAcquisition

Equivalent to hitting the 'End Data Acquisition' button in Growth Manager; this command should be sent after the growth run is completed, such that the ellipsometer can save all of its acquired data.

Command Name: StopFitting

Equivalent to hitting the 'Stop Real-Time Data Analysis' button in Growth Manager; this command cancels the current data fitting mode (which may be started by a GMan 'Custom' command).

Command Name: FastAcquisition

This command increases the data acquisition rate of the ellipsometer; this is useful during the growth of very thin layers to improve the time resolution of the measurements. The actual data acquisition period is set in the Growth Manager configuration file.

Command Name: StdAcquisition

This command sets the ellipsometer data acquisition rate to its initial value; this slower (when compared to the FastAcquisition rate) acquisition rate improves the S/N of the data, and also minimizes the amount of raw data collected.

Command Name: GlobalParmGet

This command returns the list of parameters displayed when the 'View Global Parameters' button is pressed on the GMan front panel; it is not required for the typical operation of the GMan program.

Command Name: CurrentLogData

This command returns a list of all the parameter names and current values that can be displayed with the 'Graph Analysis Parameters' button on the GMan front panel; it is not required for the typical operation of the GMan program.

GMan 'Custom' Commands

Overview

Growth Manager allows the user to extensively customize the real-time ellipsometric data analysis ability of the program. Real-Time Data Analysis Modules (which are Windows OLE objects) can be written, using the GMan programming specification which is documented elsewhere. The 'object names' of the currently available real-time data analysis modules are: SubTemp.GManObj, FastDynLayer.GManObj, and StatComp.GManObj.

Adding Custom Analysis Modules

To activate a module within the GMan program, enter the object name of the desired module in the Growth Manager configuration menu option, under the 'Custom Modules' heading. Up to 10 custom modules can be specified, and the same real-time data analysis module can be used more than once.

'Naming' Custom Analysis Buttons and Commands:

The names of the buttons on the GMan front panel are also the names of the GMan 'Custom' Commands which can sent from the external system. Each custom module has a corresponding configuration menu option which is used to specify the button/command name for each analysis module, as well as the configuration parameters specific to each analysis module.

Executing 'Custom' Commands with the External Communication Protocol

The external system can simply send a command string consisting of the GMan button name; this is equivalent to the user pressing the corresponding button on the GMan front panel. GMan will switch to Mode 4 while loading the selected analysis module, and then to Mode 5 if the module is successfully loaded (or back to Mode 3 if it is not successful; an error message will also be displayed). However, the GMan external communication protocol provides additional flexibility: any of the parameters which are accessible from the GMan custom module configuration can also be sent as arguments to the custom command. Parameters which are not specified in the argument list will use the values specified in the corresponding configuration file. For example, if a SubTemp.GManObj data analysis module was defined in GMan with a name of 'SubstrateTemp', the following command could be sent from the external system:

SubstrateTemp(Temp File=t-InP, Oxide File=InP-ox, Fit Wvls=2.5-3.3 eV)

Designing a 'Custom' command interface

There are basically 2 different ways of laying out the button/command structure within GMan:

1. For growing layers, define a single button (of the FastDynLayer.GManObj object type) on Growth Manager named something like 'GrowLayer'. To handle the different types of materials that could be grown, the external system would have to pass the material file name and all of the other associated parameters for growing a specific layer.

2. For each type of layer to be grown, define a button on Growth Manager (for example, GrowInGaAs, GrowInAlAs, etc.). Now the external system would have to know the corresponding Growth Manager button/command name, but it would not have to keep track of all the detailed parameters that the ellipsometer needs to know about the particular layer.

It is also possible to mix and match between the two command structures. The 'optimal' command structure layout depends on the particular application, the number of different types of material that will be grown, and the flexibility of the external system. It is important that the command structure is well thought out, such that it (and the external system's communication interface to GMan) does not have to be fundamentally changed to accommodate new layers and/or device structures.

Real-Time Data Analysis Module: SubTemp.GManObj

(typically assigned button/command name: SubstrateTemp)

This analysis module fits the ellipsometric data to extract a surface temperature and an overlayer thickness. It assumes that the sample is optically thick, e.g. a substrate.

Command Arguments for the SubTemp.GManObj Real-Time Analysis Module

Name	Type	Description
Temp File	string	Name of the WVASE material file which contains the substrate optical constants. This file should be stored in the MAT subdirectory under the current GMAN directory.
Nominal Temp	float	Nominal (starting) temperature for the substrate
Oxide File	string	Name of the WVASE material file which contains the optical constants for the oxide or overlayer. This file should be stored in the MAT subdirectory under the current GMAN directory.
Fit Wvls	string	String which specifies which ellipsometric data to use in the analysis. This string must use one of the following formats: 'all', 'skip=n', channel list '0 10 20', and wavelength range '1.8-2.4 eV'. The 'all' keyword will use all of the available data channels, the 'skip=n' keyword (where 'n' is replaced by an integer) will use every n'th channel, the channel list specifies a list of discrete channel numbers (separated by spaces), and the wavelength range specifies a range of channels (the range must be specified in either eV or nm).
Smoothing	integer	Specifies how many data points should be used to 'smooth' the extracted ellipsometer temperatures

Example command string:

SubstrateTemp(Temp File=t-InP, Oxide File=InP-ox, Fit Wvls=2.5-3.3 eV)

Returned 'Status' Parameters for the SubTemp.GManObj Real-Time Analysis Module

Name	Description
MSE	The 'MSE' parameter stands for Mean Squared Error, and it quantifies the 'goodness' of the ellipsometric data fit. Low numbers indicate a better fit; most 'good' fits typically have MSE's around 1. The external system could compare the reported MSE with MSE's from previous runs to verify the operation of the ellipsometer and/or the deposition system.
Temp	Ellipsometrically determined surface temperature, in °C
TempSmooth	Calculated from a running average of the 'Temp' value. The number of points used in the running average is specified in the custom module configuration file (or by

	passing the 'Smoothing=' argument to the command).
Oxide	Overlayer thickness in Angstroms
Angle	Ellipsometer beam angle of incidence in degrees

Example return string from the 'Status' command:

(in addition to the ellipsometer 'Time=' and 'RawData[...]' info described in the 'Status' command)

MSE=0.242, Temp=645.2±5.2, TempSmooth=645.6, Oxide=2.4±0.2, Angle=72.682±0.0153

The '±' values are the 90% confidence limits returned from the regression fitting procedure. These values can be loosely considered as 'error bars', and could also be utilized by the external system to establish the validity/accuracy of each parameter.

Real-Time Data Analysis Module: FastDynLayer.GManObj

(example button/command names: InGaAs_Comp, AlGaAs_Thick)

This analysis module loads the WVASE FastDyn (short for Fast Dynamic analysis) layer to fit the composition and/or thickness of a growing semiconductor layer. The Growth Manager configuration file contains a number of parameters which are used to individually tune the model fitting algorithm for each material. These parameters, which can be passed as command arguments, are listed in the table below.

Command Arguments for the FastDynLayer.GManObj Real-Time Analysis Module

Name	Type	Description
Opt Const File	string	Name of the WVASE material file which contains the optical constants. This file should be stored in the MAT subdirectory under the current GMAN directory.
Nominal Comp	float	Nominal composition for the layer
Nominal Rate	float	Nominal growth rate for the layer
Nominal Temp	float	Nominal temperature for the layer; this setting is only valid if the Opt Const File contains temperature-dependent data.
Fit Wvls	string	String which specifies which ellipsometric data to use in the analysis. This string must use one of the following formats: 'all', 'skip=n', channel list '0 10 20', and wavelength range '1.8-2.4 eV'. The 'all' keyword will use all of the available data channels, the 'skip=n' keyword (where 'n' is replaced by an integer) will use every n'th channel, the channel list specifies a list of discrete channel numbers (separated by spaces), and the wavelength range specifies a range of channels (the range must be specified in either eV or nm).
Fit Type	integer	An integer (0 - 3) which corresponds to the FastDyn Experimental Data Fit Type: 0-Entire Layer, 1-Near Surface, 2-Layer End Points, 3-Surface+Layer.
Interface Thickness	float	Specifies the interface thickness (in Å); a 'delay time' is calculated by dividing this thickness by the 'Nominal Rate' specified above. The data analysis algorithm will not use the experimental ellipsometric data acquired during this time. The interface time is 'started' when the corresponding Custom Analysis button is selected.
Num Points	integer	Number of experimental data points to use in the FastDyn analysis
Min Points	integer	Minimum number of experimental data points required before FastDyn will begin analyzing the data
Max Iter	integer	Maximum number of fit iterations used by the data analysis regression algorithm

Fill Gen Data	boolean	Enables the generation (and graphing) of the FastDyn modeled data
Fit Comp	boolean	Enables fitting of the layer composition
Comp Bounds	string	Specifies the minimum and maximum acceptable values for the layer composition, separated by a space.
Comp Min Thick	float	Specifies the minimum layer thickness (in Å) required before FastDyn begins fitting for the layer composition.
Fit Rate	boolean	Enables fitting of the layer growth rate
Rate Bounds	string	Specifies the minimum and maximum acceptable values for the layer growth rate, separated by a space.
Rate Min Thick	float	Specifies the minimum layer thickness (in Å) required before FastDyn begins fitting for the layer growth rate.
Fit Angle	boolean	Enables fitting of the angle of incidence
Angle Bounds	string	Specifies the minimum and maximum acceptable values for the angle of incidence, separated by a space.
Angle Min Thick	float	Specifies the minimum layer thickness (in Å) required before FastDyn begins fitting for the angle of incidence.
Fit VI	boolean	Enables fitting of the FastDyn virtual interface parameters
VI Min Thick	float	Specifies the minimum layer thickness (in Å) required before FastDyn begins fitting for the virtual interface parameters.
Fit Temp	boolean	Enables fitting of the layer temperature
Temp Bounds	string	Specifies the minimum and maximum acceptable values for the layer temperature, separated by a space.

Example command string:

GrowLayer(Opt Const File=InGaAs, Fit VI=ON, Fit Comp=ON, Nominal Temp=650)

When the appropriate number of data points have been acquired and/or thickness of material has been grown, the extracted parameters can be retrieved with the Status command. The returned Status string will have the following format:

MSE=.432, Comp=0.523±0.0018, Thick=534.5, Rate=2.6831±0.0004, AveComp=0.526±0.0008, Temp=645.3±2.4, Angle=72.892±0.018

A description of the 'MSE' parameter and the parameter 'Error Bars' is given in the SubTemp object above. The 'Comp' parameter gives the near surface composition, the 'Thick' parameter is the overall layer thickness in Angstroms, the 'Rate' parameter is the average layer growth rate in Angstroms/second, the 'AveComp' parameter is the average layer composition, and the 'Angle' parameter gives the angle of incidence in degrees. Notice that the 'Thick' parameter does not have an error bar, as this parameter is not actually extracted from the fit; it is *calculated* by multiplying the layer growth time times the 'Rate'. A further caveat is that not all of the parameters necessarily appear in the Status string. For example, the configuration parameters can be set to fit for composition *only after* a given layer thickness has been grown, as it is not possible to fit for the composition of a very thin or zero thickness layer. Therefore, the Status string may initially contain only the 'Rate' and 'Thick' parameters; the 'Comp' and 'AveComp' entries will appear in the Status string only when the ellipsometer has sufficient information to determine these parameters. The 'AveComp' parameter will also only appear when the Fit Type is set to 3 - Surface+Layer. Likewise, 'Comp' will not appear if the 'Fit Comp' configuration parameter is not set to 'ON'.

Comments relevant for Feedback Control of Growth using this command:

For accurate determination of layer thickness, the external system should send this command immediately after the layer growth has been started on the deposition

machine. The overall layer thickness reported by the 'Thick' parameter is subject to the following errors: 1) the coarseness of the ellipsometer data acquisition limits the resolution of the reported thicknesses, which are updated at the same discrete intervals as the data acquisition, 2) the data analysis introduces a time lag between the thickness extracted from the analysis and the current instantaneous thickness of the growing film, and 3) interfacial effects (which we have unquestionably observed for the growth of InAlAs on InP) may affect the accuracy of the reported thickness, although these effects are probably only significant for thinner (<200Å) films. Despite these potential errors, for thicker films, where a 10-20Å uncertainty in the thickness is tolerable, the external system could still just monitor the 'Thick' parameter until it exceeds the target thickness, at which time it would terminate the layer growth. For thinner films, this approach would probably not achieve the desired control accuracy. However, all of the preceding errors can be eliminated or significantly minimized by using the 'Rate' parameter for the feedback control of the thickness. The external system can at any time calculate the current thickness of the film by multiplying the 'Rate' times the total layer growth time; likewise, the external system can calculate what the 'updated' layer growth time should be by dividing the target thickness by the 'Rate'.

For the feedback control of composition, the 'Comp' parameter, which reports the near surface composition, should be monitored. The Growth Manager configuration file specifies how many data points are used in the near surface analysis, which in turn relates to the material 'depth' used for the near surface analysis. These properties can be used to calculate the effective time constant for the ellipsometrically measured near surface composition. For example, assume that 6 ellipsometric data points are used for the near surface analysis, with an ellipsometer averaging time of 5 seconds/measurement, and a layer growth rate of 3 Å/second. The effective ellipsometer 'time constant' would be 6 measurements x 5 seconds/measurement, or 30 seconds, and the material depth for the near surface analysis would be 30 seconds x 3 Å/second, or 90Å. It is important to consider the relatively large ellipsometer 'time constant' when implementing a feedback control loop: if the supervisor changes the deposition parameters to adjust the composition, it must wait for the ellipsometer 'time constant' until the ellipsometrically determined composition is based only on the 'new' deposition parameters.

8. ECR Etching Results

Monitoring the ECR etching of HgCdTe was not one of the stated requirements of the contract. However, since the etching process is important in the fabrication of IR focal plane array devices, it would also be useful to have an sensor available to monitor and optimize the etching process, and insitu SE was certainly a suitable candidate. In this chapter, some of the ECR etching of HgCdTe results which were obtained at NVESD are briefly presented.

Exsitu SE Analysis of HgCdTe

Analyzing exsitu SE data measured on HgCdTe samples is not as straightforward as one might think (this problem is directly relevant to the modeling of the insitu HgCdTe etching data, as the etching is performed at room temperature, and the HgCdTe starting material has been previously exposed to atmosphere). While room temperature composition-dependent MCT optical constants are readily available in the literature, the surface composition and morphology of most HgCdTe samples seems to be highly variable. In rare cases, a simple model consisting of a bulk MCT substrate and fitting only for the composition can yield an acceptable fit to the SE data. More often, it is necessary add some kind of overlayer to the MCT substrate. Sometimes a surface roughness layer is adequate, but sometimes a more complicated EMA mixture of MCT, amorphous tellurium (Te), and/or void is required to fit the measured data and extract correct composition values.

An example of this shown in Figure 8.1, in which two different models are used to analyze the exsitu SE data measured on a MCT sample with a composition of 0.15 (as measured by EDX). The more complicated EMA overlayer model reduced the MSE by a factor of 2. The data fits for the best fit model are shown in Figure 8.2

Model #1, Surface Roughness:			Model #2, MCT, Void, a-Te overlayer:		
1 srough		26.808 Å	1 ema (mct)/42.9% void/5.21% a-te		33.998 Å
0 mct x=0.146		1 mm	0 mct x=0.151		1 mm
MSE=12.59			MSE=6.756		
Alloy.0	0.14554±0.00149		Alloy.0	0.15069±0.000927	
Thick.1	26.808±0.25		Thick.1	33.998±2.5	
			EMA%2.1	42.893±3.97	
			EMA%3.1	5.2116±1.34	

Figure 8.1. SE data analysis models for HgCdTe sample measured exsitu

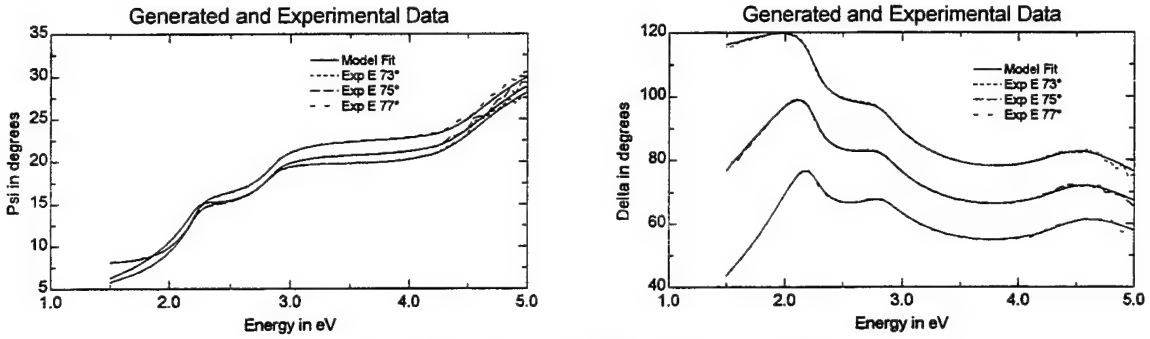

Figure 8.2. SE Data fits for HgCdTe sample measured exsitu.

Qualitative HgCdTe Etching Results

Typical dynamic SE data acquired during a ECR etching run on a HgCdTe film is shown in Figure 8.3 (the vertical lines on the graph correspond to the before and after etch timeslices which will be discussed next). Dramatic changes are observed in the data when the etch is initiated at t=1 minute.

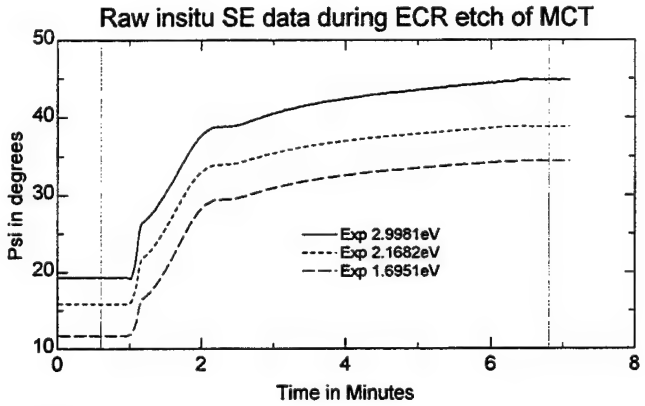

Figure 8.3. Raw insitu SE data during ECR etch of MCT layer.

Two spectroscopic timeslices are displayed before and after etching in Figure 8.4. The before etching data acquired on the HgCdTe surface is nicely fit by the simple model shown in Figure 8.5. However, the after etching SE data does not even resemble HgCdTe, as no critical point structure is observed in the pseudo <e2> curve shown in Figure 8.4. From an optical standpoint, the surface is completely changed by the ECR etching process. While it is not possible to quantitatively model the SE data during and after the etch, observing the raw SE data trajectory during the etch still provided useful information for optimizing the HgCdTe ECR etching parameters: a smaller the change observed in the raw SE data during the etching corresponds to a smaller change in the HgCdTe surface composition and/or morphology.

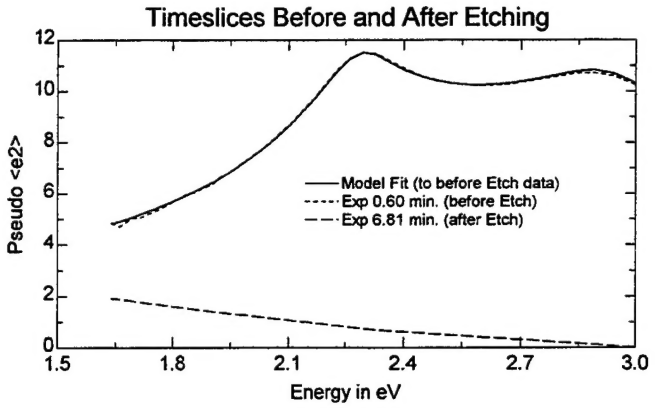

Figure 8.4. Spectroscopic timeslices before and after etching.

1	ema (mct)/8.34% void	121.33 Å
0	mct x=0.219	1 mm

Figure 8.5. Simple model to fit the SE data before etching HgCdTe.

Quantitative HgCdTe Etching Results

Using a different (proprietary) ECR etching chemistry and parameters, it was possible to etch a HgCdTe sample without severely modifying the surface composition and morphology. This is illustrated by the insitu SE data shown in Figure 8.6, which should be compared against the data shown in Figure 8.3. The change in the raw SE Psi data induced by the ECR etch has been reduced from ≈20° to ≈1°.

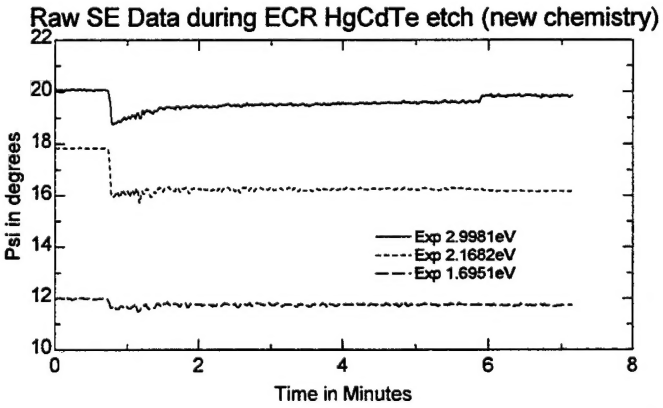

Figure 8.6. Raw SE data during ECR etch of HgCdTe with using a different etching chemistry and parameters.

The insitu SE data acquired during this new ECR etch process can be quantitatively modeled. Figure 8.7 and 8.8 show the analysis results for the HgCdTe sample before and after the etch. The Cd deficient layer which was used to fit the before etch data was postulated to come from the growth termination procedure inside the MBE system. The ECR etching removes this thin non-stoichiometric layer, leaving only small amount of surface roughness on the sample, as shown in the model of Figure 8.8. This hypothesis is also consistent with the point-by-point fit results shown in Figure 8.9.

Best Fit Model:

2	ema (mct)/50% void	7.8273 Å
1	mct x=0.056	81.94 Å
0	mct x=0.198	1 mm

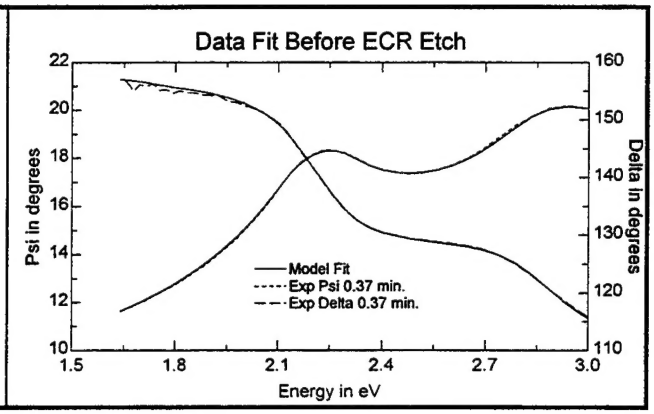

Figure 8.7. SE data fit before ECR etch.

Best Fit Model:

1	ema (mct)/50% void	29.987 Å
0	mct x=0.195	1 mm

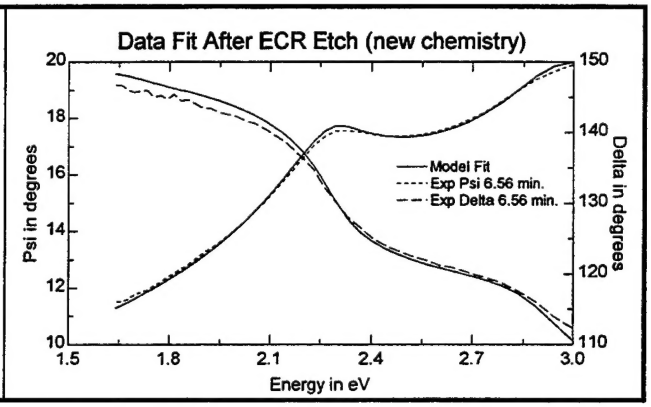

Figure 8.8. SE data fit after ECR etch.

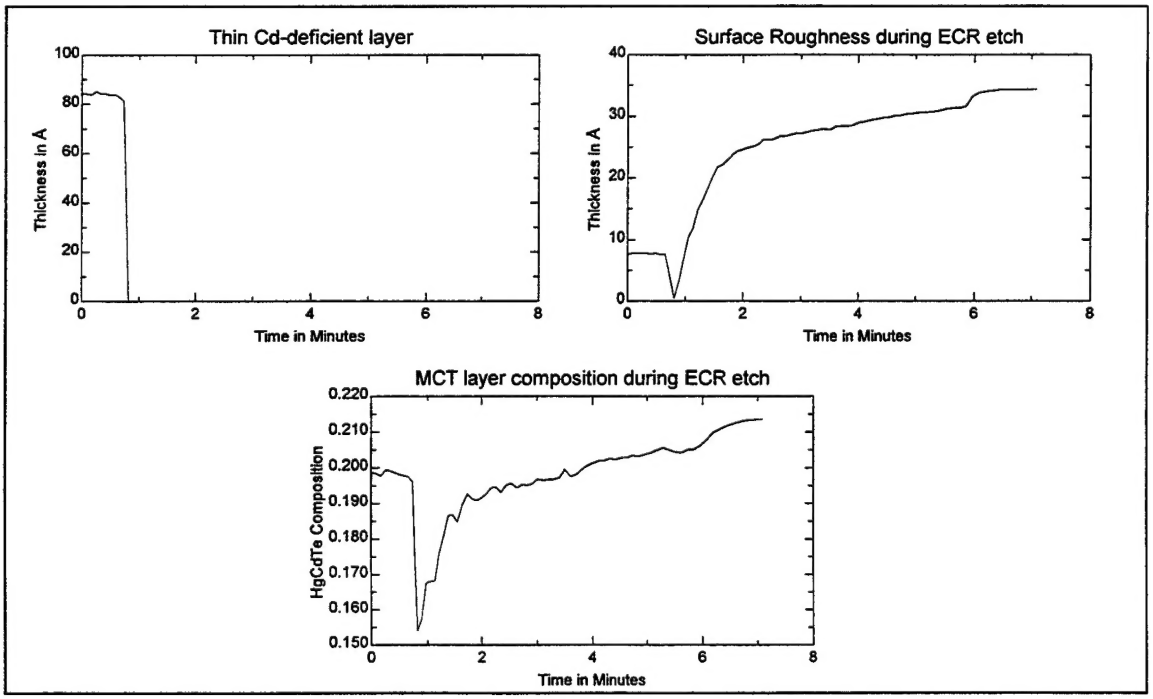

Figure 8.9. Point-by-Point fit results for ECR etch of HgCdTe sample

HgCdTe Endpoint Detection via insitu SE

The data in Figure 8.10 was acquired during the ECR etching of the multilayer MCT/HgTe structure which is shown in Table 5.3. From the large contrasts observed in the data, it is easy to determine when the various layers are etched through. Based on this observation, one might conclude that by simply monitoring the raw insitu SE data, the etching process could be stopped at a desired interface within a multiple composition HgCdTe device.

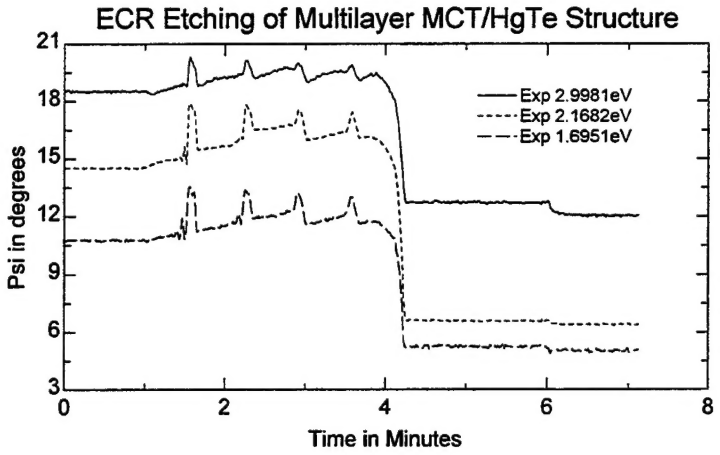

Figure 8.10. Raw insitu SE data during ECR etching of a multi-layer MCT / HgTe structure.

9. Conclusions

The primary goal of this contract was develop a real-time monitoring capability for HgCdTe composition during MBE growth. This goal was realized by demonstrating a **±0.001 accuracy in the composition** values determined by the Spectroscopic Ellipsometry (SE) insitu sensor, which was confirmed by exsitu FTIR measurements. Attaining this level of success required significant improvements in the ellipsometer system hardware and data analysis software, the creation of accurate optical constant libraries for the CdZnTe substrate and HgCdTe film materials, and the development of a systematic methodology for acquiring and analyzing insitu SE data in the MBE growth environment. These improvements and developments are part of an extensive 'knowledge base' which evolved throughout this contract, and is encapsulated in this report. This knowledge base is not specific only to HgCdTe growth; it is also directly relevant to the insitu SE monitoring of any epitaxial semiconductor growth process.

In addition to the HgCdTe composition monitoring capabilities, insitu SE was also found to be very useful in monitoring the temperature and surface condition of the CdZnTe substrate before growth. As the quality of the epitaxial HgCdTe growth can be highly dependent on the both the temperature and surface of the substrate, this added capability offered by the insitu SE sensor is highly useful. A carefully analysis of the insitu SE data also revealed interesting details about the film growth process, including the observation of surface roughening during the HgCdTe growth initiation, and changes in the film growth rate and composition due to effusion cell flux transients. Insitu SE data was also useful in monitoring the HgCdTe surface morphology during ECR etching, which is an important process used in the fabrication of focal plane array devices.

The two insitu Spectroscopic Ellipsometry systems (one M-44 and one M-88) which were delivered to NVESD on this contract are now commercially available, along with the WVASE32 software (which is used to acquire and analysis the SE data), and the Growth Manager software (which provides an easy to use interface suitable for a production environment and integration with the deposition system to support feedback control of growth). The commercial availability provides a direct path for the 'Phase III' continuation of this work. J.A. Woollam Co. will coordinate closely with its current and potential customers who are applying insitu SE to the monitor and control of the growth of HgCdTe. The most likely focus of such continuing work is to achieve *long term* HgCdTe composition accuracy by active *feedback control* during growth using the insitu SE composition sensor.